Earth-Science Reviews 259 (2024) 104985

Contents lists available at ScienceDirect

Earth-Science Reviews

journal homepage: www.elsevier.com/locate/earscirev

Precambrian tectonic evolution of the Qaidam block, northern Tibet: Implications for the assembly and breakup of Proterozoic supercontinents

Chen Wu[a,*], Jie Li[b], Wenyou Liu[c], Andrew V. Zuza[d], Peter J. Haproff[e], Lin Ding[a]

[a] State Key Laboratory of Tibetan Plateau Earth System and Resources Environment (TPESRE), Institute of Tibetan Plateau Research, Chinese Academy of Sciences, Beijing 100101, China
[b] Chongqing Key Laboratory of Complex Oil and Gas Field Exploration and Development, Chongqing University of Science and Technology, Chongqing 401331, China
[c] School of Earth Sciences and Resources, China University of Geosciences (Beijing), Beijing 100083, China
[d] Nevada Bureau of Mines and Geology, Nevada Geosciences, University of Nevada, Reno, NV 89557, USA
[e] Department of Earth and Ocean Sciences, University of North Carolina Wilmington, NC 28403, USA

ARTICLE INFO

Keywords::
Precambrian continent
North Qaidam
Columbia-Nuna supercontinent
Rodinia supercontinent
Greater North China
Laurentia

ABSTRACT

The nature of Precambrian metamorphic basement rocks and overall tectonic evolution of the Qaidam block in northern Tibet remains debated despite being important to understanding the assembly of Asia. Paleogeographic reconstructions of Precambrian supercontinents rarely consider Phanerozoic tectonic modification of its constituent Precambrian blocks. This issue is particularly relevant for the Qaidam block and its neighboring crustal fragments, which experienced significant Phanerozoic overprinting from multiple tectonic episodes. To address this problem, we systematically reviewed key geological observations and regional datasets related to Proterozoic magmatism, metamorphism, and sedimentation of major Precambrian blocks in China. This synthesis provided new constraints on the Proterozoic tectonic evolution of the Qaidam block, including paleogeographic supercontinent configurations and nature of multiple continental-drift-collision events. New results of field mapping, geochronological, and geochemical analyses allow us to divide the Precambrian rocks of the Qaidam block into four divisions: (1) Paleoproterozoic gneiss and schist; (2) Meso- and (3) Neoproterozoic metasedimentary rocks; and (4) Proterozoic intrusions. We propose that the Qaidam block was part of a "Greater North China" block, which experienced early Paleoproterozoic post-collisional extension and continental collision along the Paleoproterozoic Northern Margin orogen to form the Columbia-Nuna supercontinent. The Greater North China block subsequently experienced Mesoproterozoic extension related to supercontinent breakup. In addition, we propose that the Greater North China block was affixed to the western margin of Laurentia and Siberia as part of Rodinia in the Neoproterozoic, rifted in the late Neoproterozoic, and drifted in the early Paleozoic as a series of microcontinents.

1. Introduction

The nature and spatiotemporal evolution of the earliest supercontinent cycles remain inadequately understood and may help elucidate the oldest forms of tectonics in Earth's history (e.g., Zhang et al., 2012a; Kusky et al., 2018; Brenner et al., 2020; Brown et al., 2020; Keller and Harrison, 2020; Korenaga, 2020; Mitchell et al., 2021; Windley et al., 2021). Although existing models of the Paleoproterozoic Columbia-Nuna (Rogers and Santosh, 2002; Zhao et al., 2002; Meert, 2012) and Neoproterozoic Rodinia (Valentine and Moores, 1970; Li et al., 2008a; Cawood et al., 2010, 2016) supercontinents have been systematically tested and refined over the past decades, debate persists regarding the configurations of their constituent crustal fragments and orogens. A key lasting issue in the paleogeographic reconstructions of these supercontinents is the effect(s) of Phanerozoic tectonic modification on the original shape of their Precambrian continents (e.g., Zuza and Yin, 2017; Şengör et al., 2022). To address this problem, classical geological methods and tests of rock correlation can be employed. This problem is particularly relevant for the Qaidam block of northern Tibet and its neighboring Precambrian continents (i.e., North China craton, Tarim craton, and South China block), which have experienced significant overprinting by post-Rodinia tectonics (e.g., Yin and Harrison, 2000; Lu, 2002; Gehrels et al., 2011; Zhao and Cawood, 2012; Chen et al., 2012; Zuza and Yin, 2017; Wu et al., 2022a). Specifically, the Qaidam block

* Corresponding author.
E-mail address: wuchen@itpcas.ac.cn (C. Wu).

https://doi.org/10.1016/j.earscirev.2024.104985
Received 24 May 2024; Received in revised form 6 September 2024; Accepted 5 November 2024
Available online 9 November 2024

experienced early Neoproterozoic subduction, late Neoproterozoic continental rifting, Paleozoic to early Mesozoic subduction and continental collision, Mesozoic extension, and Cenozoic intracontinental deformation induced by the India-Asia collision (e.g., Yin and Harrison, 2000; Wu et al., 2016). The present-day Qaidam block is covered by a thick Cenozoic sedimentary succession of the Qaidam Basin, which was deposited during uplift and erosion of the Qilian Shan to the north, Eastern Kunlun Range to the south, and Altyn Tagh Range to the west (e.g., Yin et al., 2008a, 2008b).

Understanding the Precambrian evolution of the Qaidam block has two fundamental implications: (1) its rock correlations with other continental fragments provide important constraints for paleogeographic reconstruction of Asia and global supercontinents; and (2) its deformation and metamorphic histories provide an observational basis for regional paleotectonic events. However, there is no consensus regarding the nature of metamorphic basement rocks of the Qaidam block. This problem is exemplified by the three existing interpretations of correlation with the Tarim craton, North China craton, and South China block, which are mainly based on the extrapolation of local geological relationships to adjacent continental fragments. To clarify this issue and provide a new foundation for studying the Proterozoic tectonic evolution of the Qaidam block, we examined the Precambrian geology of the block and its adjacent cratons by combining geological mapping, geochronology, and geochemical analyses with existing tectonostratigraphic, magmatic, and metamorphic records. By removing the effects of Phanerozoic tectonic modification, we present a new paleogeographic reconstruction of central Asian Precambrian cratons in the context of global supercontinents.

2. Major Precambrian blocks of China

The four major Precambrian blocks of China include the North China, Tarim, South China, and Qaidam blocks (e.g., Zhao and Cawood, 2012). The North China craton is separated from the South China block by the Qinling-Dabie-Sulu orogen (Fig. 1). In the following sections, we summarize and compare the rock assemblages, tectonothermal events, and published ages among these Precambrian blocks.

2.1. North China craton

The North China craton consists of Archean–Paleoproterozoic metamorphic basement rocks overlain by Meso- and Neoproterozoic, unmetamorphosed to weakly metamorphosed cover sequences (e.g., Zhao et al., 2005; Kröner et al., 2005, 2006; Faure et al., 2007; Zhai et al., 1993, 2010; Zhai and Santosh, 2011; Zhao and Zhai, 2013; Wan et al., 2013; Zhang et al., 2014a; Kusky et al., 2016). The North China craton is traditionally divided into the Archean Eastern and Western blocks, separated by the ~1,600-km-long, northeast-striking, late Archean Central Orogenic Belt (Fig. 1A), also known as the Paleoproterozoic Trans-North China Orogen in the tectonic models of Zhao et al. (2001, 2005), Trap et al. (2012), and other papers. However, some researchers have interpreted that the Archean North China craton formed via the amalgamation of at least six microcontinents along Neoarchean greenstone belts (e.g., Zhai and Santosh, 2011; Zhai et al., 2021). The Paleoproterozoic Northern Margin orogen occurs along the northern margin of the North China craton (Fig. 1A), also known as the Inner Mongolia-Northern Hebei orogen of Kusky et al. (2016), and consists of the ca. 1.9–1.88 Ga Bayan Obo mélange, Yinshan block, and northern "Khondalite series" (e.g., Kusky et al., 2016; Wu et al., 2018, 2022a, 2023). The western continuation of the Paleoproterozoic Northern Margin orogen is the Alxa block. Numerous ca. 1.9–1.78 Ga, high-grade metamorphic rocks occur along the Northern Margin orogen. All high-pressure granulites are interpreted to have experienced ca. 1.91–1.8 Ga clockwise P-T paths related to continent-continent collision (e.g., Zhai, 2011, 2014; Zhai et al., 1993; Guo et al., 2015; Zhang et al., 2022a, 2022b; Zhao et al., 2008; Wan et al., 2009). Ca. 1.93–1.91 Ga, (ultra-)high-temperature metamorphic rocks in the Northern Margin orogen are interpreted to have been generated during subduction of a spreading ridge (e.g., Peng et al., 2010; Guo et al., 2012) (Fig. 1B).

The Paleo-Neoproterozoic unmetamorphosed rock assemblages of the North China craton include: (1) sedimentary rocks of the Changcheng, Jixian, and Qingbaikou groups that were deposited between ca. 1.8–1.4 Ga, ca. 1.4–1 Ga, and ca. 1.0–0.78 Ga, respectively; (2) ca. 1.78–1.75 Ga volcanic rocks of the Xiong'er Group and minor ca. 1.45 Ga intrusions (Zhao et al., 2002, 2004; Peng et al., 2008; He et al., 2009); (3) ca. 1.8–1.63 Ga mafic dyke swarms emplaced mainly in the central part of the craton (Peng et al., 2022); (4) a ca. 1.74–1.62 Ga anorthosite–mangerite–alkaline granite-rapakivi granite suite emplaced in the central and eastern portions of the craton (Zhang et al., 2007a); (5) ca. 1.85–1.0 Ga sedimentary rocks of the Zhaertai, Bayan Obo, and Huade groups along the northern margin of the craton (Liu et al., 2020a); and (6) ca. 1.35–1.31 Ga Yanliao diabase sills in the northeastern craton (Zhang et al., 2009a). Several researchers have proposed the development of late Paleoproterozoic–early Neoproterozoic rifts in the North China craton, including the Late Palaeoproterozoic Xiong'er rift zone in the south, Mesoproterozoic Yanliao rift zone in the east, and Late Palaeoproterozoic–Neoproterozoic Zha'ertai-Bayan Obo-Huade rift zone in the northwest (e.g., Lu et al., 2002; Zhang et al., 2009a, 2017a; Li et al., 2013a; Peng et al., 2014; Zhou et al., 2018; Liu et al., 2020a).

Magmatism in the Eastern Block of the North China craton peaked ca. 2.7 Ga and ca. 3.3 Ga, whereas magmatism in the Western Block of the craton peaked ca. 1.9 Ga (e.g., Wan et al., 2015). Wu et al. (2022a) compiled detrital zircon crystallization ages and isotope concentrations to constrain the Neoarchean–Paleoproterozoic magmatic and metamorphic history of the northern North China craton (Fig. 1C). The compilation for the Central Orogenic Belt (n = 10,370) shows the occurrence of three distinct Neoarchean–Paleoproterozoic igneous age populations of ca. 2.6–2.45 Ga, ca. 2.2–2 Ga, and ca. 1.9–1.75 Ga with four respective peaks at ca. 2.52 Ga, ca. 2.15 Ga, ca. 2.05 Ga, and ca. 1.83 Ga. The northern Central Orogenic Belt (n = 1,520) exhibits three igneous age populations that are similar to those for Central Orogenic Belt except for a ca. 2.15 Ga peak (Fig. 1C). However, the northern margin of the North China craton (n = 4,568) exhibits two zircon age populations of ca. 2.6–2.45 Ga and ca. 2.2–1.72 Ga with two respective peaks at ca. 2.5 Ga and ca. 1.95 Ga (Fig. 1C). These ages correspond with magmatic rock ages (n = 3,017) recorded in the northern North China craton (Fig. 1C). Two metamorphic episodes recorded in both the Central Orogenic Belt (n = 432) and Northern Margin orogen (n = 353) have well defined age populations of ca. 2.58–2.43 and ca. 1.98–1.77 Ga with respective peaks at ca. 2.5 and ca. 1.85 Ga (Fig. 1C). The ca. 2.5 Ga metamorphism, commonly associated with an arc-continent collision event, has been recognized in the Central Orogenic Belt and Northern Margin orogen, which was overprinted by ca. 1.93–1.8 Ga granulite-facies metamorphism (e.g., Kusky et al., 2016, 2021, 2022; Wang et al., 2017a, 2019a; Wu et al., 2018, 2022a, 2023; Zhong et al., 2021, 2022; Han et al., 2020; Ning et al., 2022). Zircon ε_{Hf}(t)-age results of the Central Orogenic Belt suggest an overall continuous evolution from ca. 2.7–1.8 Ga (Wu et al., 2022a, and references therein). In contrast, zircon ε_{Hf}(t)-age results of Northern Margin orogen suggest two distinct episodes at ca. 2.7–2.2 Ga and ca. 2.1–1.75 Ga (Wu et al., 2022a, and references therein).

Evidence for early Neoproterozoic magmatism is sparse in the North China craton, as only one ca. 965 Ma granitoid is reported in the Longshou Shan area along its southwestern margin (Wu et al., 2022b). Neoproterozoic (ultra)mafic intrusions (ca. 832–827 Ma) in the Longshou Shan area are interpreted to be related to continental rifting (e.g., Li et al., 2004, Li et al., 2005a, 2005b; Zhang et al., 2010a, 2010b; Tung et al., 2013; Tang et al., 2014). The Longshou Shan area was proposed to represent either the western extension of the North China craton since the Paleoproterozoic or the eastern extension of the North Tarim continent (e.g., Zhao et al., 2005; Zhai and Santosh, 2011; Zhang et al., 2012a; Gong et al., 2016; Zhang and Gong, 2018; Wu et al., 2021,

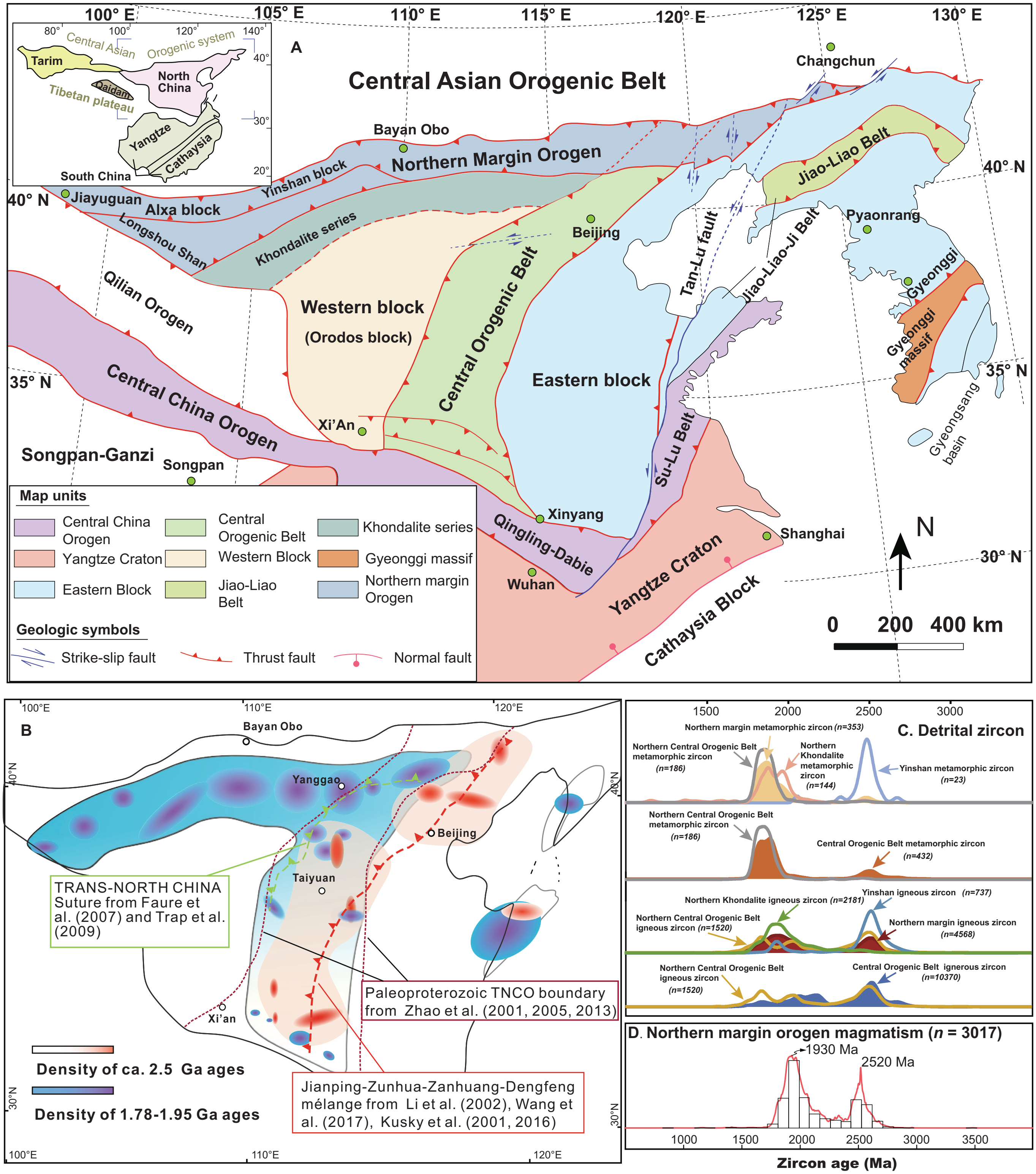

Fig. 1. (A) Simplified tectonic map of the North China craton and surrounding orogenic belts, modified from Wu et al. (2018). The North China craton is divided into the Eastern and Western blocks, Central Orogenic belt, and Northern Margin orogen. (B) Simplified tectonic map of the North China Craton, modified from Xiao et al. (2021) and Wu et al. (2022a). The different color shades represent the distribution density of ca. 2.5 Ga and ca. 1.78–1.95 Ga ages. Darker colors represent high densities of these ages. Note that records of ca. 2.5 Ga metamorphism follow the Jianping-Zunhua-Zanhuang-Dengfeng suture. In contrast, records of ca. 1.78–1.95 Ga metamorphism are widely distributed in the North China craton but decrease from north to south. High-grade metamorphism is mainly developed in the northern North China craton. The bottom right shows normalized relative probability plots of (C) Precambrian detrital zircon U-Pb ages for samples from the Central Orogenic Belt and Northern Margin orogen and (D) Precambrian magmatic records of the Northern margin orogen in the North China craton, updated from Wu et al. (2022a).

2022b). However, some workers argued that the Longshou Shan area is a block of Proterozoic basement rocks that separated from the Yangtze block or other Gondwanan subcontinents (e.g., Li et al., 2004; McKenzie et al., 2011; Dan et al., 2014; Song et al., 2017).

The Longshou Shan area consists of crystalline basement rocks of the Paleoproterozoic Longshoushan Group overlain by Mesoproterozoic–Paleozoic sedimentary cover sequences (e.g., Gong et al., 2016; Zhang and Gong, 2018; Wu et al., 2021; Su et al., 2023). The Paleoproterozoic Longshoushan Group mainly consists of migmatite intercalated with marble, schist, quartzite, and orthogneiss, which experienced Paleoproterozoic amphibolite-facies metamorphism (e.g., Gong et al., 2016; Wu et al., 2021). These rocks were subsequently folded and intruded by ca. 2.05 Ga leucogranites and Neoproterozoic ultramafic and mafic rocks (e.g., Gong et al., 2016; Zhang and Gong, 2018; Liu et al., 2020b; Wu et al., 2021). The schist of the Longshoushan Group is located in the footwall of a thrust containing ca. 2.17 Ga arc granitoid (e.g., Wu et al., 2022b). A regional angular unconformity separates the underlying Longshoushan Group from the overlying siliciclastic and carbonate rocks of the Mesoproterozoic Dunzigou Group (e.g., Gong et al., 2016; Wu et al., 2021). Metasedimentary rocks of the Longshoushan Group yield three prominent zircon age populations with peaks at ca. 1.85 Ga, ca. 2.05 Ga, and ca. 2.15 Ga, and a minor older zircon age population of ca. 2.56 Ga (e.g., Wu et al., 2022b). The Dunzigou Group has two major zircon age populations with peaks at ca. 1.82 Ga and ca. 2.05 Ga, and two minor age populations of ca. 2.31 Ga and ca. 2.6 Ga (e.g., Wu et al., 2022b). The youngest zircon age population of ca. 1.85–1.82 Ga from the Longshoushan and Dunzigou groups is interpreted to reflect a regional metamorphic event (e.g., Gong et al., 2012a, 2012b, 2016; Zhang and Gong, 2018; Wu et al., 2021, 2022b). The Archean zircon U-Pb age peak and Lu-Hf isotopes are interpreted to reflect reworking of ca. 3.04–2.76 Ga crust, which suggests a Meso–Archean basement source in the region (e.g., Gong et al., 2016; Zhang and Gong, 2018). Although Archean basement rocks are not reported in the Longshou Shan, Lu-Hf-Sr-Nd isotopes of amphibolite-facies orthogneisses of the Longshoushan Group show evidence of reworked ca. 2.7–2.4 Ga basement rocks. The Neoproterozoic Hanmushan Group consists of rift-related siliciclastic rocks, limestone, mafic rocks, and glacial deposits (e.g., Wu et al., 2022b). Detrital zircon U-Pb ages from the Hanmushan Group show two prominent age populations with peaks at ca. 1.15 Ga and ca. 1.4 Ga, and three minor age populations with peaks at ca. 1 Ga, 1.95 Ga, and 2.5 Ga (Song et al., 2017; Wu et al., 2022b).

2.2. Precambrian South China block

The South China block formed during the early Neoproterozoic (ca. 980–810 Ma) collision of the Yangtze craton in the northwest and Cathaysia block in the southeast along the Jiangnan orogen (e.g., Zheng and Zhang, 2007; Zhang and Zheng, 2013; Zhao and Cawood, 2012; Li et al., 2014; Zhao, 2015; Cawood et al., 2018; Lin et al., 2018; Shu et al., 2021) (Fig. 2A). The Kongling Complex of the South China block consists of sporadically-exposed ca. 3.3–2.7 Ga metamorphic assemblages, along with the ca. 2.78–2.74 Ga Huangtuling granulites and ca 2.7 Ga Yudongzi Group restricted to the northern Yangtze block (Fig. 2A). Paleoproterozoic rocks in the South China block include supracrustal rocks of the Houhe Complex located along the northern margin of the Yangtze craton and low-grade volcanic and sedimentary rocks of the Dahongshan, Dongchuan, and Hekou groups in the southwestern portion of the Yangtze craton (Fig. 2A). Sparse Paleoproterozoic rocks in the Cathaysia block include ca. 1.91–1.78 Ma granitoids and the Badu supracrustal rocks (e.g., Li et al., 2014). Dated Mesoproterozoic rocks are limited to the southern margin of the Yangtze craton and the Baoban Group in Hainan Island of the Cathaysia block (Cawood et al., 2018, and references therein). Scattered Archean and Paleoproterozoic rocks of the South China block are unconformably overlain by variably deformed and metamorphosed Neoproterozoic, Paleozoic, and Mesozoic igneous and sedimentary rocks (Zhao and Cawood, 2012, and references therein).

Neoproterozoic rocks are widespread across the South China block. The Neoproterozoic assembly of the South China block was followed by the development of the Nanhua rift, which is characterized by ca. 810–730 Ma, bimodal magmatic rocks and associated intracontinental rift sedimentary sequences (e.g., Wang and Li, 2003; Wang et al., 2012c; Cao et al., 2017). Upper Neoproterozoic strata conformably overlie Precambrian sequences in the Cathaysia block and unconformably overlie strata in the Yangtze craton and Jiangnan orogen (e.g., Li et al., 2014; Wang et al., 2017c). Our compilation of Precambrian zircon U-Pb ages reflecting magmatism in the South China block (n = 1,783) shows two prominent age populations with two peaks at ca. 0.82 Ga and ca. 0.98 Ga and two minor age peaks at ca. 1.4 Ga and ca. 2.5 Ga (Fig. 2B). We performed separate statistics on the magmatic peaks of the Yangtze craton (i.e., one peak at ca. 0.8 Ga; $n = 679$), Jiangnan orogen (i.e., one peak at ca. 0.82 Ga and two minor peaks at ca. 1.78 Ga and ca. 2.5 Ga; $n = 767$), and Cathaysia block (i.e., three peaks at ca. 0.83 Ga, ca. 0.98 Ga, and ca. 1.4 Ga, and one minor peak at ca. 2.5 Ga; $n = 337$) (Fig. 2B). Our compilation of Precambrian detrital zircon U-Pb ages of the South China block (n = 6,456) shows one prominent age population with a peak at ca. 0.84 Ga and two minor age peaks at ca. 1.83 Ga and ca. 2.5 Ga. These age peaks also occur in the data for the Yangtze craton, Cathaysia block, and Jiangnan orogen (Fig. 2C).

2.3. Precambrian Tarim craton

Precambrian rocks are only exposed along the margins of the Tarim craton, including the Hetian area in the southwest, Akesu area in the northwest, Kuluketage area in the northeast, North Altyn Tagh Range and Dunhuang area in the east, and Tiekelike area in the southeast (Fig. 3A). However, samples from deep drilling wells suggest that Archean–Paleoproterozoic rocks are widespread beneath the thick sedimentary sequence of the Tarim Basin (e.g., Xu et al., 2013; Yang et al., 2018; Cai et al., 2020b). Ge et al. (2018, 2020) reported ca. 3.72 Ga, high-pressure tonalitic gneisses in the North Altyn Tagh Range, providing evidence for the existence of Eoarchean basement in the Tarim craton. Although a ca. 3.3 Ga Sm-Nd isochron age was reported in the Kuruktag area (Hu and Rogers, 1992), Paleoarchean (ca. 3.6–3.2 Ga) rocks are rare in the Tarim craton. Reported Mesoarchean (ca. 3.2–2.8 Ga) rocks include ca. 2.93 Ga dioritic gneiss (Gehrels et al., 2003a) and ca. 2.83 Ga granitic gneiss (Lu et al., 2008b) in the North Altyn Tagh Range, ca. 3.05 Ga granodioritic gneiss in the Dunhuang area, and ca. 3.2–3 Ga tonalite-trondhjemite-granodiorite (TTG) gneisses, ca. 2.81 Ga high-K granite, and a ca. 3.14 Ga hypersthene granulite in the Tiekelike area (Guo et al., 2013; Ge et al., 2022). Neoarchean (ca. 2.8–2.5 Ga) TTG, dioritic and granitic gneisses, and associated metagabbro/amphibolite are widespread and well documented in the Tarim craton, mainly in the North Altyn Tagh Range and Dunhuang and Kuruktag areas (e.g., Hu and Rogers, 1992; Lu et al., 2008b; Long et al., 2014, 2015; Zhang et al., 2014c). Archean basement rocks experienced regional, high-grade metamorphism at ca. 2–1.8 Ga and ca. 1.1–1 Ga, and local metamorphism at ca. 2.5 Ga (e.g., Zhao and Cawood, 2012).

In the Tarim craton, Paleoproterozoic basement rocks are spatially associated with Archean rocks mainly exposed in the Kuruketage and Dunhuang areas. Available geochronological data show that two distinct Paleoproterozoic magmatic events occurred at ca. 2.45–2.35 Ga and ca. 1.9 Ga (Zhang et al., 2007b; Lu et al., 2008b; Long et al., 2010; Ge et al., 2022). Early Paleoproterozoic (ca. 2.4–2.35 Ga), A-type granites are reported in the Tiekelike area (Zhang et al., 2007b; Wang et al., 2014d; Ge et al., 2022). Late Mesoproterozoic, low-grade meta-sedimentary-volcanic rocks and early Neoproterozoic, high-pressure meta-sedimentary rocks occur in the Tarim craton (Lu et al., 2008b). Middle Neoproterozoic sedimentary rocks of the Tarim craton are considered to be a key record for the Neoproterozoic Snowball Earth (Kaufman et al., 1997; Hoffman et al., 1998; Hoffmann and Schrag, 2000). Neoproterozoic (ca.

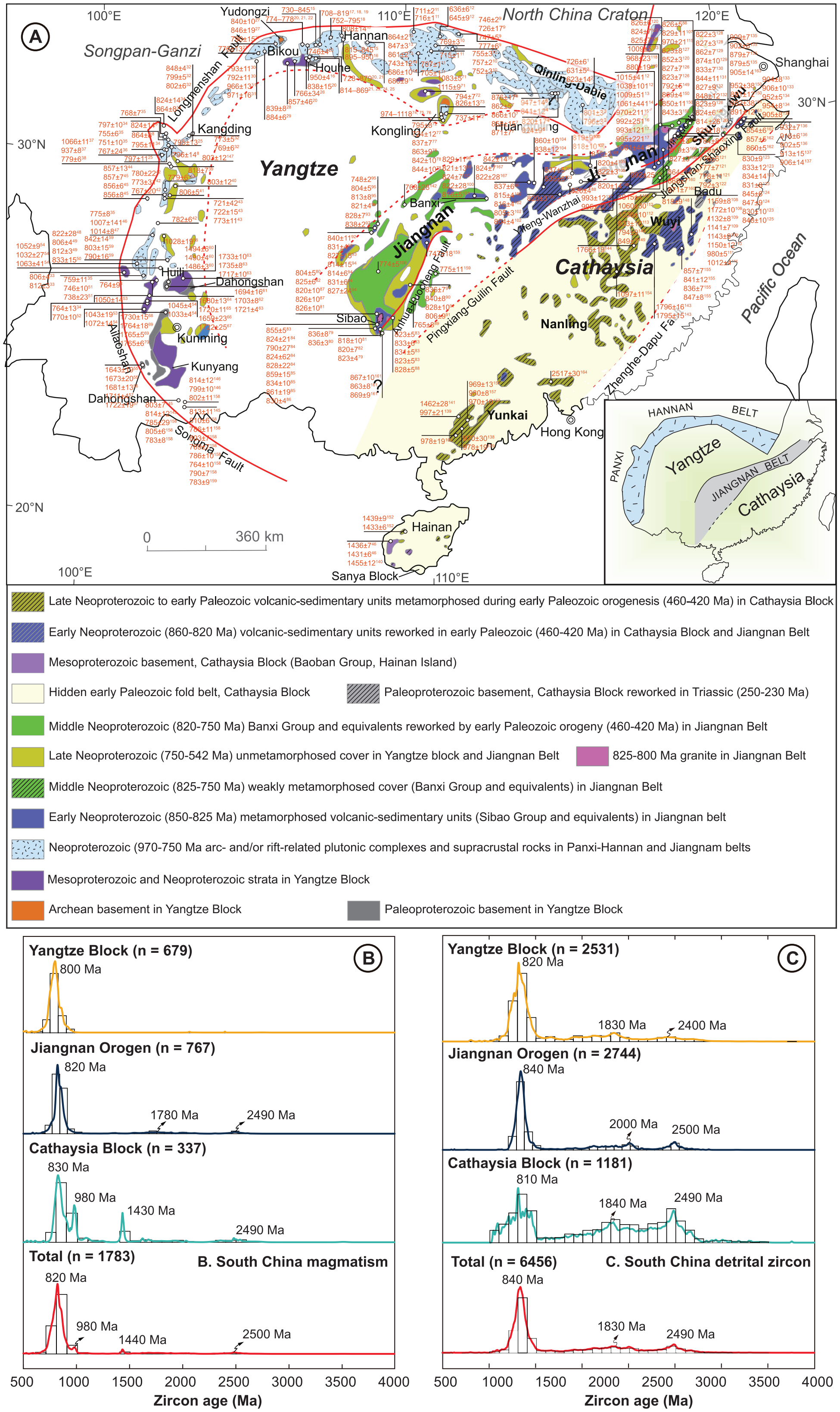

(caption on next page)

Fig. 2. (A) Simplified tectonic map of the South China block, which is divided into the Yangtze Block, Cathaysia Block, and Jiangnan orogen. The bottom shows normalized relative probability plots of Precambrian (B) magmatic records and (C) detrital zircon U-Pb ages of the total South China block, Yangtze Block, Cathaysia Block, and Jiangnan orogen. Data are compiled from: Bai et al., 2010; Cai et al., 2014, 2015, 2020a; Cao et al., 2017; Chen et al., 2016; Chen et al., 2014a, 2018; Chen et al., 2005; Chen et al., 2009a, 2009b, 2017; Chen et al., 2014b; Cui et al., 2017; Deng et al., 2012, 2017; Deng et al., 2013, 2016a, 2016b; Ding et al., 2008; Dong et al., 2011, 2012; Du et al., 2009, 2014; Fan et al., 2013; Gao et al., 2009; Gao et al., 2012, 2013, 2014; Gao and Zhang, 2009; Geng et al., 2007, 2017, 2020; Guo et al., 2007; Guo et al., 2014; Hu et al., 2017; Hu et al., 2015; Huang et al., 2008; Huang et al., 2022a; Jiang et al., 2017; Jiang et al., 2015; Jin et al., 2017; Lai et al., 2007; Li et al., 2009a; Li et al., 2013b; Li et al., 2018a; Li et al., 2013c; Li and Zhao, 2018; Li, 2010; Li et al., 2008b; Li et al., 1994, 1996, 1998, 2001a,b, 2002a, 2002b, 2003a,b, 2008c, 2009b; Li, 1999a, 1999b; Li et al., 2017; Li et al., 1999, 2002b, 2003c, 2008d; Li et al., 2005a; Lin et al., 2007; Lin, 2010; Lin et al., 2016; Ling et al., 2003, 2006, 2008; Liu et al., 2011; Liu et al., 2009; Liu et al., 2010, 2017; Liu et al., 2015; Liu et al., 2018a, 2020c; Liu et al., 2018b; Lu et al., 2019; Luo et al., 2018; Ma et al., 2009; Ma et al., 2016; Meng et al., 2015; Niu et al., 2006; Pei et al., 2009; Peng et al., 2012; Qin et al., 2006; Shi et al., 2007; Shu et al., 2008, 2011a, 2011b; Su et al., 2020; Sun et al., 2013; Sun et al., 2009; Wang et al., 2015a; Wang et al., 2012a, 2013a; Wang et al., 2018; Wang et al., 2011, 2016a, 2016b; Wang et al., 2017b; Wang et al., 2012b; Wang et al., 2006, Wang et al., 2014a; Wang et al., 2015b; Wang et al., 2013b; Wang et al., 2017c; Wang and Zhou, 2012; Wang et al., 2004, 2008a, 2012c; Wang et al., 2008b; Wang et al., 2013c, 2016c; Wei et al., 2012; Wu et al., 2005, 2006; Xia et al., 2015; Xiao et al., 2007; Xin et al., 2017; Xu et al., 2006; Xu et al., 2016; Xue et al., 2010, 2012; Yan et al., 2004; Yan et al., 2015; Yang et al., 2015; Yang et al., 2009; Yang et al., 2012; Yao et al., 2013, 2014a, 2014b, 2015, 2016a, 2016b, 2017; Ye et al., 2007; Yin et al., 2013; Yu et al., 2017a; Yu et al., 2008, 2010; Zhang et al., 2012b; Zhang et al., 2014b; Zhang et al., 2013a, 2015a; Zhang et al., 2015b; Zhang et al., 2010b; Zhang et al., 2013b, 2015c; Zhang and Wang, 2016a, 2016b; Zhang et al., 2017b; Zhang et al., 2012c; Zhang et al., 2012d; Zhao et al., 2006; Zhao and Zhou, 2007, 2009, 2013; Zhao et al., 2010, 2011, 2013a; Zhao and Zhou, 2013; Zhao et al., 2013b; Zhou et al., 2007b; Zhou et al., 2009; Zhou et al., 2011; Zhou et al., 2002a, 2002b, 2006; Zhou et al., 2007a; Zhou et al., 2020; Zhu et al., 2008a; Zhu et al., 2023; Zhuo et al., 2015.

820–780 Ma), high-pressure metamorphism may have occurred along the northern margin of the Tarim craton. Middle to late Neoproterozoic magmatism in the Kuruketage area is evidenced by ca. 820–800 Ma and ca. 780–760 Ma ultramafic–mafic rocks, ca. 740–735 Ma bimodal volcanic rocks, and minor ca. 650–635 Ma mafic dykes. Zhao and Cawood (2012) interpreted that Neoproterozoic magmatism waned since ca. 740 Ma due to the rifting of Tarim craton from the Rodinia supercontinent. Zhang et al. (2012e) argued that the middle to late Neoproterozoic magmatic rocks are related to a mantle plume event that led to the breakup of the Tarim craton from the Rodinia supercontinent.

In this study, we compiled magmatic and detrital zircon U-Pb ages for the Tarim craton (n = 3,574) (Figs. 3B and 3C). Our compilation shows the occurrence of distinct Precambrian igneous age populations with six peaks at ca. 3.65 Ga, ca. 3.15 Ga, ca. 2.46 Ga, ca. 1.85 Ga, ca. 1.4 Ga, and ca. 0.83 Ga (Fig. 3B). We conducted separate statistics on the magmatic peaks of the central (i.e., one peak at ca. 1.93 Ga; n = 83), eastern (i.e., three peaks at ca. 1.84 Ga, ca. 2 Ga, ca. 2.5 Ga; n = 1338), northeastern (i.e., Altyn Tagh Range; four peaks at ca. 0.82 Ga, ca. 0.98 Ga, ca. 1.93 Ga, ca. 2.5 Ga; n = 440), northern (i.e., five peaks at ca. 0.83 Ga, ca. 1.94 Ga, ca. 2.2 Ga, ca. 2.5 Ga, ca. 2.7 Ga; n = 765), and southeastern areas of the Tarim craton (i.e., six peaks at ca. 1.4 Ga, ca. 1.89 Ga, ca. 2.35 Ga, ca. 2.77 Ga, ca. 3.16 Ga, ca. 3.6 Ga; n = 979) (Fig. 3B). Our compilation for the Precambrian detrital zircon U-Pb ages of the Tarim craton (n = 1,504) shows two prominent age populations with peaks at ca. 0.82 Ga and ca. 1.83 Ga (Fig. 3C). The northeastern Tarim craton (i.e., Altyn Tagh Range) yields three age peaks at ca. 0.86 Ga, ca. 1.85 Ga, and ca. 2.5 Ga, whereas the southwestern Tarim craton yields four age peaks at ca. 0.82 Ga, ca. 1.4 Ga, ca. 2.1 Ga, and ca. 2.6 Ga (Fig. 3C).

2.4. Precambrian Qaidam block

The northern margin of the Qaidam block is composed of the Precambrian metamorphic basement rocks of the Quanji Massif, Cambrian shallow-marine sedimentary rocks, and Ordovician–Silurian magmatic arc rocks (e.g., Lu, 2002; Lu et al., 2002, 2006; Yin and Harrison, 2000) (Fig. 4). The geology of the southern margin of the Qaidam block is best exposed in the Eastern Kunlun Range, which is presently bounded by the Qaidam Basin in the north and active left-slip Kunlun fault in the south, the latter of which follows a Triassic suture zone (e.g., Yin and Harrison, 2000; Wu et al., 2016). Precambrian rocks of the Qaidam block are mainly exposed in the Xitie, Oulongbulak, Buhete, and southern Zongwulong mountains along the northeastern margin of the Qaidam Basin, and Eastern Kunlun Range along the southern margin of the Qaidam Basin (Fig. 3A). The oldest Precambrian basement rocks of the southern Qaidam block, exposed in the Eastern Kunlun Range, consist of ca. 1.93 Ga meta-basite, ca. 1.85 Ga meta-granite, and ca. 940–820 Ma meta-granites that are tectonically interspersed with migmatite and meta-sedimentary rocks (Tan et al., 2004; Chen et al., 2006a, 2006b; Ma et al., 2013; Wang et al., 2013d). Metamorphic basement rocks of the southern Qaidam block are intruded by Neoproterozoic mafic dikes (e.g., Ren et al., 2010).

The Quanji Massif of the northern Qaidam block is composed of medium- to high-grade metamorphic rocks of the Delingha Complex and Dakendaban Group, and low-grade, greenschist-facies Mesoproterozoic Wandonggou Group (e.g., Lu, 2002; Lu et al., 2002, 2006; Lu and Yuan, 2003; Chen et al., 2007a, 2009, 2012, 2013a, b; Wang et al., 2008c, 2009). Widespread early Paleoproterozoic granitic gneisses of the Quanji Massif include the Wulan monzogranitic and granodioritic gneisses and Delingha and Quanjishan monzogranitic gneisses (e.g., Gong et al., 2012a, 2012b). Previous studies reported the occurrence of high-grade, early Paleoproterozoic granites with enclaves of amphibolite and mafic granulite in the Delingha Complex (Lu, 2002; Huang et al., 2011; Ba et al., 2012; Gong et al., 2012a, 2012b; Liao et al., 2014). The Dakendaban Group is composed of ca. 2.32–2.2 Ga, amphibolite-facies meta-volcano-sedimentary rocks and supracrustal metapelites with ca. 2.2–1.96 Ga protolith ages (Lu, 2002; Huang et al., 2011; Chen et al., 2012). The Delingha Complex and Dakendaban Group underwent amphibolite-facies and locally granulite-facies metamorphism at ca. 1.95–1.91 Ga (Zhang et al., 2001; Wang et al., 2009; Chen et al., 2013b). This metamorphism was followed by lower pressure-temperature, amphibolite-facies metamorphism at ca. 1.82–1.8 Ga (Chen et al., 2013b). These rocks are intruded by ca. 1.83 Ga mafic dykes and ca. 1.8–1.77 Ga rapakivi granite (Lu et al., 2006; Chen et al., 2012, 2013a; Liao et al., 2014).

The Late Mesoproterozoic Wandonggou Group consists of greenschist-facies, carbonate meta-sedimentary rocks with minor mafic metavolcanics that were deposited after emplacement of ca. 1.8 Ga rapakivi granite but prior to a ca. 1 Ga low-grade metamorphic event (Yu et al., 1994; Lu et al., 2006, 2008b). The Neoproterozoic, diamictite-bearing Quanji Group and unconformably overlying Paleozoic strata were both deposited unconformably atop Paleoproterozoic metamorphic basement rocks (Lu, 2002; Lu et al., 2008a, 2008b). The Quanji Group is the oldest sedimentary sequence overlying the Precambrian basement rocks of the northern Qaidam block (Wang et al., 2013a) and is considered to have been deposited during the Ediacaran, postdating the Gaskiers glaciation (Shen et al., 2010). However, Zhang et al. (2016) argued that the Quanji Group was deposited between the Late Paleoproterozoic and Neoproterozoic based on the occurrence of ca. 1.64 Ga tuff within the lower Hongzaoshan Formation of the Quanji Group. Our compilation of magmatic zircon U-Pb ages for the Qaidam block (n = 874) shows the occurrence of distinct Precambrian igneous age populations with six peaks at ca. 2.4 Ga, ca. 1.98 Ga, ca. 1.5 Ga, ca. 1.1 Ga, ca. 0.95 Ga, and ca. 0.75 Ga (Fig. 3B). A compilation of Precambrian

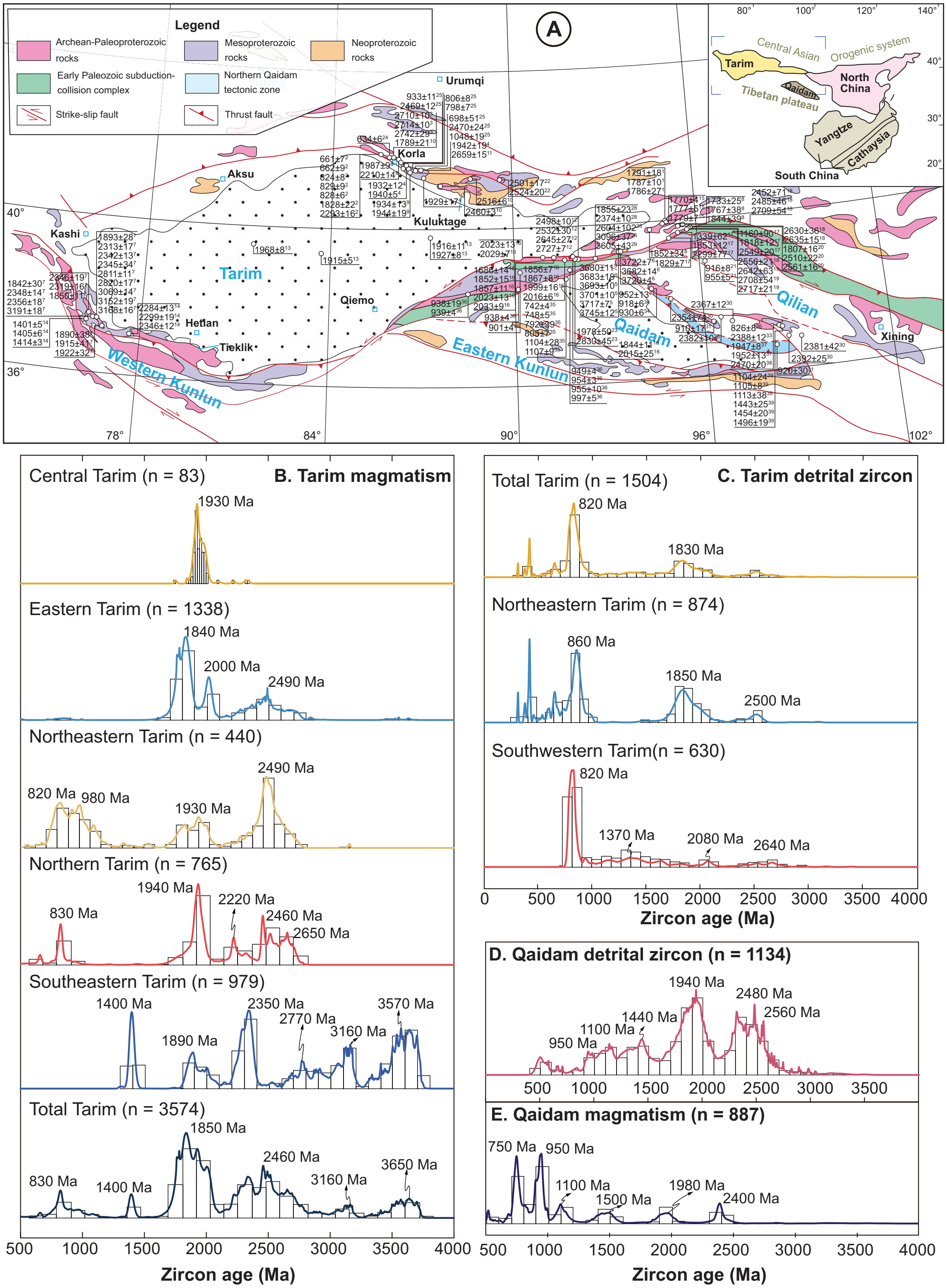

Fig. 3. (A) Simplified tectonic map of the Tarim craton and Qaidam block. The bottom shows normalized relative probability plots of Precambrian (B) magmatic records and (C) detrital zircon U-Pb ages of the Tarim craton. The bottom right shows normalized relative probability plots of Precambrian (D) magmatic records and (E) detrital zircon U-Pb ages of the Qaidam block. Data for the Tarim craton are compiled from: Cai et al., 2018, 2020b; Chen et al., 2022; Cheng et al., 2017a; Ding et al., 2015; Gan et al., 2020; Ge et al., 2013, 2014, 2015, 2018, 2020, 2022; Guo et al., 2013; He et al., 2021; He et al., 2013; Jiang et al., 2005; Lei et al., 2012; Li et al., 2001c; Long et al., 2010, 2011, 2014, 2019; Lu et al., 2008a; Lu and Yuan, 2003; Wang et al., 2020; Wu et al., 2014; Xie et al., 2023; Yang et al., 2018; Ye et al., 2013; Ye et al., 2016; Yu et al., 2014; Zhang et al., 2018; Zhang et al., 2009, 2012e, 2012f, 2014c; Zhang et al., 2013c; Zhao et al., 2015, 2019; Zhu et al., 2011; Zong et al., 2013. Data for the Qaidam block are compiled from: Chen et al., 2007a, 2009c; Cheng et al., 2017b; Fu et al., 2015; Gong et al., 2012b, 2014, 2019; Hao et al., 2022; Li et al., 2007; Li et al., 2022; Sun et al., 2018, 2019; Teng et al., 2022; Wang et al., 2015c, 2019b; Wang et al., 2021; Xia et al., 2009; Yu et al., 2017b; Zhang et al., 2003; Zhang et al., 2012f.

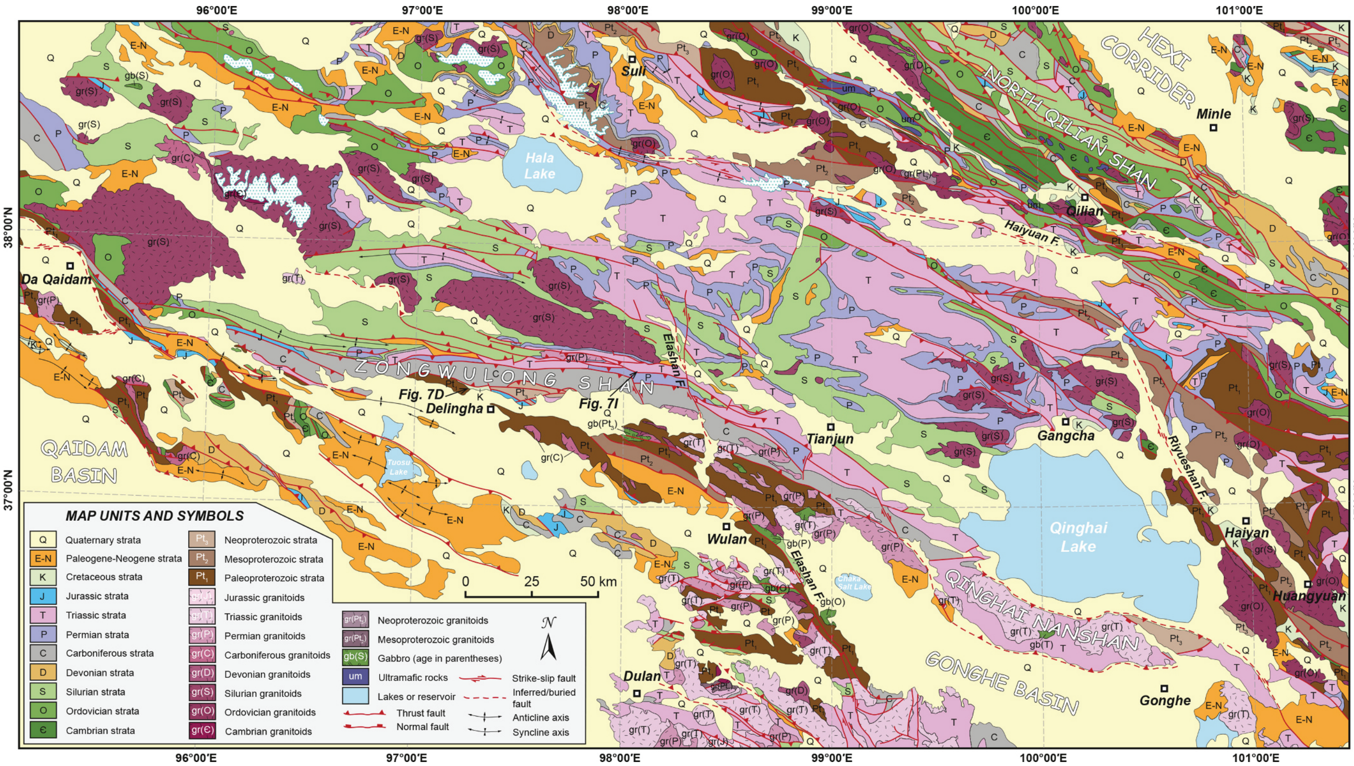

Fig. 4. Geological map of the northern Qaidam block and surrounding region of northern Tibet. Map is compiled from Pan et al. (2004) and this study.

detrital zircon U-Pb ages of the Qaidam block (n = 1,134) shows five prominent age populations with peaks at ca. 0.95 Ga, ca. 1.1 Ga, ca. 1.45 Ga, ca. 1.94 Ga, and ca. 2.5 Ga (Fig. 3C).

3. Field observations and sampling of the Precambrian Northern Qaidam block

We performed geological mapping and collected field observations in the northern Qaidam Basin with the goal of constraining the Precambrian metamorphic and magmatic evolution of the Qaidam block and northern Tibet (Fig. 4). Precambrian and early Paleozoic metamorphic rocks and foliated/undeformed granitoid plutons are widespread in the field area. Previous researchers grouped these rocks as part of the Paleoproterozoic metamorphic basement complex (Fig. 4). However, we were able to distinguish lithologic units of the metamorphic basement complex based on field observations and geochronology results. We divide the metamorphic basement complex into four lithologic units: (1) Paleoproterozoic (labeled Pt_1 in Fig. 5); (2) Mesoproterozoic (labeled Pt_2 in Fig. 5); (3) Neoproterozoic (labeled Pt_3 in Fig. 5); and (4) intrusions (labeled gr_{pz} and gr_{gb} in Fig. 5). Both the

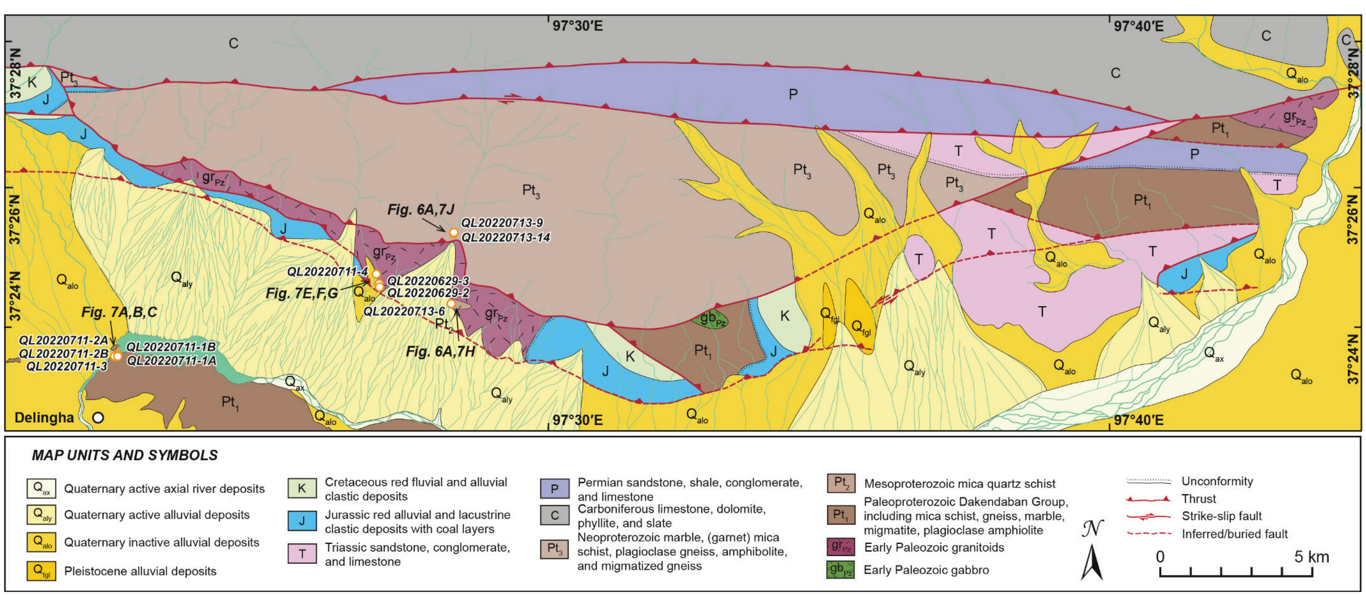

Fig. 5. Geological map of the southern edge of the Zongwulong Shan, northeast of Delingha city, in the northern Qaidam block. Map is based on Qinghai BGMR (1978) and this study. White lines are topographic contours in meters. Sample locations are shown.

Paleoproterozoic metamorphic basement rocks and Neoproterozoic metamorphic rocks experienced early Paleozoic amphibolite-facies metamorphism and were intruded by early Paleozoic plutonic rocks. In contrast, the late Paleoproterozoic meta-mafic dikes intrude early Paleoproterozoic gneiss (Fig. 5). Age assignments of the major lithologic units are primarily based on observations from Pan et al. (2004) and Wang et al. (2013e).

Paleoproterozoic, medium- to high-grade metamorphic basement rocks (i.e., Delingha Complex and Dakendaban Group) are widespread in the northern Qaidam Basin and divided into three lithologic units from older to younger: (1) gneiss; (2) metavolcanic; and (3) schist. The gneiss unit is composed of quartzo-feldspathic gneiss, mylonitic biotite

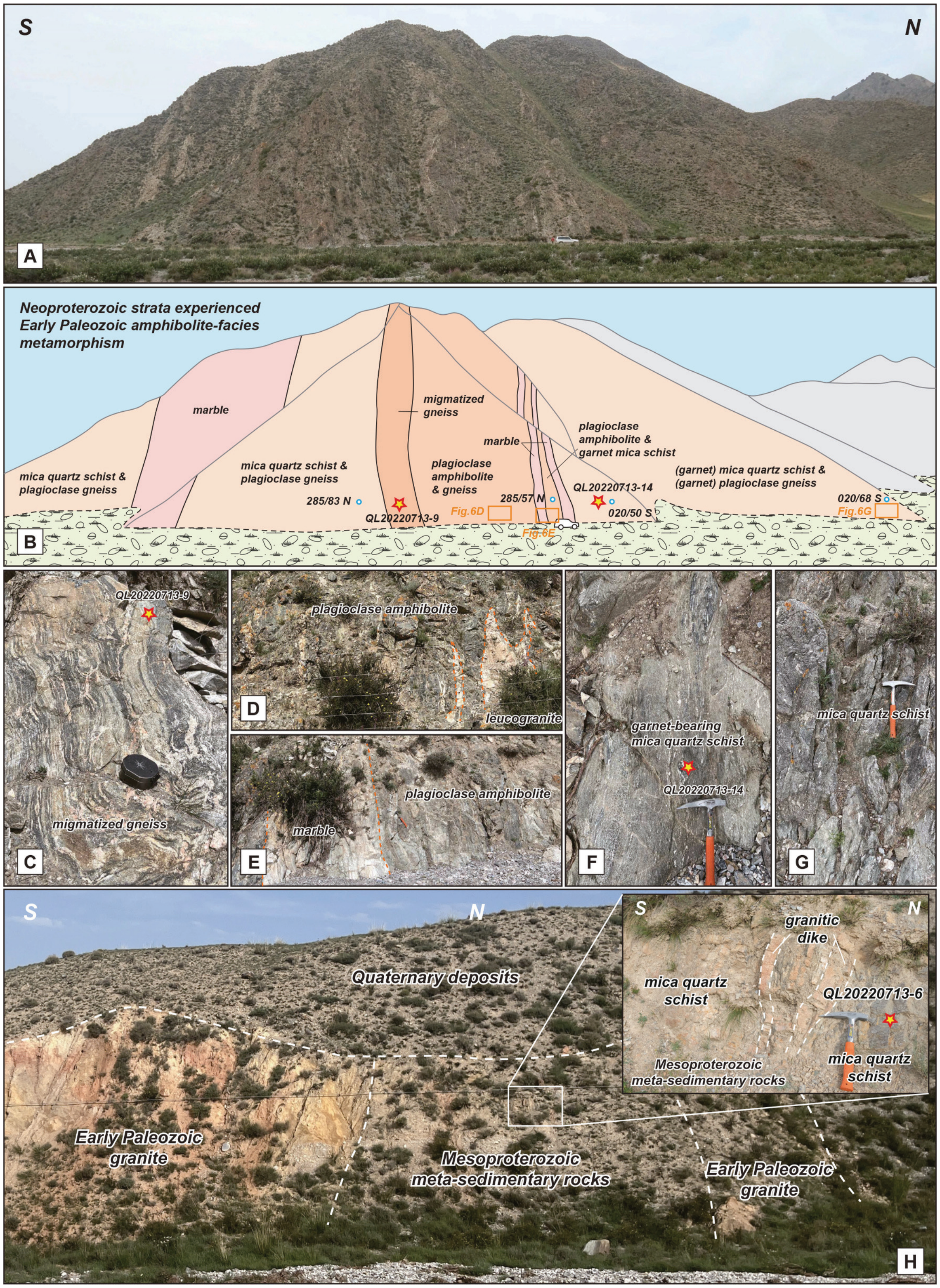

Fig. 6. Field photographs of (A) representative Neoproterozoic rock assemblages and structures and (B) Mesoproterozoic metasedimentary rocks and early Paleozoic magmatic intrusions. Note that the format of bedding and foliation attitude is strike/dip and dip quadrant.

orthogneiss, garnet-bearing syenogranite, and paragneiss. The protoliths of these rocks are inferred to be Paleoproterozoic in age based on previous geological maps (Pan et al., 2004). Mafic and leucogranite dikes occur within the gneiss unit. The metavolcanic unit consists of meta-mafic rocks and garnet amphibolite. The schist unit is characterized by mica ± garnet schist, quartzite, marble, and local phyllite. Late Mesoproterozoic meta-sedimentary rocks and Neoproterozoic sedimentary rocks are scattered in the field area. The weakly foliated, amphibolite-facies metamorphic basement rocks are intruded by early Paleozoic granitoids. The oldest unconformity in the field area, which is also widespread along the northern margin of the Qaidam block, occurs between the overlying Neoproterozoic Quanji Group and underlying Paleoproterozoic metamorphic basement rocks and local Mesoproterozoic rocks. Sedimentary bedding and metamorphic foliation generally trend northwest-southeast or north-south, parallel to the trends of mountain ranges and strikes of thrust faults.

Mesoproterozoic metasedimentary rocks exposed in the southern Zongwulong Shan consist of mica quartz schist surrounded and intruded by voluminous early Paleozoic granitoids (Figs. 5 and 6A). In the southern Zongwulong Shan, northeast of Delingha city, Neoproterozoic rocks are thrust atop Paleo- and Mesoproterozoic metamorphic rocks as a result of multiple deformation episodes. These Neoproterozoic rocks are intruded by early Paleozoic granitoids (Fig. 6B). In the north, Carboniferous and Permian sedimentary rocks were deposited atop the Precambrian rocks and the Precambrian rocks are thrust over the Permian–Cretaceous strata (Fig. 5). Neoproterozoic metamorphic rocks consist of well-layered garnet mica quartz schist, garnet plagioclase gneiss, marble, plagioclase amphibolite, and migmatitic gneiss (Fig. 6B). The observed younger-over-older stratigraphic relationships and shallow crustal intrusions suggest that the Zongwulong Shan experienced several tectonic events since the late Paleozoic (Fig. 5). These metamorphic rocks are intruded by undeformed, late Paleozoic leucogranite dikes (Fig. 6B). Field observations suggest that Neoproterozoic rocks exposed along the southern Zongwulong Shan are a suite of supracrustal sedimentary rocks that experienced early Paleozoic, amphibolite-facies metamorphism.

We collected and dated major Precambrian lithologic units of the northern Qaidam block, which consist of porphyritic gneiss, meta-mafic dikes, schist, meta-sandstone, quartzite, granitoid, and hornblende gabbro dikes (Fig. 7). Paleoproterozoic pink-red foliated granitic gneiss (i.e., samples QL20220711-2A, QL20220711-2B, QL20220711-3, and QL20220703-3) are intruded by ~3–5-m-wide, late Paleoproterozoic meta-mafic dikes (i.e., samples QL20220711-1A and QL20220711-1B) (Figs. 7A–D). Along the southern edge of the Zongwulong Shan, Paleoproterozoic gneiss is intruded by late Paleoproterozoic–Mesoproterozoic granitic dikes (i.e., samples QL20220629-2, QL20220629-3, and QL20220711-4) (Figs. 7E–G). Mesoproterozoic mica quartz schist sample QL20220713-6 is intruded by late Paleozoic granitic dikes (Fig. 7H). We also collected garnet-bearing mica quartz schist sample QL20220713-14 from the southern Zongwulong Shan and meta-sandstone sample QL20220701-5 from the core of the Zongwulong Shan (Figs. 7I–J). Mineral compositions and microscopic characteristics of these samples are shown in Fig. 8.

4. Analytical methods and results

A total of twelve Precambrian samples from the Qaidam block were analyzed via zircon U-Pb geochronology in this study. These samples include four early Paleoproterozoic gneiss samples, two late Paleoproterozoic meta-mafic dike samples, three Paleoproterozoic and Mesoproterozoic gneissic granitoid samples, one Mesoproterozoic schist sample, and two Neoproterozoic metasedimentary rocks samples. In addition, a total of eight samples from the Qaidam block were analyzed for their whole-rock, major-oxide, and trace-element geochemistry and Lu-Hf and Sr-Nd isotopes. These samples include four Paleoproterozoic gneiss samples, two late Paleoproterozoic meta-mafic dike samples, three Paleoproterozoic and Mesoproterozoic gneissic granitoid samples.

4.1. Zircon U–Pb geochronology and Hf isotopic compositions

Zircon grains used for U-Pb geochronology were separated from thirteen samples using traditional methods involving crushing, sieving, and magnetic and density separations. Individual zircon grains were picked under a binocular microscope and mounted in epoxy with standard zircon grains. Cathodoluminescence images of zircon grains were collected using a JXA-880 electron microscope with operating conditions of 20 kV and 20 nA at the Institute of Mineral Resources, Chinese Academy of Geological Sciences, Beijing.

Zircon grains were analyzed via inductively coupled plasma mass spectrometry (ICP-MS) using an Agilent 7500a instrument coupled with a New Wave Research UP193FX Excimer Laser Ablation System at the State Key Laboratory of Tibetan Plateau Earth System, Environment and Resources, Institute of Tibetan Plateau Research, Chinese Academy of Sciences, Beijing. Common Pb corrections were performed assuming an initial Pb composition from Stacey and Kramers (1975). The primary standard used was GJ1 (Jackson et al., 2004). Secondary standards included 91500 (^{238}U/^{206}Pb age of ca. 1,065 Ma; Wiedenbeck et al., 1995) and Plesovice (^{238}U/^{206}Pb age of ca. 337 Ma; Sláma et al., 2008). Reported U-Pb ages are ^{206}Pb*/^{207}Pb* ages for grains older than 1,000 Ma. Crystallization ages are interpreted from analyses with <10% discordance. Concordia diagrams and weighted mean U-Pb ages were processed using Isoplot v.3 (Ludwig, 2003). Age data and concordia plots are reported with 2σ error (Fig. 9). Uncertainties of weighted mean ages are presented at the 95% confidence level (Andersen, 2002). Sample locations and results of zircon U-Pb geochronology are shown in Table 1. Details of geochronology analyses are shown in the Supplementary Table S1.

Zircon Hf isotopes were measured in situ on a Nu Plasma II multi-collector inductively coupled plasma mass spectrometer (MC-ICP-MS, Nu Instruments Ltd., United Kingdom), which is coupled to a 193-nm New Wave laser ablation system. A beam diameter of ca. 45 μm, a 6-Hz repetition rate, and an energy density of 11.6 J/cm^2 were used during the analyses. Each measurement consists of a 10-sec pre-ablation, a 45-sec ablation, and a 30-sec washout delay. Hf isotopes were calculated using Iolite V4 (University of Melbourne). The measured Hf isotopic values are 0.282302 ± 19 for 91500, 0.281998 ± 15 for GJ-1, and 0.282475 ± 11 for Plesovice, consistent with recommended values. Details of zircon Lu-Hf isotope analyses are shown in Supplementary Table S2.

More than thirty zircon grains for each of the four granitic gneiss samples yield weighted mean Pb-Pb ages of 2,345 ± 32 Ma (MSWD = 0.64; n = 34; sample QL20220711-2A), 2,448 ± 24 Ma (MSWD = 0.49; n = 13; sample QL20220711-2B), 2,344 ± 50 Ma (MSWD = 0.052; n = 30; sample QL20220711-3), and 2,353 ± 14 Ma (MSWD = 0.13; n = 15; sample QL20220703-3) (Figs. 9A–9D). Zircon grains for these early Paleoproterozoic granitic gneiss samples have ε_{Hf}(t) values of +0.2 to +7.5 (T_{DM} = 2,753–2,515 Ma, T_{DMC} = 2,924–2,532 Ma) (Fig. 10).

Thirty zircon grains were analyzed from each of the two meta-mafic (meta-gabbro) dike samples (i.e., QL20220711-1A and QL20220711-1B) (Figs. 9E–9F). Sample QL20220711-1A yields ages ranging from ca. 826 Ma (U-Pb) to ca. 1,879 Ma (Pb-Pb). For this sample, the weighted mean U-Pb age of twenty-seven concordant analyses is 1,841 ± 38 Ma (MSWD = 0.061) (Fig. 9E). Sample QL20220711-1B yields ages ranging from a U-Pb age of ca. 268 Ma (U-Pb) to ca. 2,356 Ma (Pb-Pb). For this sample, the weighted mean U-Pb age of twenty-five concordant analyses is 1,862 ± 40 Ma (MSWD = 0.24) (Fig. 9F). The other analyses were excluded because of discordance or low radiogenic Pb. Zircon grains for these two Paleoproterozoic gabbro samples have ε_{Hf}(t) values of +0.44 to +9.79 (T_{DM} = 2,439–1,884 Ma, T_{DMC} = 2,438–1,884 Ma) (Fig. 10).

Late Paleoproterozoic granite dike sample QL20220629-3 yields Pb-Pb ages ranging from ca. 1,953–1,462 Ma. For this sample, the weighted mean Pb-Pb age is 1,746 ± 19 Ma (MSWD = 1.2; n = 7) (Fig. 9G). Zircon

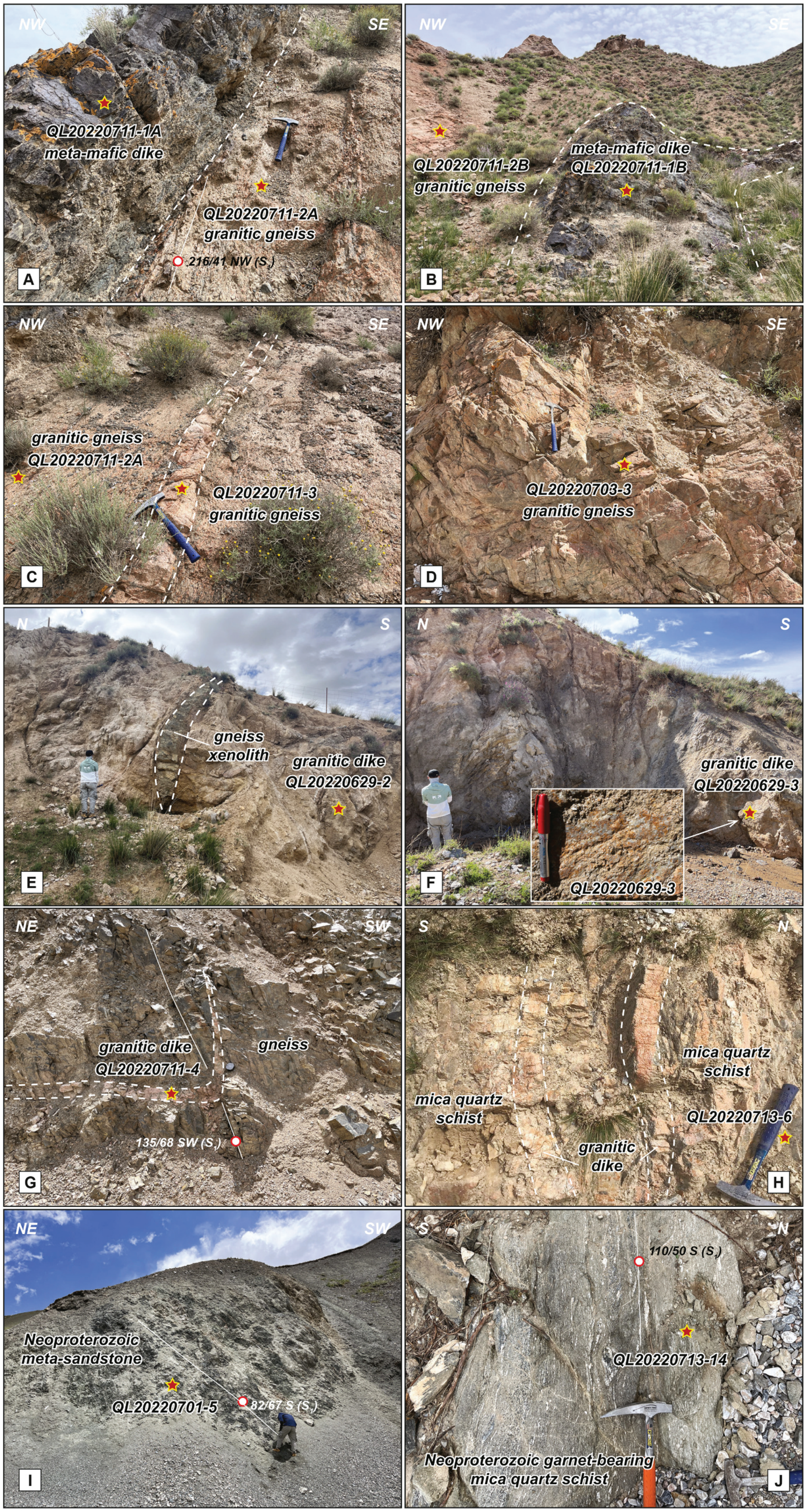

(caption on next page)

Fig. 7. Field photographs from the northern Qaidam block showing sampled Precambrian rocks. (A–D) Paleoproterozoic granitic gneiss (samples QL20220711-2A, QL20220711-2B, QL20220711-3, and QL20220703-3) is intruded by late Paleoproterozoic meta-mafic dikes (samples QL20220711-1A and QL20220711-1B). An early Mesoproterozoic granitic dike (sample QL20220629-2) contains (E) a Paleoproterozoic gneiss xenolith and (F) late Paleoproterozoic granitic dike (sample QL20220629-3). (G) A pink Mesoproterozoic granitic dike (sample QL20220711-4) intrudes Paleoproterozoic gneiss. (H) Mesoproterozoic metasedimentary rocks (sample QL20220713-6) are intruded by Paleozoic granitic dikes. (I) Neoproterozoic metasandstone (sample QL20220701-5) exposed in the core of the Zongwulong Shan. (J) Neoproterozoic garnet-bearing mica quartz schist (sample QL20220713-14) exposed along the southern edge of the Zongwulong Shan. Note that the format of bedding and foliation attitude is strike/dip and dip quadrant.

grains from this sample have $\varepsilon_{Hf}(t)$ values of -3.78 to +6.67 at 1,746 Ma (T_{DM} = 2,299–1,945 Ma, T_{DMC} = 2,638–2,037 Ma) (Fig. 10). Early Mesoproterozoic granite dike sample QL20220629-2 yields a weighted mean Pb-Pb age of 1,506 ± 24 Ma (MSWD = 1.4; *n* = 9) (Fig. 9H). Zircon grains from this sample have $\varepsilon_{Hf}(t)$ values of +0.81 to +7.06 at 1,506 Ma (T_{DM} = 1,993–1,767 Ma, T_{DMC} = 2,217–1,904 Ma) (Fig. 10). Mesoproterozoic granite dike sample QL20220711-4 yields a weighted mean Pb-Pb age of 1,349 ± 24 Ma (MSWD = 1.8; *n* = 6) (Fig. 9I). Zircon grains from this sample have $\varepsilon_{Hf}(t)$ values of +0.12 to +6.14 at 1,349 Ma (T_{DM} = 1,847–1,564 Ma, T_{DMC} = 2,116–1,705 Ma) (Fig. 10). Early Paleozoic migmatite vein sample QL20220713-9 yields ages ranging from ca. 435 Ma to ca. 710 Ma. For this sample, the weighted mean U-Pb age of concordant analyses is 506 ± 6 Ma (MSWD = 0.39; n=25) (Fig. 9J).

Mica quartz schist sample QL20220713-6 has detrital zircon age populations of ca. 1,900–1,400 Ma and ca. 2,676–2,275 Ma, with two prominent peaks at ca. 1,740 Ma and ca. 2,500 Ma, respectively (Fig. 9K). The youngest zircons grains of this sample overlap in age and have a weighted mean age of 1,367 ± 16 Ma (MSWD = 0.002; *n* = 5) (Fig. 9K), which we interpret to be the maximum depositional age for the protolith of the schist. The single youngest zircon age of the sample is ca. 1,277 Ma (Supplementary Table S1).

One hundred zircon grains were dated for each of the two Neoproterozoic metamorphic rock samples, including meta-sandstone sample QL20220701-5 and mica quartz schist sample QL20220713-14 (Figs. 9L–9M). Sample QL20220701-5 has zircon age populations between ca. 809–721 Ma and ca. 1,995–1,738 Ma, with two prominent peaks at ca. 758 Ma and ca. 1,845 Ma, respectively (Fig. 9L). Two minor age populations are ca. 2,791–2,721 Ma and ca. 2,226–2,060 Ma. The three youngest zircon grains of this sample with overlapping ages have a weighted mean age of 725 ± 20 Ma (MSWD = 0.062) (Fig. 9M). Sample QL20220713-14 has a zircon age population between ca. 995–603 Ma, with a peak at ca. 840 Ma (Fig. 9M). This sample also yields some Archean zircon ages (Fig. 9M). The three youngest zircon grains of this sample with overlapping ages have a weighted mean age of 634 ± 53 Ma (MSWD = 0.31) (Fig. 9M).

4.2. *Whole-rock major-oxide, trace-element, and Sr-Nd isotope geochemistry*

A total of eight Precambrian granitoid, granitic gneiss, and mafic dike samples were analyzed for their whole-rock major oxide, trace element, and Sr-Nd isotope compositions at the Wuhan Sample Solution Analytical Technology Co., Ltd. in Hubei, China. Prior to analysis, weathered surfaces were removed from whole-rock samples. Samples were then crushed and ground into powder (>200 mesh) using a ball mill. Major element compositions were determined via X-ray fluorescence spectrometry, which has an analytical precision of better than 2%. Trace element compositions were measured via ICP-MS, which has an analytical precision of better than 5%. Sr-Nd isotopes were measured using a Neptune Plus multi-collector ICP-MS with spectral analysis accuracy better than 0.002%. Before isotope analysis, sample dissolution was performed using acid digestion ($HF + HClO_4 + HNO_3$). Background isotope measurements were conducted within the error range. Aliquots of NIST SRM 987, JNDI-1, and JMC international standard solutions were regularly used to evaluate the reproducibility and accuracy of the instrument. Analytical results of standard sample BCR-2 (basalt) are $^{143}Nd/^{144}Nd$ = 0.512641 ± 11 (2 standard deviation) and $^{87}Sr/^{86}Sr$ = 0.705012 ± 22 (2 standard deviation) (Zhang and Hu, 2020). Data reduction for analyses of Sr isotope ratios was conducted using Iso-Compass software (Zhang and Hu, 2020). Whole-rock geochemical and Sr-Nd isotopic results are presented in Supplementary Tables S3–S4, respectively.

Three early Paleoproterozoic (ca. 2,448–2,344 Ma) granitic gneiss samples (i.e., QL20220711-2A, QL20220711-2B, QL20220711-3) have SiO_2 of 68.5–76.2 wt% and $K_2O + Na_2O$ of 8.5–9.1 wt%. The samples are classified as granite and monzonite on the $K_2O + Na_2O$ versus SiO_2 plot (Middlemost, 1994) (Fig. 11A). On the K_2O versus SiO_2 diagram (Le Maitre et al., 1989; Rickwood, 1989), the samples plot in the high-potassium calc-alkaline series field (Le Maitre et al., 1989; Rickwood, 1989) (Fig. 11B). The samples are slightly metaluminous, as indicated by their molar A/CNK of 1–0.97 and A/NK of 1.23–1.1 (Maniar and Piccoli, 1989) (Fig. 11C). On primitive mantle-normalized spider diagrams, the samples are enriched in large-ion lithophile elements (LILES), depleted in high-field strength elements (HFSEs) (Fig. 11D), and display no distinct Ce anomalies (Fig. 11D). Chondrite-normalized rare-earth element (REE) patterns are characterized by significant light rare earth element (LREE) enrichment and heavy rare-earth element (HREE) depletion, with a strong negative Eu (Eu/Eu* = 0.57–0.59) anomaly (Fig. 11E).

Late Paleoproterozoic granite dike sample QL20220629-3 (ca. 1,736 Ma) has SiO_2 of 72.4 wt% and $K_2O + Na_2O$ of 6.3 wt%. The sample is peraluminous, as indicated by its molar A/CNK of 1.3 and A/NK of 1.6 (Maniar and Piccoli, 1989) (Figs. 11A and 11C). The sample plots in the high K calc-alkaline series field (Le Maitre et al., 1989; Rickwood, 1989) (Fig. 11B). The chondrite-normalized REE pattern is characterized by LREE enrichment and slightly flat HREE slopes, with a significant negative Eu (Eu/Eu* = 0.74) anomaly and high $(La/Yb)_N$ ratio of 8 (Fig. 11E).

Mesoproterozoic granitoid dike sample QL20220711-4 (ca. 1,349 Ma) has SiO_2 of 67.75 wt% and a relatively higher Al_2O_3 of 17.14 wt% and $K_2O + Na_2O$ of 7.81 wt%. The sample is peraluminous, as indicated by its molar A/CNK of 2.85 and A/NK of 3.07 (Maniar and Piccoli, 1989) (Figs. 11A and 11C). The sample falls in the shoshonitic series field (Le Maitre et al., 1989; Rickwood, 1989) (Fig. 11B). The chondrite-normalized REE pattern of the sample is characterized by significant LREE enrichment and HREE depletion, with a strong negative Eu (Eu/Eu* = 0.55) anomaly and high $(La/Yb)_N$ ratio of 9.87 (Fig. 11E). On the primitive mantle-normalized spider diagram, the sample is enriched in LILE and depleted in HFSEs and REEs, without distinct Ce anomalies (Fig. 11D). The sample shares common trace element geochemistry of A-type granitoids (Figs. 11F–11H), specifically high Ga, Zn, Zr, Nb, and Y, and low Ba and Sr, with some variation in Rb (e.g., Collins et al., 1982; Whalen et al., 1987).

Early Mesoproterozoic granitoid dike sample QL20220629-2 (ca. 1,506 Ma) has SiO_2 of 74.82 wt%, $K_2O + Na_2O$ of 7.81 wt%, and low P_2O_5 concentrations. The sample is peraluminous as indicated by its molar A/CNK of 1.13 and A/NK of 1.34 (Maniar and Piccoli, 1989) (Figs. 11A and 11C). The sample plots in the field of the high K calc-alkaline series (Le Maitre et al., 1989; Rickwood, 1989) (Fig. 11B). The chondrite-normalized REE pattern of the sample is characterized by LREE enrichment and slight flat HREE slopes, with a significant negative Eu (Eu/Eu* = 0.51) anomaly and high $(La/Yb)_N$ ratio of 11.26 (Fig. 11E). On the primitive mantle-normalized spider diagram, the sample is enriched in LILEs and slightly depleted in HFSEs (Fig. 11D), suggesting a possible I-type protolith (Figs. 11F–11H). Negative Eu, Sr, Nb, Ta, and Ti anomalies suggest that plagioclase and rutile occurred as

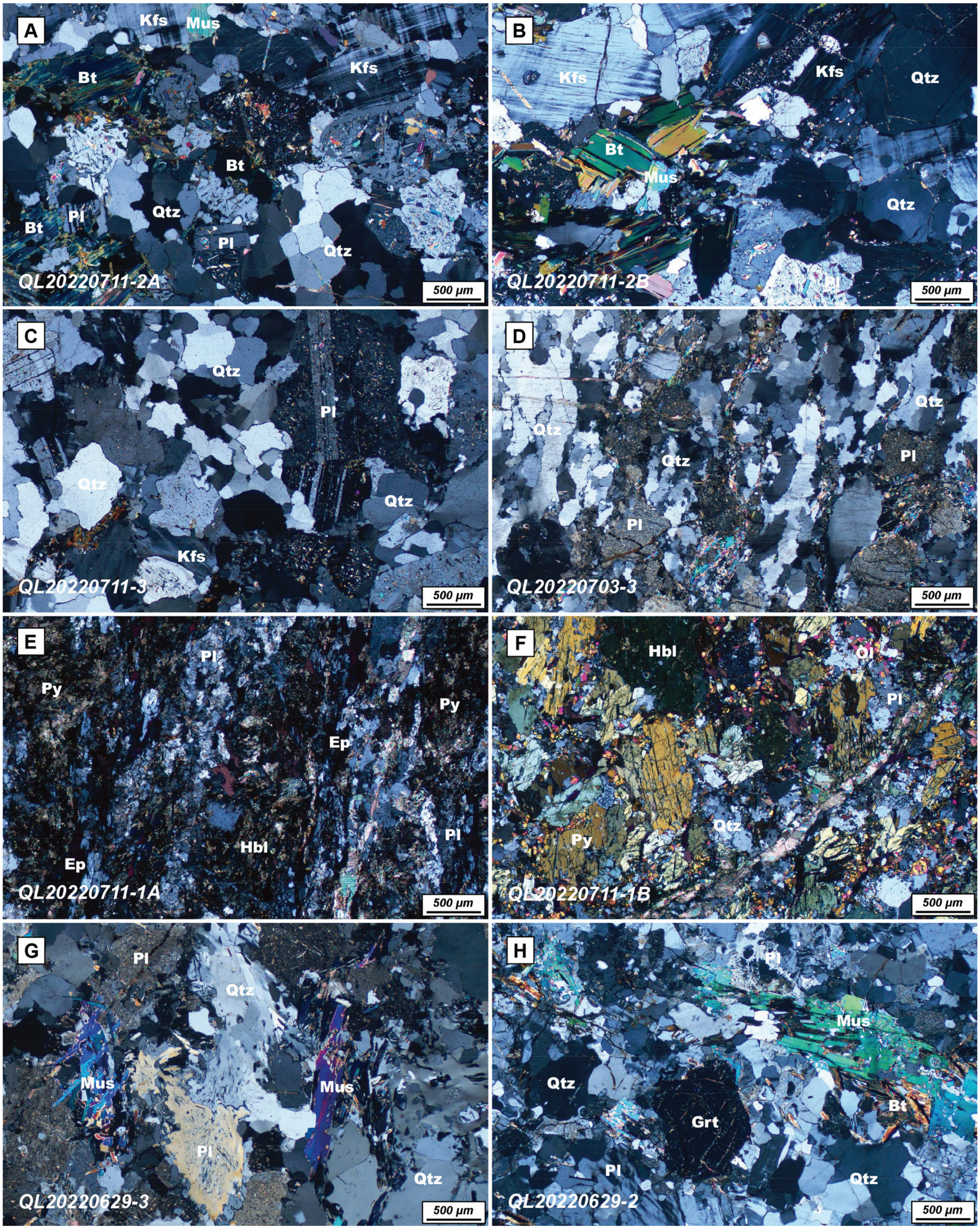

Fig. 8. Microphotographs of representative samples collected in this study.

residual phases in the source. As such, the precursor magma was likely produced by dehydration melting in a predominantly lower crustal setting under relatively low pressures.

Two late Paleoproterozoic gabbro dike samples QL20220711-1A and QL20220711-1B (ca. 1,862–1,841 Ma) have SiO_2 of 46.3–49.0 wt%, high MgO of 5.5–6.8 wt%, and Ni of 71.5–84.3 ppm. The samples are

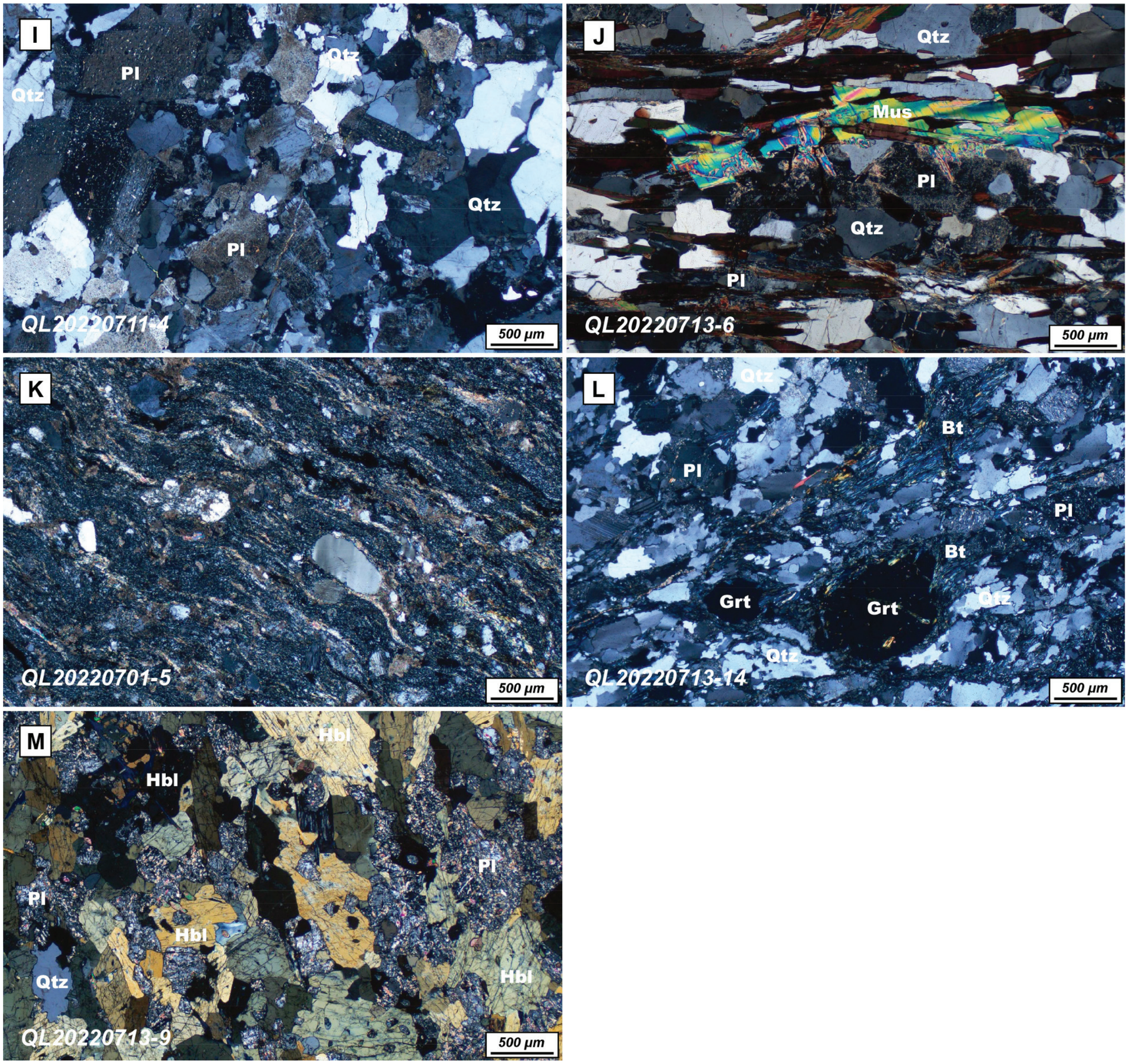

Fig. 8. (*continued*).

metaluminous, as indicated by their molar A/CNK of 0.59–0.77 and A/NK of 2.02–2.46 (Maniar and Piccoli, 1989) (Figs. 11A and 11C). Chondrite-normalized REE patterns of the samples are characterized by slight LREE enrichment (La_N/Yb_N = 2.10–2.41) and flat HREE slopes with no obvious Eu anomaly (Eu/Eu* = 0.91–1) (Fig. 11E). On primitive mantle-normalized spider diagrams, the samples are enriched in LILES (e.g., U and K) and depleted in HFSEs (e.g., Nb and Ta) (Fig. 11E).

Three granitic gneiss samples QL20220711-2A, QL20220711-2B, QL20220711-3 (ca. 2,344–2,335 Ma) have consistent lower initial $^{87}Sr/^{86}Sr$ ratios of 0.702914–0.688088 and $\varepsilon_{Nd}(t)$ values of 1.85 to 3.14 (Fig. 11I). Two meta-gabbro samples QL20220711-1A and QL20220711-1B (ca. 1,862–1,841 Ma) have consistent lower initial $^{87}Sr/^{86}Sr$ ratios of 0.706941–0.694602 and $\varepsilon_{Nd}(t)$ values of 0.63–0.64 (Fig. 11I). In contrast, granite dike sample QL20220629-3 (ca. 1,746 Ma) has higher initial $^{87}Sr/^{86}Sr$ ratios of 0.741077 and $\varepsilon_{Nd}(t)$ values of 2.09 (Fig. 11I). Granitoid sample QL20220629-2 (ca. 1,506 Ma) has initial $^{87}Sr/^{86}Sr$ ratios of 0.696976 and $\varepsilon_{Nd}(t)$ values of -3.67 (Fig. 11I), whereas granitoid sample QL20220711-4 (ca. 1,349 Ma) has anomalous Rb/Sr ratio with no usual $^{87}Sr/^{86}Sr$ analyze and $\varepsilon_{Nd}(t)$ values of -11.42 (Fig. 11I). Our study shows that the whole rock Nd-Hf isotopes of these samples yield linear trends in Nd-Hf space that mostly overlap with the terrestrial array (Fig. 11J).

5. Discussion

5.1. *Precambrian magmatism of the Qaidam block*

Zircon Pb-Pb ages of Precambrian granitoid samples from the northern Qaidam block fall into six main age groups (Fig. 3E): (1) an early Paleoproterozoic group with a ca. 2.4 Ga peak; (2) a late Paleoproterozoic group with a ca. 1.98 Ga peak; (3) an early Mesoproterozoic group with a ca. 1.5 Ga peak; (4) a late Mesoproterozoic group with a ca. 1.1 Ga peak; (5) an early Neoproterozoic group with a ca. 0.95 Ga peak; and (6) a middle Neoproterozoic group with a ca. 0.75 Ga peak. Contemporary debate regarding the evolution of the Qaidam block has focused on the tectonic settings during emplacement of the early

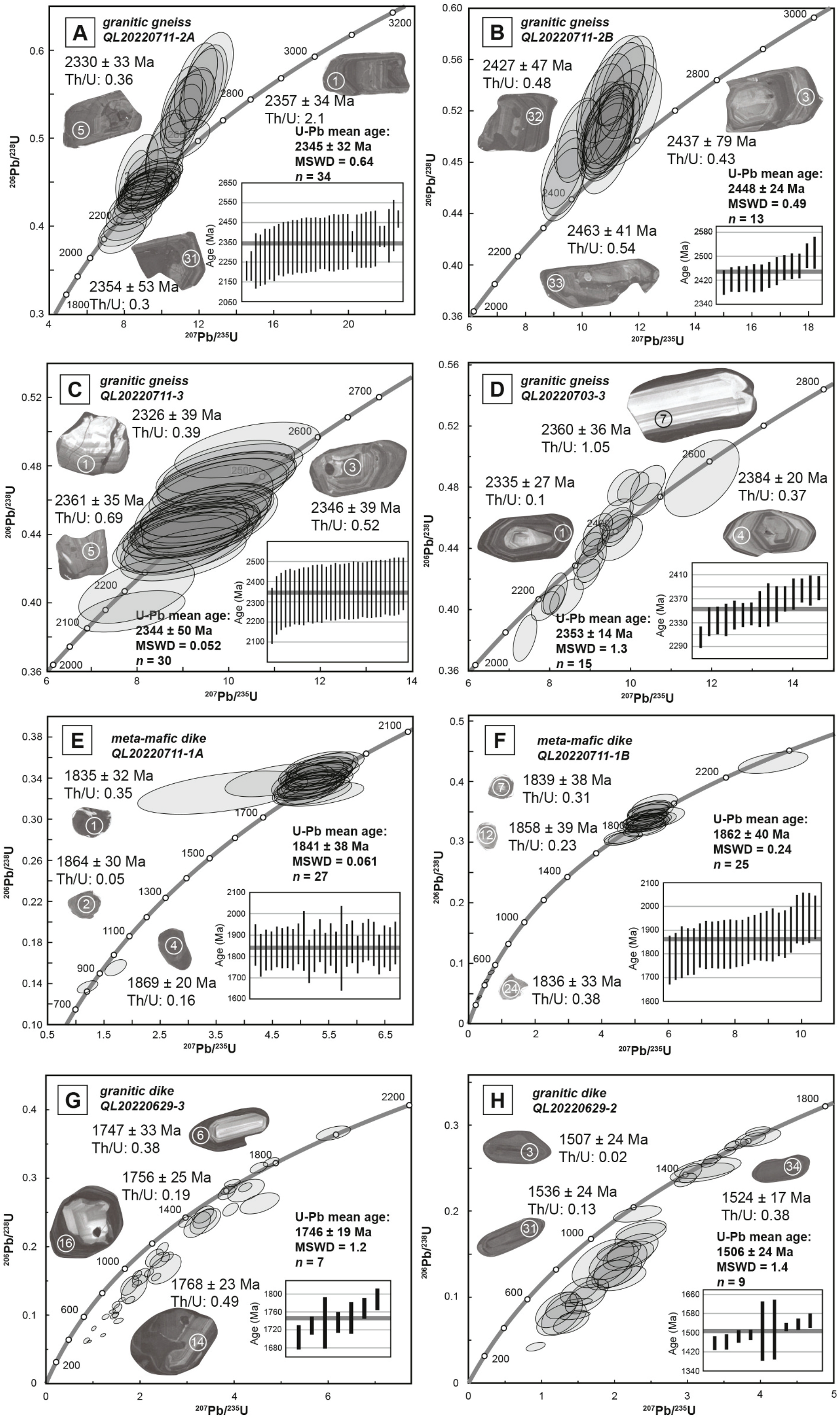

Fig. 9. U-Pb concordia diagrams showing results of single-shot zircon analyses. Error ellipses are 2σ. Circles represent ~30 μm analyzed spots. Insets show the weighted mean age for selected zircon grains. MSWD-mean square of weighted deviates.

Paleoproterozoic (ca. 2.4 Ga) granitic gneisses; specifically, whether the granitic gneisses were generated in a magmatic arc during subduction or rifting associated with continental breakup (e.g., Lu et al., 2006, 2008b; Gong et al., 2012a, 2012b; Yu et al., 2017b). Our granitic gneiss samples have major and trace elements characteristics similar to typical adakites with their depleted in HREE, high Sr, and low Y contents. However, low MgO, Cr, Ni, and Sc contents and $Mg^{\#}$ suggest that the magma was not derived from a subducted oceanic slab. Positive $\varepsilon_{Nd}(t)$ values indicate that the granitic gneisses are derived from a depleted mantle source. A low initial Sr ratio implies that portions of this source magma are

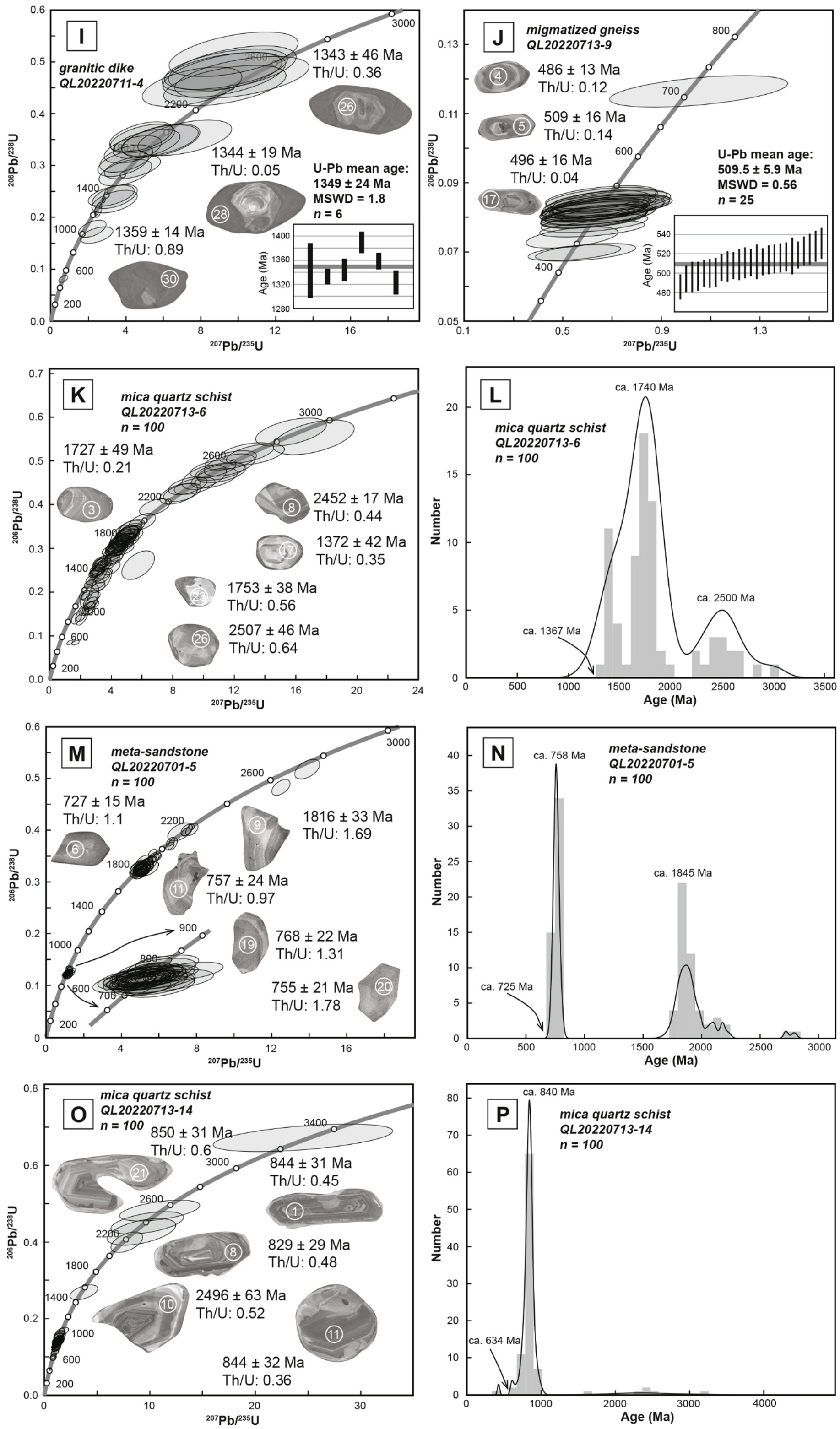

Fig. 9. (*continued*).

possibly derived from partial melting of juvenile crust, resulting in high temperature-pressure metamorphism. This magma may have been supplied via mantle upwelling and underplating in an extensional setting following collision and crustal thickening. Therefore, we interpret that the ca. 2.4 Ga granitic gneisses were generated during regional extension.

Previously reported geochemistry results for both the late Paleoproterozoic and late Mesoproterozoic–early Neoproterozoic granitoids with ca. 1.98 Ga and ca. 1.1–0.9 Ga zircon age peaks, respectively, suggest generation in a magmatic arc (e.g., Gehrels et al., 2003a). Emplacement of the late Paleoproterozoic gabbro dikes (ca. 1.86–1.84 Ga) is thought to have occurred during regional extension. In this study, the major- and trace-element and Sr-Nd isotope geochemistry of late Paleoproterozoic gabbro samples exhibit a strong affinity with magma

Table 1
Summary of sample locations and geochronology results from this study.

Sample number	Rock type	Lattitude (°N)	Longitude (°E)	Elevation (m)	Methods	Ages
QL20220711-2A	granitic gneiss	37°23′31.60″	97°22′04.10″	3006	zircon U-Pb/zircon Lu-Hf/whole-rock geochemistry/Sr-Nd isotope	2345 ± 32 Ma
QL20220711-2B	granitic gneiss	37°23′31.60″	97°22′04.10″	3006	zircon U-Pb/zircon Lu-Hf/whole-rock geochemistry/Sr-Nd isotope	2448 ± 24 Ma
QL20220711-3	granitic gneiss	37°23′31.60″	97°22′04.10″	3006	zircon U-Pb/zircon Lu-Hf/whole-rock geochemistry/Sr-Nd isotope	2344 ± 50 Ma
QL20220703-3	granitic gneiss	37°27′00.30″	97°15′04.60″	3469	zircon U-Pb/zircon Lu-Hf	2353 ± 14 Ma
QL20220711-1A	meta-gabbro dike	37°23′31.79″	97°22′04.03″	3009	zircon U-Pb/zircon Lu-Hf/whole-rock geochemistry/Sr-Nd isotope	1841 ± 38 Ma
QL20220711-1B	meta-gabbro dike	37°23′31.60″	97°22′04.10″	3006	zircon U-Pb/zircon Lu-Hf/whole-rock geochemistry/Sr-Nd isotope	1862 ± 40 Ma
QL20220629-3	granitic dike	37°24′49.36″	97°26′56.64″	3236	zircon U-Pb/zircon Lu-Hf/whole-rock geochemistry/Sr-Nd isotope	1746 ± 19 Ma
QL20220629-2	granitic dike	37°24′44.09″	97°26′55.19″	3240	zircon U-Pb/zircon Lu-Hf/whole-rock geochemistry/Sr-Nd isotope	1506 ± 24 Ma
QL20220711-4	granitic dike	37°23′11.10″	97°21′40.00″	3008	zircon U-Pb/zircon Lu-Hf/whole-rock geochemistry/Sr-Nd isotope	1349 ± 24 Ma
QL20220713-9	migmatized gneiss vein	37°25′14.73″	97°28′15.27″	3401	zircon U-Pb	506 ± 6 Ma
QL20220713-6	mica quartz schist	37°24′27.10″	97°28′13.76″	3271	zircon U-Pb	
QL20220701-5	meta-sandstone	37°30′30.87″	98°08′54.89″	4066	zircon U-Pb	
QL20220713-14	mica quartz schist	37°25′16.54″	97°28′15.79″	3404	zircon U-Pb	

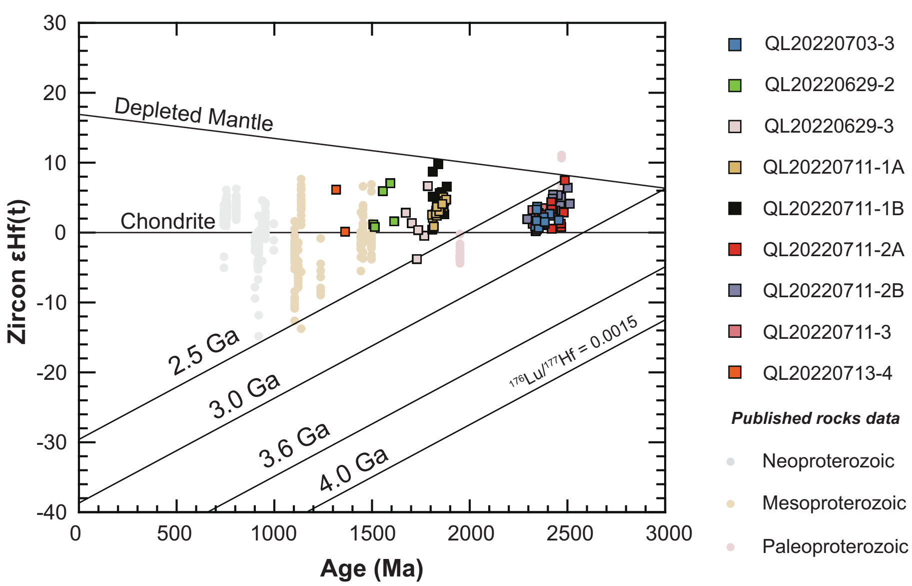

Fig. 10. Plot of zircon age versus zircon $\varepsilon_{Hf}(t)$. Data for magmatic zircons from Precambrian intrusions in the North Qaidam block (Fu et al., 2015; Wang et al., 2021; Teng et al., 2022; Chen et al., 2007a, 2007b, 2009; Hao et al., 2022; Li et al., 2007) are shown for comparison.

derived from ocean island basalt-type sources. Ca. 1.74 Ga and ca. 1.35 Ga granite dikes analyzed in this study show A-type granite and "within-plate" geochemical characteristics generally associated with extension regardless of the origin of the magma source (e.g., Whalen et al., 1987; Eby, 1990, 1992; Turner et al., 1992). The REE pattern of the A-type intrusions seems to reflect the tetrad effect attributed to melt-fluid interaction during a late stage of the magma evolution (Jahn et al., 2001). Positive $\varepsilon_{Nd}(t)$ and Sr isotopes indicate that the source magma of the granitic dikes is derived from the partial melting of juvenile lower crust that originated from a depleted mantle. These high-K, calc-alkaline series granitic dikes are possibly a product of post-orogenic magmatism. Previously reported geochemical results (e.g., Wang et al., 2016d; Wang et al., 2021) and the ca. 1.5 Ga, I-type granitic gneiss analyzed in this study suggest generation in an anorogenic setting, possibly a rift featuring mantle upwelling. Early Neoproterozoic magmatism and continent-continent collision in the northern Qaidam block were followed by ca. 0.75–0.53 Ga, rift-related magmatic and/or plume activity, which are generally associated with opening of the Qilian Ocean in the north and Paleo-Kunlun Ocean in the south (e.g., Wu et al., 2016; Zuza et al., 2018). Neoproterozoic rifting and continental breakup were followed by deposition of passive continental margin sequences in the Qaidam block and surrounding regions (e.g., Wu et al., 2016, 2017).

5.2. Proterozoic tectonostratigraphy of the Qaidam block

The metamorphic basement of the Qaidam block is referred to as the Quanji massif, which consists of the Delingha complex, Dakendaban Group, and Wandonggou Group. The oldest basement rock of the Qaidam block is the Delingha complex, which includes ca. 2.4–2.2 Ga, highly metamorphosed granitic gneiss, and amphibolite and mafic granulite enclaves. The geochemistry and isotope characteristics of ca. 2.39–2.34 Ga granodioritic and monzonitic gneisses from previous

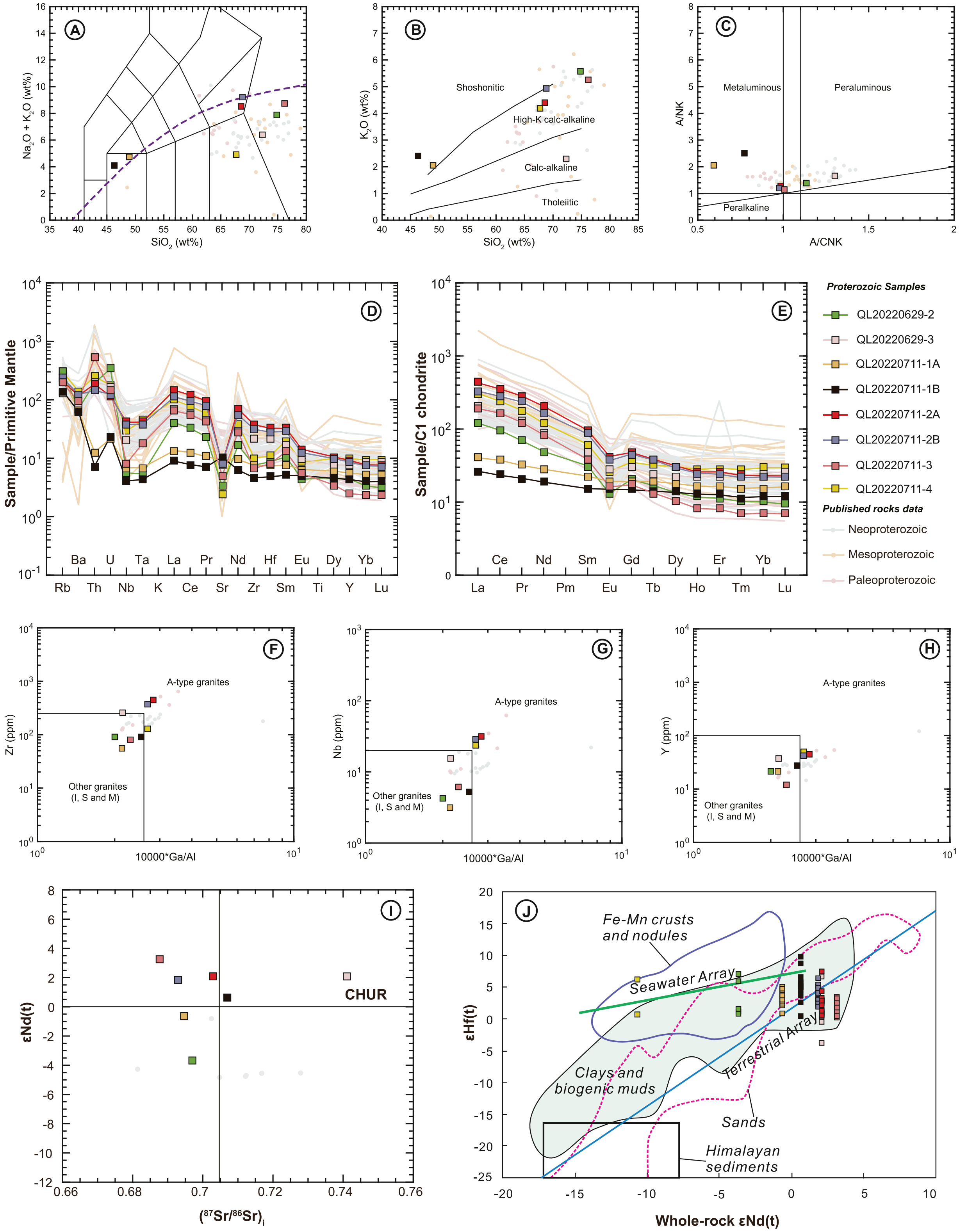

Fig. 11. Geochemical plots of the Precambrian rock samples collected in this study. Data for Precambrian intrusions in the North Qaidam block (Fu et al., 2015; Wang et al., 2021; Cheng et al., 2017b; Gong et al., 2014, 2019; Teng et al., 2022; Chen et al., 2007a, 2007b, 2009; Hao et al., 2022; Yu et al., 2017b; Li et al., 2007) are shown for comparison. (A) ($K_2O + Na_2O$) versus SiO_2 plot (Middlemost, 1994). (B) K_2O versus SiO_2 diagram (Le Maitre et al., 1989; Rickwood, 1989). (C) A/CNK versus A/NK plot (Maniar and Piccoli, 1989). (D) Primitive mantle-normalized and (E) chondrite-normalized rare earth element multi-element patterns. Primitive mantle and chondrite data are from McDonough and Sun (1995). (F–H) Plots of Zr, Nb, and Y versus 10,000*Ga/Al. (I) Plots of whole-rock $(^{87}Sr/^{86}Sr)_i$ versus εNd(t) and (J) whole-rock εNd(t) versus zircon εHf(t). Oceanic sediments including Fe-Mn crust and nodules, deep-sea clays and biogenic sediments, sands, Himalayan continental sediments, the seawater array, and terrestrial array are from Chauvel et al. (2008) and Vervoort et al. (2011). Literature data are from Wang et al. (2018).

studies and this study suggest generation in a post-collisional environment (Lu et al., 2008b; Gong et al., 2012a, 2012b; Wang et al., 2015c; He et al., 2018). These granitic gneisses are correlative with similar-aged granitic gneisses in the North Tarim-North China craton. Specifically, Paleoproterozoic tectono-thermal events in both the Delingha Complex and North Tarim-North China craton include: (1) ca. 1.96–1.9 Ga, medium pressure-temperature, amphibolite-facies metamorphism and local granulite-facies metamorphism (Chen et al., 2013b; Yu et al., 2017a, 2017b); (2) ca. 1.85–1.83 Ga emplacement of amphibolite dykes with arc-related geochemical features that formed in a back-arc basin (Liao et al., 2014); and (3) ca. 1.82–1.8 Ga, medium pressure-temperature, amphibolite-facies metamorphism related to continental collision (Chen et al., 2013b). Detrital zircon U-Pb data from late Paleoproterozoic metasedimentary rocks of the Quanji massif yield two distinct age populations of ca. 2.5–2.2 Ga and ca. 2.05–1.75 Ga (Sun et al., 2019). These age populations reflect a single regionally extensive unit that extended from the North Tarim to the North China craton.

Detrital zircon U-Pb ages commonly represent the timing of crystallization of an igneous source rock and/or metamorphic overprinting, and thus, can only be used to estimate a maximum depositional age of detrital zircon-hosting strata. For metasedimentary rocks of the Qaidam block, detrital zircon U-Pb ages constrain their provenance. Here, we revise the debated stratigraphic divisions of Precambrian metamorphic and metasedimentary rocks in the Qaidam block based on their zircon ages. Detrital zircon U-Pb ages of late Paleoproterozoic–early Mesoproterozoic metasedimentary rocks of the Quanji massif yield two distinct age populations with ca. 2.6–2.2 Ga and ca. 2.05–1.75 Ga peaks and a maximum depositional age of ca. 1.65 Ga (Zhang et al., 2012g; Li

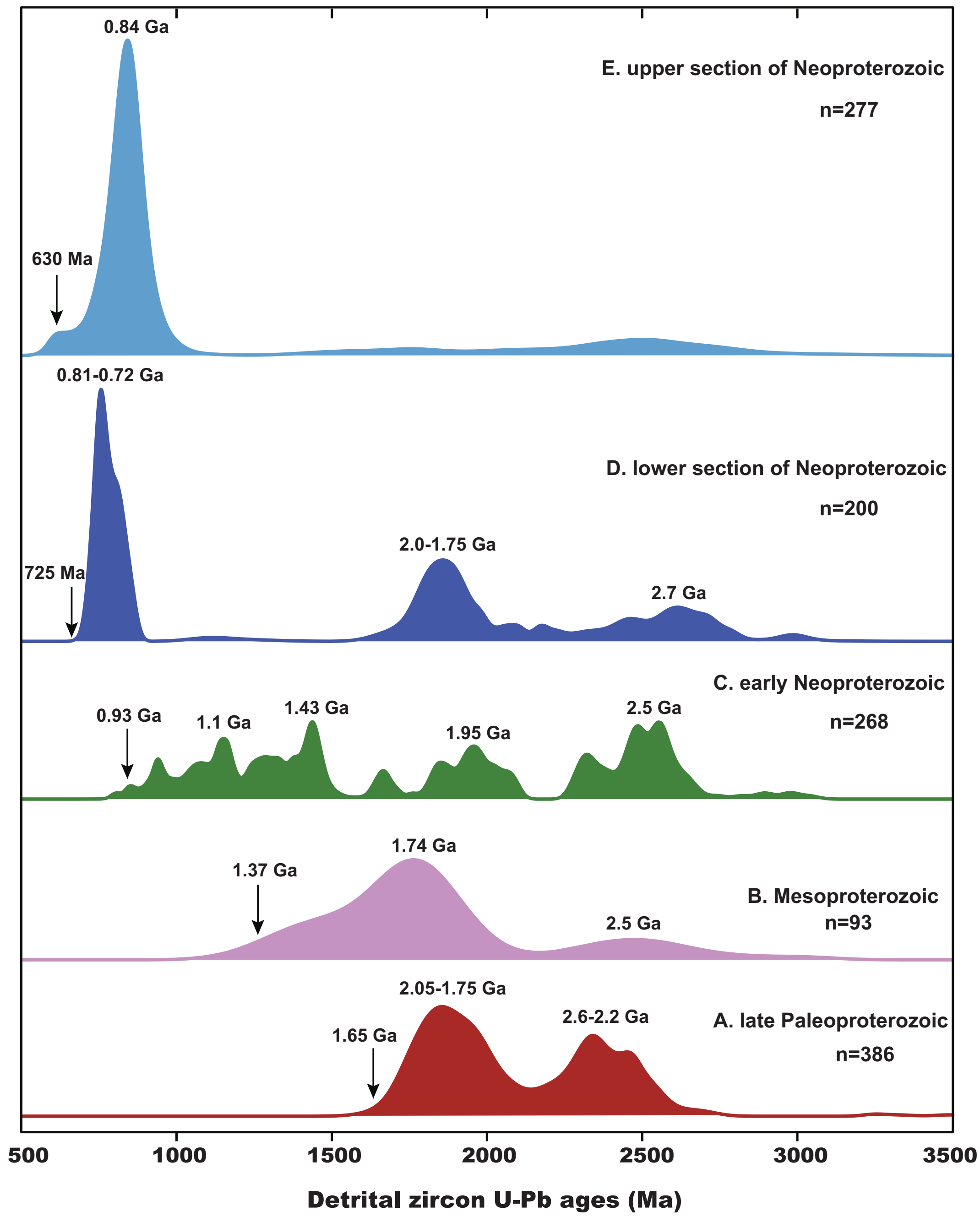

Fig. 12. Normalized probability plot of Precambrian detrital zircon ages from the Qaidam block. Data are from: Zhang et al., 2012f; Li et al., 2018a, 2018b; Sun et al., 2019, Wang et al., 2019a, 2019b; Li et al., 2022; and this study.

et al., 2018a, 2018b; Sun et al., 2019, Wang et al., 2019b; Li et al., 2022) (Fig. 12). Metavolcanic tuff layers aged at ca. 1.65–1.64 Ga are also present in the late Paleoproterozoic–early Mesoproterozoic metasedimentary rocks (Zhang et al., 2016). Field observations show ca. 1.5 Ga trondhjemite intruded the late Paleoproterozoic–early Mesoproterozoic metasedimentary rocks (Wang et al., 2016d and this study), all of which subsequently experienced ca. 1.47–1.3 Ga regional metamorphism and anatexis (Wang et al., 2021; Li et al., 2022). These ages constrain the deposition of the protoliths of the metasedimentary rocks to between ca. 1.65–1.5 Ga, potentially in a rift basin (Wang et al., 2019b). The provenance of the late Paleoproterozoic–early Mesoproterozoic metasedimentary rocks may be the Neoarchean-Paleoproterozoic North Tarim-North China craton and Paleoproterozoic gneiss and intrusions in the Qaidam block.

Mesoproterozoic mica quartz schist sample (QL20220713-6) has a maximum depositional age of ca. 1.37 Ga and contains a single youngest zircon grain age of ca. 1,277 Ma (Fig. 12), which confirms Mesoproterozoic deposition. In addition, two prominent zircon age populations with ca. 1.74 Ga and ca. 2.5 Ga peaks suggest a source in the North Tarim-North China craton and local Qaidam block. The detrital zircon ages of the late Mesoproterozoic–early Neoproterozoic metasedimentary rocks yield age peaks at ca. 1.43 Ga, ca. 1.3–1.2 Ga, ca. 1.1 Ga, and ca. 0.95 Ga, with a ca. 0.93 Ga maximum depositional age (Wang et al., 2019b) (Fig. 12). In addition, these metasedimentary rocks contain a ca. 1.1 Ga metavolcanic tuff layer (Wang et al., 2019a, 2019b) and are intruded by ca. 0.9 Ga garnet-bearing granitic gneiss (Ma et al., 2018). Correlative Proterozoic rocks have been reported in northern Tibet. Gehrels et al. (2003b) reported detrital zircon ages from two Proterozoic samples, one in the central Qilian Shan and another from the Altyn Tagh Range, both of which are intruded by ca. 925 Ma granitoid (Gehrels et al., 2003a, 2003b). Wu et al. (2017) and Zuza et al. (2018) reported two Mesoproterozoic quartzo-feldspathic schist samples in the central Qilian block that were deposited between ca. 1,200–960 Ma based on their detrital zircon ages and intrusive relationships with early Neoproterozoic arc granitoids. In addition, the northern and southwestern North China craton contain numerous correlative rocks (e.g., Wu et al., 2017, 2021, Wu et al., 2022a, 2022b, 2022c). Thus, we interpret that the North China craton, local Qaidam block, and western Laurentia were sources of the late Mesoproterozoic–early Neoproterozoic metasedimentary rocks examined in this study (e.g., Wen et al., 2017; Wu et al., 2017; Zuza and Yin, 2017; Wang et al., 2019b).

In the Qaidam block, we mapped a Neoproterozoic metasedimentary sequence, which can be divided into two sections (Fig. 12). The lower section consists of undeformed metasandstone and metavolcanic layers in the northern part of the study area. The upper section consists of deformed garnet mica quartz schist intruded by ca. 506 Ma gneiss in the southern part of the study area. A metasandstone sample from the lower section has two main zircon age populations of ca. 809–721 Ma and ca. 1,995–1,738 Ma, and a ca. 725 Ma maximum depositional age (Fig. 12). In this sample, two minor age populations occur at ca. 2,226–2,060 Ma and ca. 2,791– 2,721 Ma. Metavolcanic layers in the lower section are ca. 740–734 Ma (Ji et al., 2018; Bai et al., 2019). A schist sample from the upper section has a dominant age population of ca. 995–603 Ma with one peak at ca. 840 Ma and a few Archean ages. For this sample, the deposition age is estimated to be ca. 634–506 Ma (Fig. 12). The Archean and Paleoproterozoic aged zircon grains from this sample may be sourced from the North Tarim-North China craton and local Qaidam block. Although Li et al. (2019) argued a Gondwanan provenance for the Neoproterozoic-aged zircon grains, the local Qaidam block, central Qilian-Altyn Tagh terrane, and western North China craton are likely detrital sources for the Neoproterozoic metasedimentary sequence (e.g., Gehrels et al., 2003a, 2003b, 2011; Wu et al., 2017, 2019, 2021, 2022a; Zuza and Yin, 2017; Zuza et al., 2018). We observed that the Neoproterozoic metasedimentary sequence and early Paleozoic gneiss intrusion are thrust over Paleoproterozoic gneiss. Some researchers have linked northern Tibet to the Yangtze block of southern China or other Gondwana continents based on records of ca. 1.3–0.9 Ga magmatism (e.g., Wan et al., 2006; Tung et al., 2013; Xu et al., 2007; Lu et al., 2008b, 2009; Han et al., 2016). However, we note that these ca. 1.3–0.9 Ga ages are not particularly useful for correlating continents, as such ages are found in East Antarctica, India, Australia, central Asia, southern China, southwestern North China, and Tarim (e.g., Fitzsimons, 2000; Ling et al., 2003; Chen et al., 2006a; Wu et al., 2006; Ye et al., 2007; Hu et al., 2010; Song et al., 2012; Kröner et al., 2013; Meng et al., 2013; Xu et al., 2013; Dan et al., 2014; Wang et al., 2014b; Wang et al., 2014c; Chattopadhyay et al., 2015; Wu et al., 2017, 2022a).

5.3. Precambrian tectonic evolution of the Qaidam block

Based on our results and a regional synthesis of the Precambrian tectonostratigraphy and magmatic records (Figs. 13–14), we describe the Proterozoic tectonic evolution of the Qaidam block and its relationships to the neighboring North China craton, Tarim craton, and South China block. In our Proterozoic reconstruction of the Qaidam block, we interpret a combined Tarim–North China continental strip (i.e., Greater North China), which separated the Paleo-Asian and Tethyan oceans in the Neoproterozoic–Paleozoic following global Neoproterozoic rifting. We also assume that the Neoproterozoic shape of the northern margin of the North China-Tarim craton was modified by rifting in the Neoproterozoic–Cambrian. The Tarim craton consists of the North Tarim and South Tarim blocks that were sutured in the Proterozoic (e.g., Guo et al., 2005; Xu et al., 2013). South Tarim correlates with the Kunlun-Qaidam continent and North Tarim correlates with the North China craton. We also suggest the Songpan-Ganzi terrane is the westward extension of the Yangtze craton of western South China since the Mesoproterozoic (i.e., Greater South China; e.g., Wu et al., 2016). Lastly, restoring Cenozoic slip on the Altyn Tagh fault and removing effects of the early Paleozoic Qilian orogeny suggests that the Kunlun-Qaidam-Qilian continent was part of the North China-Tarim craton in the Neoproterozoic. This interpretation is viable according to global plate reconstructions that imply Tarim and North China were adjacent throughout the Phanerozoic (e.g., Domeier and Torsvik, 2014).

In the North Tarim–North China continent and Quanji massif of the Qaidam block, ca. 2.45–2.34 Ga, highly metamorphosed granitic gneiss, ca. 2.32–1.96 Ga amphibolite-facies, metavolcanic-sedimentary and supracrustal rocks, and late Paleoproterozoic metamorphic rocks were emplaced, which supports a close connection between the Qaidam block and North Tarim–North China continent in the Paleoproterozoic (Fig. 13A). In addition, the Qaidam block contains ca. 2 Ga arc granitoid, ca. 1.86–1.83 Ga meta-mafic dikes, ca. 1.8–1.77 Ga rapakivi granites, ca. 1.74 Ga A-type granite, and evidence of late Paleoproterozoic–early Mesoproterozoic (ca. 1.65–1.5 Ga) rifting. From this, we interpret that modern-style plate tectonics operated in the Paleoproterozoic during the assembly of the Columbia-Nuna supercontinent, including oceanic subduction, continent-continent collision, and post-collisional extension (Figs. 13B–13E). Furthermore, the occurrence of ca. 1.5–1.4 Ga anorogenic magmatic, metamorphic, and anatectic events in the North Qaidam block may have been related to the initial break-up of the Columbia-Nuna supercontinent (e.g., Fan et al., 2013; Wu et al., 2014; Wang et al., 2016d, 2019b; Wu et al., 2017; Sun et al., 2019; Wang et al., 2021; Li et al., 2024), which may have continued to ca. 1.37–1.35 Ga (Fig. 13E). An analogous tectonic event is proposed for the North China craton (e.g., Zhang et al., 2022a, 2022b; Liu et al., 2023; Zhou et al., 2018).

Wu et al. (2016) suggested that the Paleo-Qilian Ocean opened between the North China-Tarim craton and Qilian-Qaidam-Kunlun continent within the Greater North China craton (e.g., Wu et al., 2022b; i.e., part of the larger Balkatach continent of Zuza and Yin, 2017). They also interpreted that the Proto-Kunlun Ocean opened between the Songpan-Ganzi terrane and Qilian-Qaidam-Kunlun continent beginning in the Mesoproterozoic (Fig. 14A). Early Neoproterozoic (ca. 1–0.9 Ga) magmatic arcs developed along the northern and southern margins of

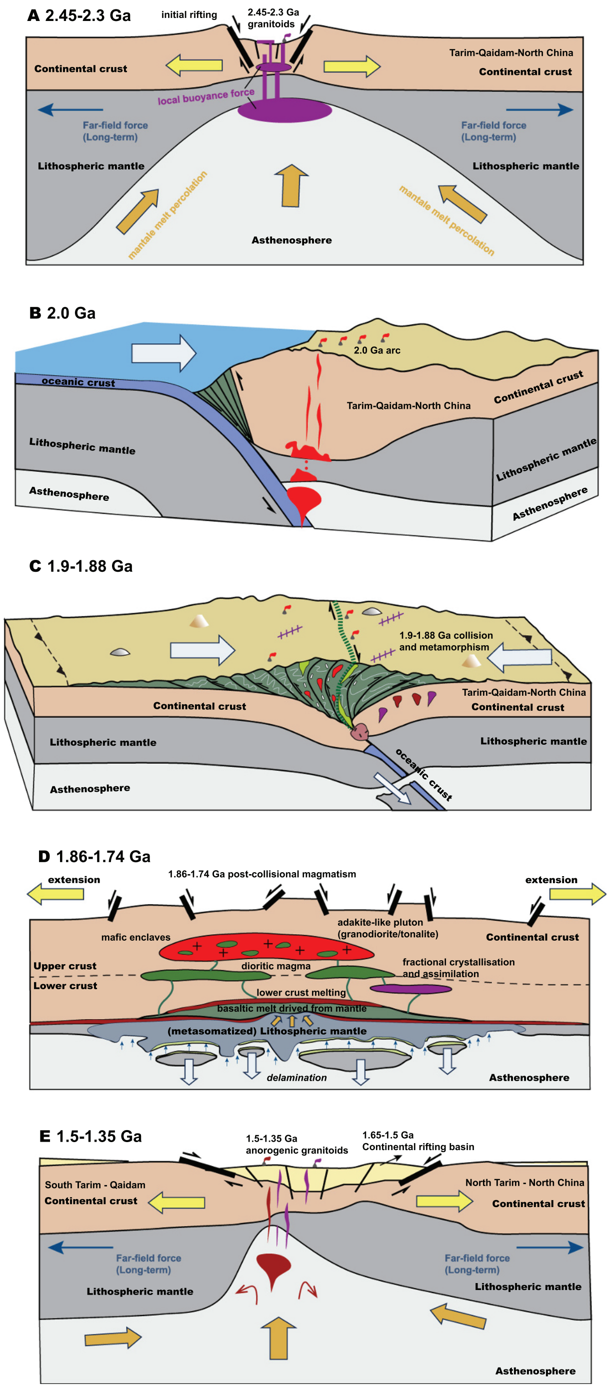

Fig. 13. Schematic, lithospheric-scale cross sections and block diagrams depicting the tectonic evolution of the Qaidam block from the onset of the Paleoproterozoic to the Mesoproterozoic: (A) ca. 2.45–2.3 Ga, (B) ca. 2 Ga, (C) 1.9–1.88 Ga, (D) 1.86–1.74 Ga, and (E) ca. 1.5–1.35 Ga.

the Qilian-Qaidam-Kunlun continent during subduction of Paleo-Qilian and Proto-Kunlun oceanic lithosphere (Fig. 14A). Closure of these ocean basin and cessation of subduction occurred ca. 0.85–0.75 Ma (e.g., Wu et al., 2016, 2017, 2022b; Zuza and Yin, 2017; Zuza et al., 2018) (Fig. 14B). Late Neoproterozoic rifting of this sutured continental landmass opened the Qilian oceans in the south and the Paleo-Asian Ocean in the north. The lack of Phanerozoic sutures or amalgamation structures between the South Tarim and Qaidam blocks suggests that the landmasses were connected prior to and during the opening of the Qilian oceans (e.g., Wu et al., 2017; Zuza et al., 2018). Evidence for bimodal volcanism and passive-margin sedimentation in the North Tarim and North China cratons suggest that the opening of the Paleo-Asian Ocean started ca. 0.8 Ga (e.g., Li et al., 2005a, 2005b; Zhu et al., 2008b; Turner, 2010; Shu et al., 2011a; Wu et al., 2016; Zuza and Yin, 2017) (Fig. 14B). Opening of the North and South Qilian oceans may have commenced ca. 750–730 Ma, whereas opening of the Paleo-Kunlun Ocean occurred just prior to ca. 680 Ma (Wu et al., 2016, 2017, 2019, 2022b; Zuza et al., 2018) (Fig. 14C).

5.4. Proterozoic supercontinent reconstruction

Debate has focused on the paleogeographic configuration of the North China craton in the Columbia-Nuna supercontinent. Most researchers have interpreted that the north-south-striking Trans-North China orogen in the center of the North China craton is a collisional suture. The Trans-North China orogen between the Eastern and Western blocks (Zhao et al., 2001, 2005; Zhao et al., 2012) was delineated by its regional high-grade metamorphism and clockwise P-T-t paths at ca. 1.85 Ga. However, others have argued that a ~1600-km-long, east-west-striking collisional orogen occurs along the northern margin of the North China craton, marking the suture where the craton joined the Columbia-Nuna supercontinent. In this model, the center of the North China craton formed via arc-continent collision in the Neoarchean (ca. 2.5 Ga), during which at least one intra-oceanic arc accreted to the eastern margin of the craton. This proposed collisional orogen is referred to as the Central Orogenic Belt (Kusky and Li, 2003; Kusky et al., 2007, 2016), which is thought to have formed by the accretion of magmatic arcs between ca. 2.7–2.55 Ga (Kusky et al., 2016; Zhai et al., 2021; Peng et al., 2023). In this collisional orogen, field-based studies document: (1) ca. 2.55–2.5 Ga ophiolite fragments and mélanges (Kusky et al., 2001, 2007, 2016; Wang et al., 2017a, 2019a; Ning et al., 2020); (2) ca. 2.7 Ga and ca. 2.55 Ga fore-arc subduction sequences and accretionary nappes (Ning et al., 2020; Zhong et al., 2021; Huang et al., 2023); (3) ca. 2.5 Ga paired metamorphic belts and foreland basin sequences with ages reflecting ca. 2.5 Ga arc/continent collision (Huang et al., 2020, 2022b); and (4) evidence of ca. 2.5–2.45 Ga erosion denudation of the orogen. Intracontinental rifting of Archean cratons since ca. 2.4 Ga, prior to subduction initiation, may reflect the onset of the Paleoproterozoic Columbia-Nuna supercontinent cycle (e.g., Zhou and Zhai, 2022; Zhou et al., 2024) (Fig. 13A).

Following the arc(s)/protocontinent collision, subduction polarity flipped (e.g., Kusky et al., 2007; Wang et al., 2017a) and a new east-dipping subduction zone resulted in the accretion of new crustal fragments, including the Ordos Block (i.e., a possible oceanic plateau; Kusky and Mooney, 2015) and the Yinshan ribbon continent (i.e., the Khondalite belt after its metamorphic grade). By ca. 2.3 Ga, subduction and magmatism were initiated along the present-day northern margin of the craton (Kusky et al., 2016). In this model, subduction and magmatism along the northern cratonic margin occurred along a ~600-km-long distance and protracted duration from ca. 2.3–1.85 Ga, both similar to the modern southern Andes (e.g., Horton et al., 2022). During this time, many episodes of slab rollback, ridge subduction, back-arc extension, and sedimentation/magmatism occurred. Subduction ceased when the possible Siberian craton collided with the growing Columbia-Nuna Supercontinent (Fig. 13B). Wu et al. (2018) initially recognized an east-west-striking, ca. 1.9–1.88 Ga tectonic mélange and mylonitic shear zones along the northern margin of the craton. Further field studies by Wu et al. (2022b, 2023) documented the presence of an east-west striking belt of ca. 2.2–2 Ga magmatic arc rocks (Fig. 13B) and lower Paleoproterozoic strata folded by north-south-oriented contraction, all of which experienced ca. 1.9–1.8 Ga, granulite-facies metamorphism (Fig. 13C). The Paleoproterozoic Northern Margin orogen contains evidence of overprinting by a ca. 1.85 Ga metamorphic event and intrusion by ca. 1.87–1.78 plutons in a post- collisional setting, such as in the Rodinian belts. In this context, the ca. 2.45–2.34 Ga, highly metamorphosed and extension-related gneiss, ca. 2.32–1.96 Ga amphibolite-

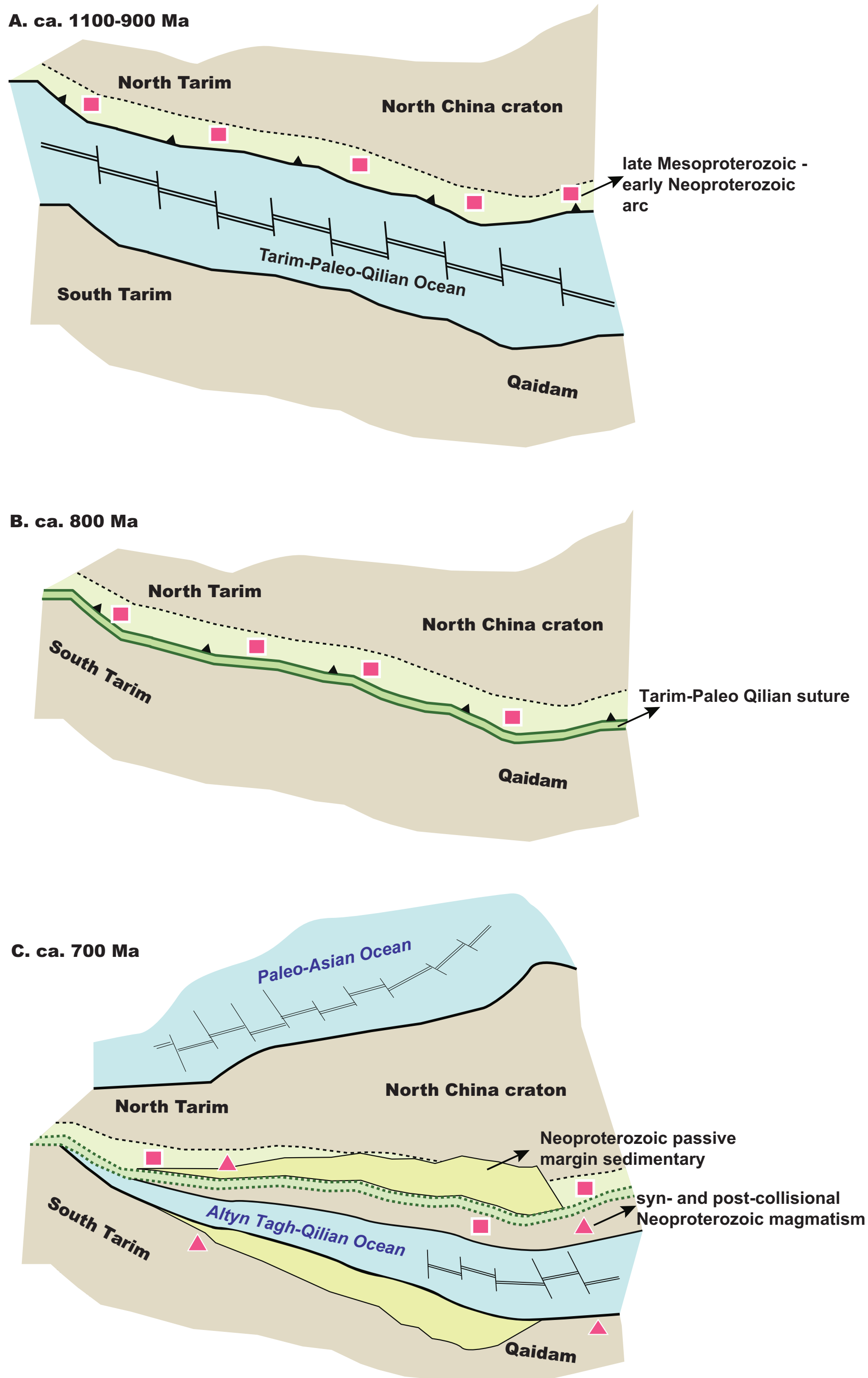

Fig. 14. Map-view diagrams depicting the Neoproterozoic tectonic evolution of the Qaidam block at (A) ca. 1,100–900 Ma, (B) ca. 800 Ma, and (C) ca. 700 Ma.

facies rocks, and ca. 1.86–1.74 Ga extension-related intrusions also developed in the North Tarim and Qaidam block (Fig. 13C). The occurrence of these rocks supports a contiguous North Tarim-North China-Qaidam continent for the Neoarchean arc-continent and Paleoproterozoic continent-continent collisional orogens.

Supercontinent reconstructions are partly based on spatial and temporal correlations of key geological features. Zhao et al. (2002) established connections between the North China and Indian cratons based on a similar ca. 1.85 Ga orogeny. The reconstruction of Kusky and Santosh (2009) used the Paleoproterozoic Northern Margin orogen to fit the North China craton into a supercontinent, correlating the orogen with the Trans-Amazonian of South America and Eburnian/Birimian orogens of West Africa. Grenholm (2019) fits most cratons of Columbia into the "Atlantica" configuration, wherein the Northern Margin orogen of the North China craton accreted with the Birimian terranes during the Eburnia orogeny (Kusky and Traore, 2023). Wu et al. (2021) suggested a correlation between the Limpopo belt in South Africa and Longshou Shan along the southwestern margin of the North China craton. Although these hypotheses successfully link specific features and piercing points, ambiguous paleomagnetic data and non-unique linkages open these configurations to new interpretations. Here, we emphasize the importance of using the Northern Margin orogen to fit the North China craton into the Columbia-Nuna Supercontinent reconstruction.

In many Rodinia reconstructions, the North China craton is commonly placed on the outside of the supercontinent, and its shape is considered limited based on the geographically defined, modern shape of northern China, north of the Qinling-Dabie orogenic belt (e.g., Halls et al., 2000; Zhang et al., 2006; Li et al., 2008d). Three fundamental issues exist with this configuration: (1) the North China craton was much larger in the Precambrian, as far west in present coordinates as the Karakum or potentially Baltica cratons (e.g., Yin and Nie, 1996; Heubeck et al., 2001; Zuza and Yin, 2017; Wu et al., 2022a); (2) Paleo- and Mesoproterozoic structures are truncated by Neoproterozoic rift and passive margin sequences (e.g., Badarch et al., 2002; Guo et al., 2005), which requires the North China craton to fit into a larger continental assemblage before this time; and (3) Paleozoic arc-continent collisional events across central Asia and Cenozoic intracontinental deformation (e.g., Şengör and Natal'in, 1996; Yin, 2010) significantly modified the

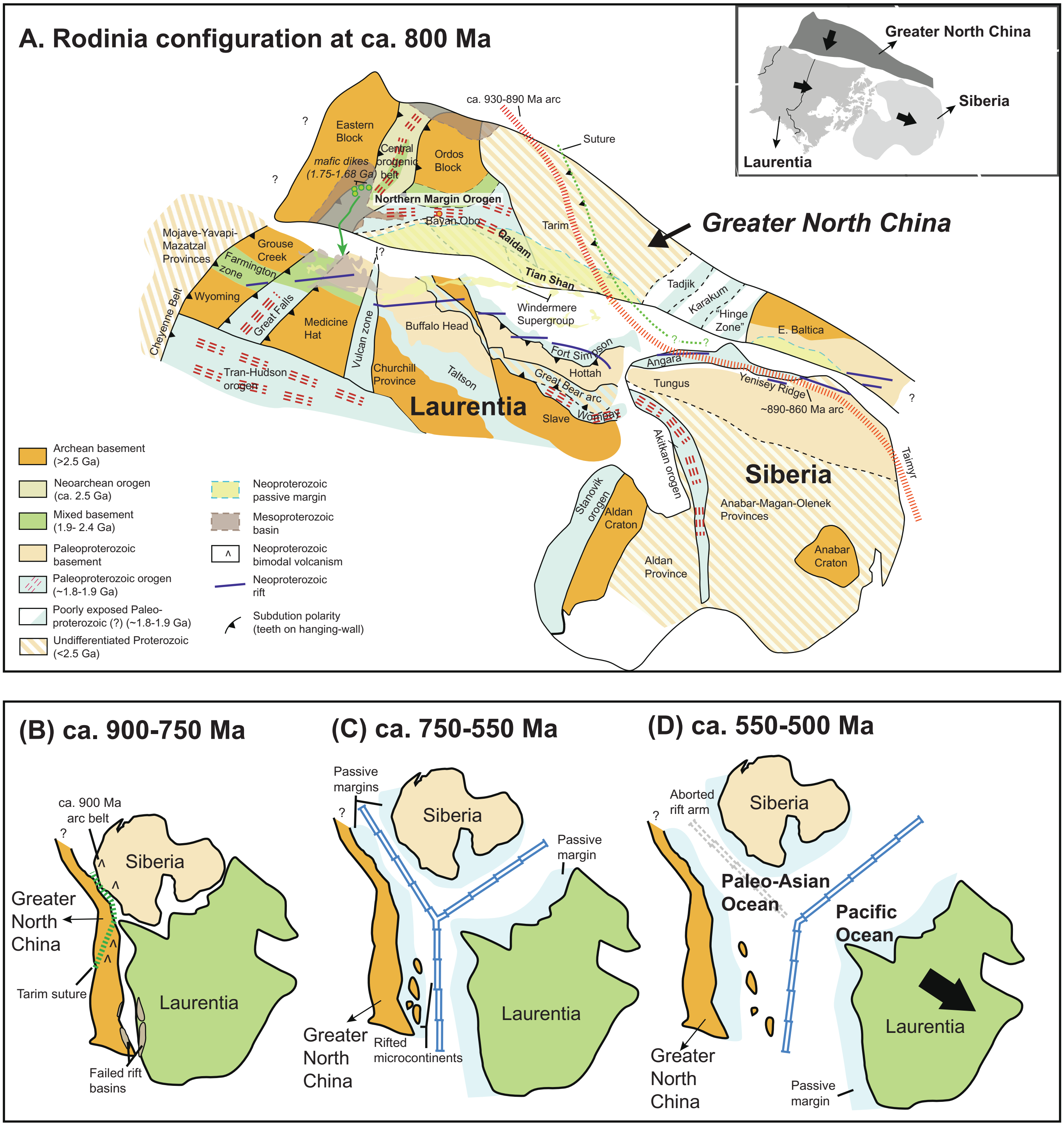

Fig. 15. (A) Neoproterozoic paleogeographic reconstruction of Rodinia showing the Great North China-Laurentia-Siberian craton and correlative geological features. The positions of Laurentia and Siberia are based on Li et al. (2008a) and Rainbird et al. (1998), respectively. (B–D) Tectonic model for the opening of the Paleo-Asian and Pacific oceans.

original shape of the craton. The northern rim of the Neoproterozoic North China-Tarim craton was significantly modified by the Paleozoic–early Mesozoic arc-continent collisional events and Cenozoic deformation. This modification is most evident in the Cenozoic Tian Shan, where the northern margin of the Tarim craton has subducted beneath the Tian Shan range up to 200 km in the west (e.g., Burtman, 2012). The northern continental margin of the Tarim craton may have subducted beneath a Devonian magmatic arc (e.g., Charvet et al., 2011), implying its original size is larger than its present exposure. The original Neoproterozoic shape of the northern margin of the North China-Tarim craton has further been modified by Neoproterozoic–Cambrian rifting (e.g., Zuza and Yin, 2017). Greater North China likely contributed the micro-continental fragments that formed the eventual building blocks of the Paleozoic Central Asian Orogenic System (e.g., Kelty et al., 2008; Briggs et al., 2009; Şengör et al., 1993; Windley et al., 2007; Kröner et al., 2013; Zuza and Yin, 2017). Sedimentological, paleontological, and geochronological data indicate that the Kazak-Yili-Tian Shan (Biske and Seltmann, 2010; Levashova et al., 2011; Meert, 2012), Tuva-Mongol (Rojas-Agramonte et al., 2011), and Erguna-Xing'an-Songliao (Han et al., 2011) microcontinents were linked to the northern margin of Tarim and North China in the Neoproterozoic.

The issue of which continent(s) were once linked with the western margin of Laurentia as part of Rodinia remains controversial (e.g., Dalziel, 1991; Hoffman, 1991; Moores, 1991; Li et al., 1995; Karlstrom et al., 1999; Burrett and Berry, 2000; Wingate et al., 2002; Wang et al., 2022). As described above, our newly reconstructed and previously unrecognized Greater North China must fit in a Rodinia configuration (Fig. 15A). We propose that Greater North China was affixed in a north-south orientation along the western margin of Laurentia (e.g., Zuza and Yin, 2017; Wu et al., 2022a) (Fig. 15A). If Siberia was in a slightly modified position from that proposed by Rainbird et al. (1998), Greater North China fits along this western margin (e.g., Zuza and Yin, 2017; Wu et al., 2022a) (Fig. 15A). The major cratons in western Laurentia include the Wyoming craton and Medicine Hat-Hearne provinces, which are joined by the ca. 1.86–1.8 Ga, granulite-facies Great Falls Tectonic Zone (e.g., Mueller et al., 2002; Foster et al., 2006). The presence of a north-dipping, paleo-subducted slab under the Medicine Hat block, imaged by geophysical studies (Kanasewich et al., 2002; Ross and Eaton, 2002), and a ca. 1.86 Ga calc-alkaline suite (i.e., the Little Belt arc) in the same block suggest that north-dipping subduction accommodated convergence of the Wyoming craton and Medicine Hat block before collision. The westernmost cratons (i.e., those that would have been in contact with Greater North China) include the Grouse Creek and Priest River blocks. The Grouse Creek orthogneiss complex contains ca. 2.55–2.53 Ga leucogranite that intrudes older schist with ≥3–2.5 Ga detrital zircon ages (e.g., Strickland et al., 2011). These rocks are exposed in northern Nevada and Utah, just west of the Wyoming craton. The Priest River block is a complex assemblage of ca. 2.67–2.56 Ga migmatitic paragneiss, lenses of coarse-grained amphibolite, and quartzo-feldspathic orthogneiss, which are intruded by ca. 1.58 Ga felsic granitoids (e.g., Doughty et al., 1998). Evidence of a similar Neoarchean orogeny is observed in the Central Orogenic belt of the North China craton (cf. Kusky et al., 2007; Trap et al., 2012). Between these Archean cratons within Laurentia is the Selway terrane, which consists of ca. 2.4–1.8 Ga arc fragments (e.g., Foster et al., 2006). We note that ca. 1.7–1.6 Ga detrital zircon ages are observed in the northern North China and Longshou Shan regions (e.g., Zhou et al., 2018; Liu et al., 2020a; Wu et al., 2021, 2022b; ZJ Wu et al., 2022c), suggesting that the western margin of Laurentia may have contributed detritus at that time.

The occurrence of plate tectonic processes on Earth during the Paleoproterozoic along the northern margin of the North China-Tarim craton is supported by ca. 2.2–1.8 Ga subduction-collision orogens associated with the assembly of the Columbia-Nuna supercontinent (e.g., Kusky et al., 2016; Wu et al., 2018, 2022a, 2022b, 2022c, 2023). The basement rocks of Greater North China and Laurentia both involve similar Archean cratons that collided in the Paleoproterozoic. This stabilized craton, with the Eastern domain of Greater North China (e.g., Zuza and Yin, 2017; Wu et al., 2022a, 2022b, 2022c), also consisted of Siberia to the north. With our proposed fit, the Northern Margin orogen is linked with the Great Falls Tectonic Zone. Overlying these metamorphic basement rocks are thick Proterozoic sequences of low-grade to unmetamorphosed sedimentary strata. A majority of the exposed basement rocks in the Karakum and Tajikistan terranes consist of ca. 1.9–1.8 Ga gneiss and greenstone rocks (e.g., Zonenshain et al., 1990). These terranes are interpreted to align with the ca. 1.9–1.85 Ga Fort Simpson belt (Ross et al., 2000) in western Laurentia. The Belt-Purcell Supergroup (ca. 1.47–1.35 Ga; Winston, 1986) spatially and temporally correlates with similarly-aged Jixian strata in the North China craton (e.g., Zhang et al., 2007a). Both sedimentary sequences are thick (i.e., >10 km) and consist of carbonate and mudrock strata deposited in rift basins (e.g., Ross et al., 1992; Zhang et al., 2007a; Meng et al., 2011; Liu et al., 2023).

Recent paleomagnetic datasets from both Tarim and North China have been used to support the separate linkage of each continent to the western margin of Laurentia in the Neoproterozoic (e.g., Wen et al., 2017, 2018; Ding et al., 2021). In these reconstructions, the traditional Tarim and North China cratons are separated in the Neoproterozoic. However, we interpret these datasets to suggest that these two continental regions were at similar paleo-latitudes along the western margin of Laurentia in the Neoproterozoic, and thus, the simplest interpretation is that they were connected and contiguous. For example, a problem with the reconstruction of Ding et al. (2021), which places eastern North China adjacent to the western Tarim craton, requires the collision of the two continents after Neoproterozoic rifting. The products of such a collision, and preceding arc subduction, have not been identified between the two cratons, as outlined in this work and Zuza and Yin (2017).

Additional support for the linkage between Greater North China and western Laurentia is the potential correlation of the ca. 1.4–1.3 Ga carbonatite-related REE deposits in Mountain Pass of western North America and Bayan Obo of northern China within an intra-plate rift system (Zhang et al., 2022a, 2022b). These regions are the two of the largest and most economically productive REE deposits in the world. In our proposed reconstruction, the ca. 1.3 Ga Bayan Obo rocks (e.g., Li et al., 2021; Zhou et al., 2018; Liu et al., 2020a) are contiguous with the ca. 1.38 Ga Mountain Pass rocks (Castor and Hedrick, 2006; Watts et al., 2022).

In light of the proposed linkages described above, we interpret that Greater North China and Laurentia became separated in the late Neoproterozoic, forming the Paleo-Asian and Pacific oceans. The Central Asian microcontinents formed during this rifting, and the final division of the Paleo-Asian and Pacific oceans occurred in the late Paleozoic. Possible east-dipping subduction facilitated the motion of western Greater North China toward Laurentia-Siberia (Zuza and Yin, 2017) (Fig. 15B). The collision of western Greater North China was diachronous from south to north with final suturing occurring by ca. 800 Ma (Fig. 15A). Following collision events in the north, western Laurentia and Greater North China experienced coeval Neoproterozoic rifting. In western Laurentia, unsuccessful rifting started at ca. 750 Ma and progressed northward (Fig. 15C), leading to the development of widespread intracontinental basins. Final rift separation was complete by ca. 550 Ma, leading to the development of a Cambrian passive continental margin outboard of Laurentia (e.g., Lund et al., 2010; Balgord et al., 2013) (Fig. 15D). Neoproterozoic rift deposits and bimodal volcanic rocks are widespread in the northern Tarim craton, North China craton, and Central Asian microcontinents (e.g., Han et al., 2011; Meert et al., 2011; Shu et al., 2011a).

The observations described above also suggest that rifting started ca. 765 Ma (Levashova et al., 2011) and fully developed in the latest Neoproterozoic to earliest Cambrian (e.g., Levashova et al., 2010). The rifted Central Asian microcontinents can be thought to be the result of "tectonic calving" during extension and asymmetric rift development—a process that may have been thermally enhanced by diffuse bimodal volcanism and a warmed lithosphere (e.g., Müller et al., 2001). Additionally, similar-aged (i.e., ca. 710 Ma, ca. 655 Ma, and ca. 630 Ma) diamictites in the Windermere (Lund et al., 2003, 2010; Balgord et al., 2013) and Qurutagh groups (Xu et al., 2005; Shu et al., 2011a), as well as in the Central Asian microcontinents (Levashova et al., 2011; Meert et al., 2011), further support coeval rifting of Greater North China and Laurentia in a similar paleogeographic position. By the early Cambrian, both the Greater North China and Laurentian margins experienced passive-margin sedimentation as the cratons and terranes separated. With progressive continental separation, Laurentia was removed from the Central Asian microcontinents that accreted to form the Central Asian Orogenic System in the Paleozoic (e.g., Windley et al., 2007; Rojas-Agramonte et al., 2014; Zuza and Yin, 2017; Wu et al., 2022b).

6. Conclusions

In this study, we compiled a large dataset of previous and new U-Pb zircon and Lu-Hf isotope, whole-rock major, trace-element, and Sr-Nd isotopic results for Precambrian metamorphic, magmatic, and sedimentary sequences of the Qaidam block. Zircon Pb-Pb ages of Precambrian magmatic rocks fall into six main age groups with peaks at ca. 2.4 Ga, ca. 1.98 Ga, ca. 1.5 Ga, ca. 1.1 Ga, ca. 0.95 Ga, and ca. 0.75 Ga. Geochemistry results support an interpretation that magmatism at ca. 2.4 Ga, ca. 1.5 Ga, and ca. 0.75 Ga was associated with post-collisional extension, whereas magmatism at ca. 1.1 Ga and ca. 0.95 Ga was associated with subduction. Newly reported ca. 1.86–1.84 Ga gabbro, ca. 1.74 Ga and ca. 1.35 Ga A-type granitoids, and ca. 1.5 Ga I-type granitoids in the northern Qaidam block are attributed to magmatism during intracontinental extension. Detrital zircon ages of late Paleo- to Mesoproterozoic metasedimentary rocks reflect sources in the coherent Tarim-North China craton and Paleoproterozoic Quanji massif of the northern Qaidam block. Western Laurentia was an additional detrital source of late Mesoproterozoic–early Neoproterozoic metasedimentary rocks in the Qaidam block. However, the Qaidam block, central Qilian-Altyn Tagh terrane, and western North China craton (i.e., Longshou Shan) likely were the detrital sources of Neoproterozoic metasedimentary rocks in the northern Qaidam block. Based on the data collected in this study and a regional synthesis of Precambrian tectonostratigraphy and magmatic records, we present a new model for the protracted Proterozoic tectonic evolution of the Qaidam block and relationships to the neighboring cratons. We interpret that the Qaidam block was part of a combined "Greater North China" continental strip. When placing our results in the global context, Greater North China fits within the paleogeographic configurations of the Columbia-Nuna and Rodinia supercontinents. Great North China subsequently separated from Laurentia during global Neoproterozoic rifting.

Supplementary data to this article can be found online at https://doi.org/10.1016/j.earscirev.2024.104985.

Declaration of competing interest

The authors declare that they have no known competing financial interests or personal relationships that could have appeared to influence the work reported in this paper.

Acknowledgments

We thank Editor Yildirim Dilek, Prof. Brendan Murphy and an anonymous reviewer for constructive reviews. This research was supported by grants from the National Natural Science Foundation of China (project no. 42372256), the Basic Science Center for Tibetan Plateau Earth System (CTPES, 41988101), the Second Tibetan Plateau Scientific Expedition and Research Program (2019QZKK0708), and the Tectonics Program of the National Science Foundation of U.S.A. (EAR 1914503 and EAR 1914501). This research and the ideas presented within this paper benefited from discussions with the late Professor An Yin over the past decade.

Data availability

Data will be made available on request.

References

Andersen, T., 2002. Correction of common lead in U-Pb analyses that do not report ^{204}Pb. Chem. Geol. 192, 59–79.

Ba, J., Gong, S.L., Liao, F.X., Zhang, L., 2012. Re-determining the intrusion age for the protolith of the Mohe gneiss in the Quanji Massif. Geol. Sci. Technol. 31 (6), 98–101 in Chinese with English abstract.

Badarch, G., Cunningham, W.D., Windley, B.F., 2002. A new terrane subdivision for Mongolia: Implications for the Phanerozoic crustal growth of Central Asia. J. Asian Earth Sci. 21, 87–110 [in Chinese with English abstract].

Bai, D.Y., Jia, B.H., Liu, W., Chen, B.H., Liu, Y.R., Zhang, X.Y., 2010. Zircon SHRIMP U-Pb dating of the igneous rocks from Chengbu, Hunan:Constraint on the Neoproterozoic tectonic evolution of the Jiangnan Orogenic Belt. Acta Geol. Sin. 84 (12), 1715–1726 (in Chinese with English abstract).

Bai, C.D., Zhuan, S.P., Mao, Z.F., Chen, Y.Y., Li, J., 2019. LA-ICP-MS Zircon U-Pb ages, geochemical characteristics and geotectonic significance of the metamorphosed volcanic rocks in Neoproterozoic Balongonggaer Formation in Tianjun County, Southern Qilian Mountain. Geol. Rev. 65 (3), 755–771.

Balgord, E., Yonkee, W., Link, P.K., Fanning, C.M., 2013. Stratigraphic, geochronologic, and geochemical record of the Cryogenian Perry Canyon Formation, northern Utah: Implications for Rodinia rifting and snowball Earth. Geol. Soc. Am. Bull. 125, 1442–1467.

Biske, Y.S., Seltmann, R., 2010. Paleozoic Tian-Shan as a transitional region between the Rheic and Urals-Turkestan oceans. Gondwana Res. 17, 602–613.

Brenner, A.R., Fu, R.R., Evans, D.A.D., Smirnov, A.V., Trubko, R., Rose, I.R., 2020. Paleomagnetic evidence for modern-like plate motion velocities at 3.2 Ga. Sci. Adv. 6, eaaz8670.

Briggs, S.M., Yin, A., Manning, C.E., Chen, Z.L., Wang, X.F., 2009. Tectonic development of the southern Chinese Altai Range as determined by structural geology, thermobarometry, ^{40}Ar/^{39}Ar thermochronology, and Th/Pb ion-microprobe monazite geochronology. Geol. Soc. Am. Bull. 121, 1381–1393.

Brown, M., Johnson, T., Gardiner, N.J., 2020. Plate tectonics and the Archean Earth. Annu. Rev. Earth Planet. Sci. 48, 12.

Burrett, C., Berry, R., 2000. Proterozoic Australia–Western United States (AUSWUS) fit between Laurentia and Australia. Geology 28 (2), 103–106.

Burtman, V.S., 2012. Geodymanics of Tibet, Tarim, and the Tien Shan in the late Cenozoic. Geotectonics 46 (3), 185–211.

Cai, Y., Wang, Y., Cawood, P.A., Fan, W., Liu, H., Xing, X., Zhang, Y., 2014. Neoproterozoic subduction along the Ailaoshan zone, South China: Geochronological and geochemical evidence from amphibolite. Precambrian Res. 245, 13–28.

Cai, Y., Wang, Y., Cawood, P.A., Zhang, Y., Zhang, A., 2015. Neoproterozoic crustal growth of the Southern Yangtze Block: Geochemical and zircon U–Pb geochronological and Lu-Hf isotopic evidence of Neoproterozoic diorite from the Ailaoshan zone. Precambrian Res. 266, 137–149.

Cai, Z., Xu, Z., Yu, S., Li, S., He, B., Ma, X., 2018. Neoarchean magmatism and implications for crustal growth and evolution of the Kuluketage region, northeastern Tarim Craton. Precambrian Res. 304, 156–170.

Cai, Y., Liu, H., Feng, Z., Zhou, Y., Liu, X., Wang, Z., Ma, L., Li, Z., Xu, J., 2020a. Neoproterozoic active margin of the SW South China Block: Constraints from U Pb ages, Sr Nd isotopes and geochemical data for the gabbro and granodiorite along the Ailaoshan tectonic belt. Lithos 358–359, 105387.

Cai, Z., Jiao, C., He, B., Qi, L., Ma, X., Cao, Z., 2020b. Archean–Paleoproterozoic tectonothermal events in the central Tarim Block: Constraints from granitic gneisses revealed by deep drilling wells. Precambrian Res. 347, 105776.

Cao, Z.Q., Cai, Y.T., Zeng, Z.X., Hu, Z.X., Chen, J., Jiang, X.F., Sun, Z.Q., Wu, B., Liu, C. X., Guo, P., 2017. Discovery of Neoproterozoic A-type granite in northern Yangtze Craton and its tectonic significance. Earth Sci. 42 (6), 957–973 (in Chinese with English abstract).

Castor, S.B., Hedrick, J.B., 2006. Rare earth elements. Indust. Miner. Rocks 7, 769–792.

Cawood, P.A., Strachan, R., Cutts, K., Kinny, P.D., Hand, M., Pisarevsky, S., 2010. Neoproterozoic orogeny along the margin of Rodinia: Valhalla Orogen, North Atlantic. Geology 38 (2), 99–102.

Cawood, P.A., Strachan, R.A., Pisarevsky, S.A., Gladkochub, D.P., Murphy, J.B., 2016. Linking collisional and accretionary orogens during Rodinia assembly and breakup: Implications for models of supercontinent cycles. Earth Planet. Sci. Lett. 449, 118–126.

Cawood, P.A., Zhao, G., Yao, J., Wang, W., Xu, Y., Wang, Y., 2018. Reconstructing South China in phanerozoic and precambrian supercontinents. Earth Sci. Rev. 186, 173–194.

Charvet, J., Shu, L., Laurent-Charvet, S., Wang, B., Faure, M., Cluzel, D., Yan, C., De Jong, K., 2011. Palaeozoic tectonic evolution of the Tianshan belt, NW China. Sci. China Earth Sci. 54, 166–184.

Chattopadhyay, S., Upadhyay, D., Nanda, J.K., Mezger, K., Pruseth, K.L., Berndt, J., 2015. Proto-India was a part of Rodinia: evidence from Grenville-age suturing of the Eastern Ghats Province with the Paleoarchean Singhbhum Craton. Precambrian Res. 266, 506–529.

Chauvel, C., Lewin, E., Carpentier, M., Arndt, N.T., Marini, J.C., 2008. Role of recycled oceanic basalt and sediment in generating the Hf–Nd mantle array. Nat. Geosci. 1, 64–67. https://doi.org/10.1038/ngeo.2007.51.

Chen, Y.L., Luo, Z.H., Zhao, J.X., Li, Z.H., Zhang, H.F., Song, B., 2005. Petrogenesis and dating of the Kangding complex, Sichuan Province. Sci. China (Ser. D) 48 (5), 622–634.

Chen, N.S., Li, X.Y., Wang, X.Y., Chen, Q., Wang, Q.Y., Wan, Y.S., 2006a. Zircon U-Pb SHRIMP dating of Neoproterozoic metagranite in the North Kunlun unit on the southern margin of the Qaidam block in China. Geol. Bull. China 25, 1311–1314.

Chen, N.S., Li, X.Y., Zhang, K.X., Wang, G.C., Zhu, Y.H., Hou, G.J., Bai, Y.S., 2006b. Lithological characteristics of the Baishahe Formation south of Xiangride town, Eastern Kunlun Mountains, and its age constrained from zircon Pb-Pb dating. Geol. Sci. Technol. Inform. 25, 1–7 [in Chinese with English abstract].

Chen, N.S., Wang, X.Y., Zhang, H.F., Sun, M., Li, X.Y., Chen, Q., 2007a. Geochemistry and Nd–Sr–Pb isotopic compositions of granitoids from Qaidam and Oulongbuluke micro-blocks, NW China: constraints on basement nature and tectonic affinity. Earth Sci. 32 (1), 7–21 [in Chinese with English abstract].

Chen, N.S., Xia, X.P., Li, X.Y., Sun, M., Xu, P., Liu, X.M., Wang, X.Y., Wang, Q.Y., 2007b. Timing of magmatism of the gneissic-granite plutons along north Qaidam margin and implications for Precambrian crustal accretions: zircon U-Pb dating and Hf isotope evidences. Acta Petrol. Sin. 23 (2), 501–512 (in Chinese with Englishi abstract).

Chen, Z.H., Xing, G.F., Guo, K.Y., Dong, Y.G., Chen, R., Zeng, Y., Li, L.M., He, Z.Y., Zhao, L., 2009a. Petrogenesis of keratophyes in the Pingshui Group, Zhejiang: Constraints from zircon U-Pb ages and Hf isotopes. Chin. Sci. Bull. 54 (9), 1570–1578.

Chen, Z.H., Guo, K.Y., Dong, Y.G., Chen, R., Li, L.M., Liang, Y.H., Li, C.H., Yu, X.M., Zhao, L., Xing, G.F., 2009b. Possible Early Neoproterozoic magmatism associated with slab window in the Pingshui segment of the Jiangshan-Shaoxing suture zone: Evidence from zircon LA-ICP-MS U-Pb geochronology and geochemistry. Sci. China (Ser. D) 52 (7), 925–939.

Chen, N.S., Gong, S.L., Sun, M., Li, X.Y., Long, X.P., Wang, Q.Y., Wu, F.Y., Xu, P., 2009c. Precambrian evolution of the Quanji block, northeastern margin of Tibet: Insights from zircon U-Pb and Lu-Hf isotope compositions. J. Asian Earth Sci. 35, 367–376.

Chen, N.S., Zhang, L., Sun, M., Wang, Q., Kusky, T.M., 2012. U-Pb and Hf isotopic compositions of detrital zircons from the paragneisses of the Quanji Massif, NW China: Implications for its early tectonic evolutionary history. J. Asian Earth Sci. 54–55, 110–130.

Chen, N.S., Gong, S.L., Long, X.P., Geng, H.Y., Wang, L., Sun, M., Kusky, T.M., 2013a. Zircon Hf isotope of Yingfeng Rapakivi granites from the Quanji Massif and ~2.7 Ga crustal growth. J. Earth Sci. 24, 29–41.

Chen, N.S., Liao, F.X., Wang, L., Santosh, M., Sun, M., Wang, Q.Y., Mustafa, H.A., 2013b. Late Paleoproterozoic multiple metamorphic events in the Quanji Massif: Links with Tarim and North China cratons and implications for assembly of the Columbia supercontinent. Precambrian Res. 228, 102–116.

Chen, W.T., Sun, W.H., Wang, W., Zhao, J.H., Zhou, M.F., 2014a. "Grenvillian" intra-plate mafic magmatism in the southwestern Yangtze Block, SW China. Precambrian Res. 242, 138–153.

Chen, X., Wang, D., Wang, X.L., Gao, J.F., Shu, X.J., Zhou, J.C., Qi, L., 2014b. Neoproterozoic chromite-bearing high-Mg diorites in the western part of the Jiangnan orogen, southern China: Geochemistry, petrogenesis and tectonic implications. Lithos 200–201, 35–48.

Chen, H., Ni, P., Chen, R.Y., Lü, Z.C., Pang, Z.S., Wang, G.G., Yuan, H.X., 2016. Chronology and geological significance of spillite-keratophyre in Pingshui Formation, Northwest Zhejiang Province. Geol. China 43 (2), 410–418 (in Chinese with English abstract).

Chen, Z.H., Zhao, L., Chen, D.D., Zhao, X.L., Xing, G.F., 2017. First discovery of a Palaeoproterozoic A-type granite in southern Wuyishan terrane, Cathaysia Block: Evidence from geochronology, geochemistry, and Nd-Hf-O isotopes. Int. Geol. Rev. 59 (1), 80–93.

Chen, W.T., Sun, W.H., Zhou, M.F., Wang, W., 2018. Ca. 1050Ma intra-continental rift-related A-type felsic rocks in the southwestern Yangtze Block, South China. Precambrian Res. 309, 22–44.

Chen, W., Lü, X., Yuan, Q., Huang, C., Cao, X., 2022. Petrogenesis and metallogenesis of the Kawuliuke Fe-P-Ti oxide-rich intrusive complex in the Kuluketage Block, northeastern Tarim Craton. Precambrian Res. 379, 106816.

Cheng, Z., Zhang, Z., Hou, T., Santosh, M., Chen, L., Ke, S., Xu, L., 2017a. Decoupling of Mg–C and Sr–Nd–O isotopes traces the role of recycled carbon in magnesiocarbonatites from the Tarim Large Igneous Province. Geochim. Cosmochim. Acta 202, 159–178.

Cheng, F., Jolivet, M., Hallot, E., Zhang, D., Zhang, C., Guo, Z., 2017b. Tectono-magmatic rejuvenation of the Qaidam craton, northern Tibet. Gondwana Res. 49, 248–263.

Collins, W.J., Beams, S.D., White, A.J.R., Chappell, B.W., 1982. Nature and origin of A-type granites with particular reference to southeastern Australia. Contrib. Mineral. Petrol. 80, 189–200. https://doi.org/10.1007/BF00374895.

Cui, X., Zhu, W.B., Fitzsimons, I.C.W., Wang, X., Lu, Y.Z., Wu, X.H., 2017. A possible transition from island arc to continental arc magmatism in the eastern Jiangnan Orogen, South China:Insights from a Neoproterozoic (870~860 Ma) gaboric-dioritic complex near the Fuchuan ophiolite. Gondwana Res. 46, 1–16.

Dalziel, I.W., 1991. Pacific margins of Laurentia and East Antarctica-Australia as a conjugate rift pair: evidence and implications for an Eocambrian supercontinent. Geology 19 (6), 598–601.

Dan, W., Li, X.H., Wang, Q., Tang, G.J., Liu, Y., 2014. An Early Permian (ca. 280 Ma) silicic igneous province in the Alxa Block, NW China: A magmatic flare-up triggered by a mantle-plume? Lithos 204, 144–158.

Deng, H., Kusky, T.M., Wang, L., Peng, S.B., Jiang, X.F., Wang, J.P., Wang, S.J., 2012. Discovery of a sheeted dike complex in the northern Yangtze Craton and its implications for craton evolution. J. Earth Sci. 23 (5), 676–695.

Deng, Q., Wang, J., Wang, Z.J., Wang, X.C., Qiu, Y.S., Yang, Q.X., Du, Q.D., Cui, X.Z., Zhou, X.L., 2013. Continental flood basalts of the Huashan Group, northern margin of the Yangtze block: Implications for the breakup of Rodinia. Int. Geol. Rev. 55 (15), 1865–1884.

Deng, Q., Wang, Z.J., Wang, J., Hu, Z.Z., Cui, X.Z., Du, Q.D., Ma, L., Xiong, X.H., Yang, F., 2016a. 800~780 Ma continental rift magmatism in the eastern part of the Jiangnan Orogen: Implications from ~790 Ma aluminous A-type granites in Zhejiang-Anhui-Jiangxi border area. Geol. Bull. China 35 (11), 1855–1868 (in Chinese with English abstract).

Deng, Q.Z., Yang, Q.X., Mao, X.W., Kong, L.Y., 2016b. Study of lithostratigraphic sequences and chronology of middle-late Nanhua in Wudang-Suizhou area. Resour. Environ. Eng. 30 (2), 132–142 (in Chinese with English abstract).

Deng, H., Peng, S.B., Polat, A., Kusky, T., Jiang, X.F., Han, Q.S., Wang, L., Huang, T., Wang, J.P., Zeng, W., Hu, Z.X., 2017. Neoproterozoic IAT intrusion into Mesoproterozoic MOR Miaowan ophiolite, Yangtze Craton:Evidence for evolving tectonic settings. Precambrian Res. 289, 75–94.

Ding, B.H., Shi, R.D., Zhi, X.C., Zheng, L., Chen, L., 2008. Neoproterozoic (~850Ma) subduction in the Jiangnan orogen: Evidence from the SHRIMP U-Pb dating of the SSZ-type ophiolite in southern Anhui Province. Acta Petrol. Mineral. 27 (5), 375–388 (in Chinese with English abstract).

Ding, H., Ma, D., Lin, Q., Jing, L., 2015. Age and nature of Cryogenian diamictites at Aksu, Northwest China: implications for Sturtian tectonics and climate. Int. Geol. Rev. 57, 2044–2064.

Ding, J., Zhang, S., Evans, D.A., Yang, T., Li, H., Wu, H., Chen, J., 2021. North China craton: The conjugate margin for northwestern Laurentia in Rodinia. Geology 49 (7), 773–778.

Domeier, M., Torsvik, T.H., 2014. Plate tectonics in the late Paleozoic. Geosci. Front. 5, 303–350. https://doi.org/10.1016/j.gsf.2014.01.002.

Dong, Y.P., Liu, X.M., Santosh, M., Zhang, X.N., Chen, Q., Yang, C., Yang, Z., 2011. Neoproterozoic subduction tectonics of the northwestern Yangtze Block in South China: Constrains from zircon U-Pb geochronology and geochemistry of mafic intrusions in the Hannan Massif. Precambrian Res. 189 (1-2), 66–90.

Dong, Y.P., Liu, X.M., Santosh, M., Chen, Q., Zhang, X.N., Li, W., He, D.F., Zhang, G.W., 2012. Neoproterozoic accretionary tectonics along the northwestern margin of the Yangtze Block, China: Constraints from zircon U-Pb geochronology and geochemistry. Precambrian Res. 196-197, 247–274.

Doughty, P.T., Price, R.A., Parrish, R.R., 1998. Geology and U-Pb geochronology of Archean basement and Proterozoic cover in the Priest River complex, northwestern United States, and their implications for Cordilleran structure and Precambrian continent reconstructions. Can. J. Earth Sci. 35 (1), 39–54.

Du, L.L., Yang, C.H., Geng, Y.S., Wang, X.S., Ren, L.D., Zhou, X.W., 2009. Petrogenesis of the Gaojiacun mafic-ultramafic pluton at the southwestern margin of Yangtze Block: Evidence from petrology, geochemistry and geochronology. Acta Petrol. Sin. 25 (8), 1897–1908 (in Chinese with English abstract).

Du, L.L., Guo, J.H., Nutman, A.P., Wyman, D., Geng, Y.S., Yang, C.H., Liu, F.L., Ren, L.D., Zhou, X.W., 2014. Implications for Rodinia reconstructions for the initiation of Neoproterozoic subduction at ~860Ma on the western margin of the Yangtze Block: Evidence from the Guandaoshan pluton. Lithos 196-197, 67–82.

Eby, G.N., 1990. The A-type granitoids: A review of their occurrence and chemical characteristics and speculations on their petrogenesis. Lithos 26, 115–134. https://doi.org/10.1016/0024-4937(90)90043-Z.

Eby, G.N., 1992. Chemical subdivision of the A-type granitoids:Petrogenetic and tectonic implications. Geology 20, 641–644. https://doi.org/10.1130/0091-7613(1992)020<0641:CSOTAT>2.3.CO;2.

Fan, H.P., Zhu, W.G., Li, Z.X., Zhong, H., Bai, Z.J., He, D.F., Chen, C.J., Cao, C.Y., 2013. Ca. 1.5 Ga mafic magmatism in South China during the break-up of the supercontinent Nuna/Columbia: the Zhuqing Fe–Ti–V oxide ore-bearing mafic intrusions in western Yangtze Block. Lithos 168, 85–98.

Faure, M., Trap, P., Lin, W., Monie, P., Bruguier, O., 2007. Polyorogenic evolution of the Paleoproterozoic Trans-North China Belt, new insights from the in Luliangshan-Hengshan-Wutaishan and Fuping massifs. Episodes 30 (2), 95–106.

Fitzsimons, I.C., 2000. Grenville-age basement provinces in East Antarctica: evidence for three separate collisional orogens. Geology 28 (10), 879–882.

Foster, D.A., Mueller, P.A., Mogk, D.W., Wooden, J.L., Vogl, J.J., 2006. Proterozoic evolution of the western margin of the Wyoming craton: Implications for the tectonic and magmatic evolution of the northern Rocky Mountains. Can. J. Earth Sci. 43 (10), 1601–1619.

Fu, J., Liang, X., Zhou, Y., Wang, C., Jiang, Y., Zhong, Y., 2015. Geochemistry, zircon U–Pb geochronology and Hf isotopes of granitic rocks in the Xitieshan area, North Qaidam, Northwest China: Implications for Neoproterozoic geodynamic evolutions of North Qaidam. Precambrian Res. 264, 11–29.

Gan, B., Diwu, C., Yan, J., Wang, T., Li, J., 2020. Formation and stabilization of the Dunhuang Block, NW China: Constraints from the Late Paleoproterozoic A-type granites of the Dunhuang Complex. Precambrian Res. 346, 105791.

Gao, W., Zhang, C.H., 2009. Zircon SHRIMP U-Pb ages of the Huangling granite and the tuff beds from Liantuo Formation in the Three Gorges area of Yangtze River, China and its geological significance. Geol. Bull. China 28 (1), 45–50 (in Chinese with English abstract).

Gao, J., Klemd, R., Long, L.L., Xiong, X.M., Qian, Q., 2009. Adakitic signature formed by fractional crystallization: An interpretation for the Neo-proterozoic meta-plagiogranites of the NE Jiangxi ophiolitic mélange belt, South China. Lithos 110 (1-4), 277–293.

Gao, L.Z., Liu, Y.X., Ding, X.Z., Zhang, C.H., Wang, Z.Q., Chen, J., Liu, Y.R., 2012. SHRIMP dating of Cangshuipu Group in the middle part of the Jiangnan Orogen and its implications for tectonic evolutions. Geol. China 39 (1), 12–20 (in Chinese with English abstract).
Gao, L.Z., Liu, Y.X., Ding, X.Z., Song, Z.R., Huang, Z.Z., Zhang, C.H., Zhang, H., Shi, Z.G., 2013. Geochronographic dating of the Tieshajie Formation in the Jiangshan-Shaoxing fault zone and its implications. Geol. Bull. China 32 (7), 996–1005 (in Chinese with English abstract).
Gao, L.Z., Zhang, H., Ding, X.Z., Liu, Y.X., Zhang, C.H., Huang, Z.Z., Xu, X.M., Zhou, Z.Y., 2014. SHRIMP zircon U-Pb dating of the Jiangshan-Shaoxing faulted zone in Zhejiang and Jiangxi. Geol. Bull. China 33 (6), 763–775 (in Chinese with English abstract).
Ge, R., Zhu, W., Wu, H., Zheng, B., He, J., 2013. Timing and mechanisms of multiple episodes of migmatization in the Korla Complex, northern Tarim Craton, NW China: Constraints from zircon U–Pb–Lu–Hf isotopes and implications for crustal growth. Precambrian Res. 231, 136–156.
Ge, R., Zhu, W., Wilde, S.A., Wu, H., He, J., Zheng, B., 2014. Archean magmatism and crustal evolution in the northern Tarim Craton: Insights from zircon U–Pb–Hf–O isotopes and geochemistry of ~2.7Ga orthogneiss and amphibolite in the Korla Complex. Precambrian Res. 252, 145–165.
Ge, R., Zhu, W., Wilde, S.A., He, J., Cui, X., 2015. Synchronous crustal growth and reworking recorded in late Paleoproterozoic granitoids in the northern Tarim craton: In situ zircon U-Pb-Hf-O isotopic and geochemical constraints and tectonic implications. Geol. Soc. Am. Bull. 127 (5–6), 781–803.
Ge, R., Zhu, W., Wilde, S.A., Wu, H., 2018. Remnants of Eoarchean continental crust derived from a subducted proto-arc. Sci. Adv. 4 (2), eaao3159.
Ge, R., Wilde, S.A., Kemp, A.I., Jeon, H., Martin, L.A., Zhu, W., Wu, H., 2020. Generation of Eoarchean continental crust from altered mafic rocks derived from a chondritic mantle: The ~ 3.72 Ga Aktash gneisses, Tarim Craton (NW China). Earth Planet. Sci. Lett. 538, 116225.
Ge, R., Wilde, S.A., Zhu, W., Zhou, T., Si, Y., 2022. Formation and evolution of Archean continental crust: A thermodynamic–geochemical perspective of granitoids from the Tarim Craton, NW China. Earth Sci. Rev. 234, 104219.
Gehrels, G.E., Yin, A., Wang, X.F., 2003a. Detrital-zircon geochronology of the northeastern Tibetan Plateau. Geol. Soc. Am. Bull. 115, 881–896.
Gehrels, G.E., Yin, A., Wang, X.F., 2003b. Magmatic history of the northeastern Tibetan Plateau. J. Geophys. Res. 108, 1–14.
Gehrels, G., Kapp, P., DeCelles, P., Pullen, A., Blakey, R., Weislogel, A., Ding, L., Guynn, J., Martin, A., McQuarrie, N., Yin, A., 2011. Detrital zircon geochronology of pre-Tertiary strata in the Tibetan-Himalayan orogen. Tectonics 30 (5), 2011TC002868.
Geng, Y.S., Yang, C.H., Du, L.L., Wang, X.S., Ren, L.D., Zhou, X.W., 2007. Chronology and tectonic environment of the Tianbaoshan Formation: New evidence from zircon SHRIMP U-Pb age and geochemistry. Geol. Rev. 53 (4), 323–334 (in Chinese with English abstract).
Geng, Y.S., Kuang, H.W., Liu, Y.Q., Du, L.L., 2017. Subdivision and correlation of the Mesoproterozoic stratigraphy in the western and northern margins of Yangtze Block. Acta Geol. Sin. 91 (10), 2151–2174 (in Chinese with English abstract).
Geng, Y.S., Du, L.L., Kuang, H.W., Liu, Y.Q., 2020. Ca. 1.7 Ga Magmatism on Southwestern Margin of the Yangtze Block: Response to the Breakup of Columbia. Acta Geol. Sin.-English Edition 94 (6), 2031–2052.
Gong, J.H., Zhang, J.X., Yu, S.Y., Li, H.K., Hou, K.J., 2012a. Ca. 2.5 Ga TTG rocks in the western Alxa Block and their implications. Chin. Sci. Bull. 57, 4064–4076.
Gong, S.L., Chen, N.S., Wang, Q.Y., Kusky, T.M., Wang, L., Zhang, L., Ba, J., Liao, F.X., 2012b. Early Paleoproterozoic magmatism in the Quanji Massif, northeastern margin of the Qinghai-Tibet Plateau and its tectonic significance: LA-ICP-MS U-Pb zircon geochronology and geochemistry. Gondwana Res. 21, 152–166.
Gong, S., Chen, N., Geng, H., Sun, M., Zhang, L., Wang, Q., 2014. Zircon Hf isotopes and geochemistry of the early Paleoproterozoic high-Sr low-Y quartz-diorite in the Quanji massif, NW China: crustal growth and tectonic implications. J. Asian Earth Sci. 25 (1), 74–86.
Gong, J.H., Zhang, J.X., Wang, Z.Q., Yu, S.Y., Li, H.K., Li, Y.S., 2016. Origin of the Alxa Block, western China: New evidence from zircon U-Pb geochronology and Hf isotopes of the Longshoushan Complex. Gondwana Res. 36, 359–375.
Gong, S., He, C., Wang, X.-C., Chen, N., Kusky, T., 2019. No plate tectonic shutdown in the early Paleoproterozoic: Constraints from the ca. 2.4 Ga granitoids in the Quanji Massif, NW China. J. Asian Earth Sci. 172, 221–242.
Grenholm, M., 2019. The global tectonic context of the ca. 2.27-1.96 Ga Birimian Orogen–Insights from comparative studies, with implications for supercontinent cycles. Earth Sci. Rev. 193, 260–298.
Guo, Z.-J., Yin, A., Robinson, A., Jia, C.-Z., 2005. Geochronology and geochemistry of deep drill-core samples from the basement of the central Tarim basin. J. Asian Earth Sci. 25, 45–56.
Guo, C.L., Wang, D.H., Chen, Y.C., Zhao, Z.G., Wang, Y.B., Fu, X.F., Fu, D.M., 2007. SHRIMP U-Pb zircon ages and major element, trace element and Nd-Sr isotope geochemical studies of a Neoproterozoic granitic complex in western Sichuan: Petrogenesis and tectonic significance. Acta Petrol. Sin. 23 (10), 2457–2470 (in Chinese with English abstract).
Guo, J.H., Peng, P., Chen, Y., Jiao, S., Windley, B.F., 2012. UHT sapphirine granulite metamorphism at 1.93–1.92 Ga caused by gabbronorite intrusions: Implications for tectonic evolution of the northern margin of the North China Craton. Precambrian Res. 222–223, 124–142.
Guo, X.C., Zheng, Y.Z., Gao, J., Zhu, Z.X., 2013. Determination and Geological significance of the Mesoarchean Craton in Western Kunlun Mountains, Xinjiang, China. Geol. Rev. 59, 401–412 (in Chinese with English abstract).
Guo, Y., Wang, S.W., Sun, X.M., Wang, Z.Z., Yang, B., Liao, Z.W., Zhou, B.G., Jiang, X.F., Hou, L., Yang, B., 2014. The Paleoproterozoic breakup event in the Southwest Yangtze Block: Evidence from U-Pb zircon age and geochemistry of diabase in Wuding, Yunnan Province, SW China. Acta Geol. Sin. 88 (9), 1651–1665 (in Chinese with English abstract).
Guo, J.H., Zhai, M.G., Peng, P., Jiao, S., Zhao, L., Wang, H., 2015. Paleoproterozoic granulites in the North China Craton and their geological implications. In: Precambrian Geology of China. Springer, Berlin, Heidelberg, pp. 137–169.
Halls, H.C., Li, J., Davis, D., Hou, G., Zhang, B., Qian, X., 2000. A precisely dated Proterozoic palaeomagnetic pole from the North China craton, and its relevance to palaeocontinental reconstruction. Geophys. J. Int. 143 (1), 185–203.
Han, G., Liu, Y., Neubauer, F., Genser, J., Li, W., Zhao, Y., Liang, C., 2011. Origin of terranes in the eastern Central Asian Orogenic Belt, NE China: U-Pb ages of detrital zircons from Ordovician–Devonian sandstones, North Da Xing'an Mts. Tectonophysics 511, 109–124.
Han, Y., Zhao, G., Cawood, P.A., Sun, M., Eizenhöfer, P.R., Hou, W., et al., 2016. Tarim and North China cratons linked to northern Gondwana through switching accretionary tectonics and collisional orogenesis. Geology 44 (2), 95–98.
Han, S.X., Wu, C., Zhou, Z.G., Wang, G.S., 2020. Geology, geochemistry, and geochronology of the paleoproterozoic Donggouzi mafic-ultramafic complex: Implications for the evolution of the North China craton. Lithos 366, 105567.
Hao, J., Wang, C., Liu, L., Wu, H., Yang, W., Kang, L., Gai, Y., Cao, Y., Meert, J.G., Ma, D., Li, H., Yu, Z., Sun, X., Zhang, S., 2022. Reappraisal of the petrogenetic processes of Neoproterozoic granitoids in the Altyn Tagh, NW China: Implications for reconstruction of the Qaidam block in Rodinia. Precambrian Res. 379, 106782.
He, B., Xu, Y.G., Paterson, S., 2009. Magmatic diapirism of the Fangshan pluton, southwest of Beijing, China. J. Struct. Geol. 31 (6), 615–626.
He, Z.-Y., Zhang, Z.-M., Zong, K.-Q., Dong, X., 2013. Paleoproterozoic crustal evolution of the Tarim Craton: Constrained by zircon U–Pb and Hf isotopes of meta-igneous rocks from Korla and Dunhuang. J. Asian Earth Sci. 78, 54–70.
He, C., Gong, S.L., Wang, L., Chen, N.S., Santosh, M., Wang, Q.Y., 2018. Protracted postcollisional magmatism during plate subduction shutdown in early Paleoproterozoic: insights from post-collisional granitoid suite in NW China. Gondwana Res. 55, 92–111.
He, J., Pan, X., Li, S., Li, D., Tao, X., Xu, B., 2021. Early Neoproterozoic continuous oceanic subduction along the northern margin of the Tarim Block: Insights from ca. 910–870 Ma arc-related magmatism in the Aksu area, NW China. Precambrian Res. 360, 106236.
Heubeck, C., Hendrix, M.S., Davis, G.A., 2001. Assembly of central Asia during the middle and late Paleozoic. MEMOIRS-Geol. Soc. Am. 1–22.
Hoffman, P.F., 1991. Did the breakout of Laurentia turn Gondwanaland inside-out? Science 252 (5011), 1409–1412.
Hoffman, P.F., Kaufman, A.J., Halverson, G.P., Schrag, D.P., 1998. Comings and goings of global glaciations on a Neoproterozoic tropical platform in Namibia. GSA Today 8 (5), 1–9.
Hoffmann, P.F., Schrag, D.P., 2000. Snowball earth. Sci. Am. 282 (1), 68–75.
Horton, B.K., Capaldi, T.N., Perez, N.D., 2022. The role of flat slab subduction, ridge subduction, and tectonic inheritance in Andean deformation. Geology 50 (9), 1007–1012.
Hu, A.-Q., Rogers, G., 1992. Discovery of 3.3 Ga Archaean rocks in north Tarim Block of Xinjiang, western China. Chin. Sci. Bull. 37, 1546–1549.
Hu, A.Q., Wei, G.J., Jiang, B.M., Zhang, J.B., Deng, W.F., Chen, L.L., 2010. Formation of the 0.9 Ga Neoproterozoic granitoids in the Tianshan orogen, NW China: Constraints from the SHRIMP zircon age determination and its tectonic significance. Geochimica 39, 197–212 [in Chinese with English abstract].
Hu, Z.X., Chen, C., Mao, X.W., Deng, Q.Z., Yang, J.X., Li, L.J., Kong, L.Y., 2015. Documentation of Jinningian island-arc volcanic rocks and accretionary complexes in the Dahongshan region, northern Hubei and its tectonic significance. Resour. Environ. Eng. 29 (6), 757–766 (in Chinese with English abstract).
Hu, P.Y., Zhai, Q.G., Wang, J., Tang, Y., Ren, G.M., 2017. The Shimian ophiolite in the western Yangtze Block, SW China: Zircon SHRIMP U-Pb ages, geochemical and Hf-O isotopic characteristics, and tectonic implications. Precambrian Res. 298, 107–122.
Huang, X.L., Xu, Y.G., Li, X.H., Li, W.X., Lan, J.B., Zhang, H.H., Liu, Y.S., Wang, Y.B., Li, H.Y., Luo, Z.Y., Yang, Q.J., 2008. Petrogenesis and tectonic implications of Neoproterozoic, highly fractionated A-type granites from Mianning, South China. Precambrian Res. 165 (3-4), 190–204.
Huang, W., Zhang, L., Ba, J., Liao, F.X., Chen, N.S., 2011. Detrital zircon LA-ICP-MS U-Pb dating for K-feldspar leptite of Quanji massif in the north margin of Qaidam Block: constraint on the age of Dakendaban Group. Geol. Bull. Chin. 30, 1353–1359 (in Chinese with English abstract).
Huang, B., Kusky, T., Johnson, T., Wilde, S., Wang, L., Polat, A., Fu, D., 2020. Paired metamorphism in the Neoarchean: a record of accretionary-to-collisional orogenesis in the North China Craton. Earth Planet. Sci. Lett. 543, 116355.
Huang, R., He, Z., De Grave, J., 2022a. Did a Late Paleoproterozoic-Early Mesoproterozoic Landmass Exist in the Eastern Cathaysia Block? New Evidence from Detrital Zircon U-Pb Geochronology and Sedimentary Indicators. Minerals 12, 1199.
Huang, B., Johnson, T.E., Wilde, S.A., Polat, A., Fu, D., Kusky, T., 2022b. Coexisting divergent and convergent plate boundary assemblages indicate plate tectonics in the Neoarchean. Nat. Commun. 13 (1), 6450.
Huang, B., Liu, M., Kusky, T.M., Johnson, T.E., Wilde, S.A., Fu, D., Deng, H., Qian, Q., 2023. Changes in orogenic style and surface environment recorded in Paleoproterozoic foreland successions. Nat. Commun. 14 (1), 7997.
Jackson, S.E., Pearson, N.J., Griffin, W.L., Belousova, E.A., 2004. The application of laser ablation-inductively coupled plasma-mass spectrometry to in situ U-Pb zircon geochronology. Chem. Geol. 211 (1–2), 47–69.

Jahn, B., Wu, F., Capdevila, R., Martineau, F., Zhao, Z., Wang, Y., 2001. Highly evolved juvenile granites with tetrad REE patterns: the Woduhe and Baerzhe granites from the Great Xing'an Mountains in NE China. Lithos 59, 171–198.
Ji, B., Yu, J.Y., Li, X.M., Huang, B.T., Wang, L., 2018. The disintegration of Balonggongge'er Formation and the definition of lithostratigraphic unit in Danghenanshan area of South Qilian Mountain: Evidence from petrology and chronology. Geol. Bull. China 37 (4), 621–633 (in Chinese with English abstract).
Jiang, C.Y., Jiang, C., Jiang, H.B., Ye, S.F., Xia, M.Z., Lu, D.X., 2005. Petrochemical characteristics, Nd, Sr, Pb isotopic compositions and petrogenesis of Permian dike swarm, Kuruktag Region, Xinjiang. Acta Geol. Sin. 6 (79), 823–833.
Jiang, Y., Zhao, X.L., Xing, G.F., Li, L.M., Duan, Z., 2015. Arc magmatic activity of Qingbaikou Period along the southeastern margin of Yangtze Block: Implications from the zircon U-Pb age and geochemical characteristics of Nb-enriched gabbro and high-Mg diorite in the Jinhua plutonic complex. Geol. Bull. China 34 (8), 1550–1561 (in Chinese with English abstract).
Jiang, X.F., Peng, S.B., Kusky, T., Wang, L., Deng, H., Wang, J.P., 2017. Formation time of the northeastern Jiangxi ophiolite in the eastern Jiangnan Orogenic Belt: Evidence from LA-ICP-MS zircon U-Pb dating of the gabbro. Geoscience 31 (4), 697–704 (in Chinese with English abstract).
Jin, T.F., Li, Y.G., Fei, G.C., Feng, Y.C., Zhou, H., Sha, X.B., Wu, K., 2017. Geochronology of zircon U-Pb from Hongshan Formation in the Dahongshan Group in the Southwest Yangtze block for the redefinitions of the forming age of the protolith and metamorphic age. Geol. Rev. 63 (4), 894–910 (in Chinese with English abstract).
Kanasewich, E., Gorman, A., Asudeh, I., Clowes, R., Hajnal, Z., Ellis, R., Miller, K., Henstock, T., Spence, G., Keller, R., Levander, A., Snelson, C., Burianyk, M., 2002. Deep Probe: Imaging the roots of western North America. Can. J. Earth Sci. 39, 375–398.
Karlstrom, K.E., Harlan, S.S., Williams, M.L., McLelland, J., Geissman, J.W., Ahall, K.I., 1999. Refining Rodinia: Geologic evidence for the Australia–western US connection in the Proterozoic. GSA Today 9 (10), 1–7.
Kaufman, A.J., Knoll, A.H., Narbonne, G.M., 1997. Isotopes, ice ages, and terminal Proterozoic earth history. Proc. Natl. Acad. Sci. 94 (13), 6600–6605.
Keller, C.B., Harrison, T.M., 2020. Constraining the crustal silica on ancient Earth. Proc. Natl. Acad. Sci. 117 (35), 21101–21107.
Kelty, T.K., Yin, A., Dash, B., Gehrels, G.E., Ribeiro, A.E., 2008. Detrital-zircon geochronology of Paleozoic sedimentary rocks in the Hangay-Hentey basin, north-central Mongolia: Implications for the tectonic evolution of the Mongol–Okhotsk Ocean in central Asia. Tectonophysics 451, 290–311.
Korenaga, J., 2020. Plate tectonics and surface environment: Role of the oceanic upper mantle. Earth Sci. Rev. 205, 103185.
Kröner, A., Wilde, S.A., Li, J.H., Wang, K.Y., 2005. Age and evolution of a late Archean to Paleoproterozoic upper to lower crustal section in the Wutaishan/Hengshan/Fuping terrain of northern China. J. Asian Earth Sci. 24 (5), 577–595.
Kröner, A., Wilde, S.A., Zhao, G.C., O'Brien, J., Sun, M., Liu, D.Y., 2006. Zircon geochronology and metamorphic evolution of mafic dykes in the Hengshan Complex of northern China: Evidence for late Palaeoproterozoic extension and subsequent high pressure metamorphism in the North China craton. Precambrian Res. 146 (1–2), 45–67.
Kröner, A., Alexeiev, D.V., Rojas-Agramonte, Y., Hegner, E., Wong, J., Xia, X., Belousova, E., Mikolaichuk, A.V., Seltmann, R., Liu, D., Kiselev, V.V., 2013. Mesoproterozoic (Grenville-age) terranes in the Kyrgyz North Tianshan: Zircon ages and Nd-Hf isotopic constraints on the origin and evolution of basement blocks in the southern Central Asian orogen. Gondwana Res. 23, 272–295.
Kusky, T.M., Li, J.H., 2003. Paleoproterozoic tectonic evolution of the North China craton. J. Asian Earth Sci. 22 (4), 383–397. https://doi.org/10.1016/S1367-9120(03)00071-3.
Kusky, T., Mooney, W., 2015. Is the Ordos Basin floored by a trapped oceanic plateau? Earth Planet. Sci. Lett. 429, 197–204.
Kusky, T.M., Santosh, M., 2009. The Columbia connection in North China. In: Reddy, S. M., Mazumder, R., Evans, D.A.D., Collins, A.S. (Eds.), Palaeoproterozoic Supercontinents and Global Evolution. Geological Society of London, p. 0. https://doi.org/10.1144/SP323.3.
Kusky, T.M., Traore, A., 2023. A paradigm shift: North China craton's North Margin Orogen is the collisional suture with the Columbia supercontinent. Geochem. Geophys. Geosyst. 24 (2), e2022GC010797.
Kusky, T.M., Li, J.H., Tucker, R.D., 2001. The Archean Dongwanzi ophiolite complex, North China Craton: 2.505-billion-year-old oceanic crust and mantle. Science 292 (5519), 1142–1145.
Kusky, T.M., Li, J.H., Santosh, M., 2007. The Paleoproterozoic North Hebei orogen: North China craton's collisional suture with the Columbia supercontinent. Gondwana Res. 12 (1–2), 4–28.
Kusky, T.M., Polat, A., Windley, B.F., Burke, K.C., Dewey, J.F., Kidd, W.S.F., 2016. Insights into the tectonic evolution of the North China craton through comparative tectonic analysis: A record of outward growth of Precambrian continents. Earth Sci. Rev. 162, 387–432.
Kusky, T.M., Windley, B.F., Polat, A., 2018. Geological Evidence for the Operation of Plate Tectonics throughout the Archean: Records from Archean Paleo-Plate Boundaries. J. Earth Sci. 29 (6), 1291–1303.
Kusky, T.M., Windley, B.F., Polat, A., Wang, L., Ning, W.B., Zhong, Y.T., 2021. Archean dome-and-basin style structures form during growth of intraoceanic and continental margin arcs and their death by slab failure and collision. Earth Sci. Rev. 220, 103725.
Kusky, T., Huang, Y., Wang, L., Robinson, P., Wirth, R., Polat, A., Wei, H., 2022. Vestiges of early Earth's deep subduction and CHONSP cycle recorded in Archean ophiolitic podiform chromitites. Earth Sci. Rev. 227, 103968.
Lai, S.C., Li, Y.F., Qin, J.F., 2007. Geochemistry and LA-ICP-MS zircon U-Pb dating of the Dongjiahe ophiolite complex from the western Bikou terranein. Sci. China (Ser. D) 50 (2), 305–313.
Le Maitre, R.W.B., Dudek, P., Keller, A., Lameyre, J., Le Bas, J., Sabine, M.J., Schmid, P. A., Sorensen, R., Streckeisen, H., Woolley, A., Zanettin, A.R., 1989. A Classification of Igneous Rocks and Glossary of terms. In: Recommendations of the International Union of Geological Sciences, Subcommission on the Systematics of Igneous Rocks (No. 552.3 CLA). International Union of Geological Sciences, Oxford, Blackwell, 193 p.
Lei, R., Wu, C., Chi, G., Chen, G., Gu, L., Jiang, Y., 2012. Petrogenesis of the Palaeoproterozoic Xishankou pluton, northern Tarim block, northwest China: implications for assembly of the supercontinent Columbia. Int. Geol. Rev. 54 (15), 1829–1842.
Levashova, N.M., Kalugin, V.M., Gibsher, A.S., Yff, J., Ryabinin, A.B., Meert, J.G., Malone, S.J., 2010. The origin of the Baydaric microcontinent, Mongolia: Constraints from paleomagnetism and geochronology. Tectonophysics 485, 306–320.
Levashova, N.M., Meert, J.G., Gibsher, A.S., Grice, W.C., Bazhenov, M.L., 2011. The origin of microcontinents in the Central Asian Orogenic Belt: constraints from paleomagnetism and geochronology. Precambrian Res. 185 (1–2), 37–54.
Li, X.H., 1999a. U-Pb zircon ages of granites from northern Guangxi and their tectonic significance. Geochimica 28 (1), 1–9 (in Chinese with English abstract).
Li, X.H., 1999b. U-Pb zircon ages of granites from the southern margin of the Yangtze Block: timing of Neoproterozoic Jinning: Orogeny in SE China and implications for Rodinia assembly. Precambrian Res. 97 (1-2), 43–57.
Li, T., 2010. The study of Neoproterozoic tectonic-magmatic events in the northern margin of the Yangtze continental. Master Degree Thesis. Chang'an University, Xi'an, pp. 1–55 (in Chinese).
Li, Q.W., Zhao, J.H., 2018. The Neoproterozoic high-Mg dioritic dikes in South China formed by high pressures fractional crystallization of hydrous basaltic melts. Precambrian Res. 309, 198–211.
Li, X.H., Zhou, G.Q., Zhao, J.X., Fanning, C.M., Compston, W., 1994. SHRIMP ion microprobe zircon U-Pb age of the NE Jiangxi ophiolite and its tectonic implications. Geochimica 23 (2), 125–131.
Li, Z.X., Zhang, L., Powell, C.M., 1995. South China in Rodinia: Part of the missing link between Australia–East Antarctica and Laurentia? Geology 23, 407–410.
Li, X.H., Liu, Y., Tu, X.L., Liu, H.C., Ling, X.S., 1996. Multiple-stage evolution of zircon U-Pb isotopic systematics in S-type granites and its chronological significance: A case study on Sanfang granite, northern Guangxi. Acta Mineral. Sin. 16 (2), 170–177 (in Chinese with English abstract).
Li, X.H., Wang, Y.X., Zhao, Z.H., Chen, D.F., Zhang, H., 1998. SHRIMP U-Pb zircon geochronology for amphibolite from the Precambrian basement in SW Zhejiang and NW Fujian provinces. Geochimica 27 (4), 327–334 (in Chinese with English abstract).
Li, Z.X., Li, X.H., Kinney, P.D., Wang, J., 1999. The breakup of Rodinia: Did it start with a mantle plume beneath South China. Earth Planet. Sci. Lett. 173 (3), 171–181.
Li, X.H., Zhou, H.W., Li, Z.X., Liu, Y., 2001a. Zircon U-Pb age and petrochemical characteristics of the Neoproterozoic bimodal volcanics from western Yangtze block. Geochimica 30 (4), 315–322 (in Chinese with English abstract).
Li, X.H., Li, Z.X., Ge, W.C., Zhou, H.W., Li, W.X., Liu, Y., 2001b. U-Pb zircon ages of the Neoproterozoic granitoids in South China and their tectonic implications. Bull. Mineral. Petrol. Geochem. 20 (4), 271–273 (in Chinese with English abstract).
Li, H.M., Lu, S.N., Zheng, J.K., 2001c. Dating of 3.6 Ga zircon in granite gneiss from the eastern Altyn Mountain and its geological significance. J. Bull. Mineral. Petrol. Geochem. 20, 259–262 in Chinese with English abstract.
Li, X.H., Li, Z.X., Zhou, H.W., Liu, Y., 2002a. SHRIMP U-Pb zircon geochronological geochemical and Nd isotopic study of the Neoproterozoic granitoids in southern Anhui. Geol. Rev. 48 (Suppl), 8–16 (in Chinese with English abstract).
Li, Z.X., Li, X.H., Zhou, H.W., Kinny, P.D., 2002b. Grenvillian continental collision in South China: New SHRIMP U-Pb zircon results and implications for the configuration of Rodinia. Geology 30 (2), 163–166.
Li, X.H., Li, Z.X., Zhou, H.W., Liu, Y., Liang, X.R., Li, W.X., 2003a. SHRIMP U-Pb zircon age, geochemistry and Nd isotope of the Guandaoshan pluton in SW Sichuan: Petrogenesis and tectonic significance. Sci. China (Ser. D) 46 (1), 73–83.
Li, X.-H., Li, Z.-X., Ge, W., Zhou, H., Li, W., Liu, Y., Wingate, M.T.D., 2003b. Neoproterozoic granitoids in South China: crustal melting above a mantle plume at ca. 825 Ma? Precambrian Res. 122 (1), 45–83.
Li, Z.X., Li, X.H., Kinny, P.D., Wang, J., Zhang, S., Zhou, H., 2003c. Geochronology of Neoproterozoic syn-rift magmatism in the Yangtze Craton, South China and correlations with other continents: evidence for a mantle superplume that broke up Rodinia. Precambrian Res. 122 (1), 85–109.
Li, X.H., Su, L., Song, B., Liu, D.Y., 2004. SHRIMP U-Pb zircon age of the Jinchuan ultramafic intrusion and its geological significance. Chin. Sci. Bull. 49, 420.
Li, W.X., Li, X.H., Li, Z.X., 2005a. Neoproterozoic bimodal magmatism in the Cathaysia Block of South China and its tectonic significance. Precambrian Res. 136 (1), 51–66.
Li, X.H., Su, L., Chung, S.L., Li, Z.X., Liu, Y., Song, B., Liu, D.Y., 2005b. Formation of the Jinchuan ultramafic intrusion and the world's third largest Ni-Cu sulfide deposit: Associated with the ~825 Ma south China mantle plume? Geochem. Geophys. Geosyst. 6, Q11004.
Li, X.Y., Chen, N.S., Xia, N.P., Sun, M., Xu, P., Wang, Q.Y., Wang, X.Y., 2007. Onstraints on timing of the early Paleoproterozoic magmatism and crustal evolution of the Oulongbuluke microcontinent: U-Ph and Lu-Hf isotope systematics of zircons from Mohe granitic pluton. Acta Petrol. Sin. 23 (2), 513–522.
Li, Z.-X., Li, X.-H., Li, W.-X., Ding, S., 2008a. Was Cathaysia part of Proterozoic Laurentia? – new data from Hainan Island, south China. Terra Nova 20 (2), 154–164.

Li, W.X., Li, X.H., Li, Z.X., Lou, F.S., 2008b. Obduction-type granites within the NE Jiangxi Ophiolite: Implications for the final amalgamation between the Yangtze and Cathaysia blocks. Gondwana Res. 13 (3), 288–301.
Li, X.-H., Li, W.-X., Li, Z.-X., Liu, Y., 2008c. 850–790 Ma bimodal volcanic and intrusive rocks in northern Zhejiang, South China: A major episode of continental rift magmatism during the breakup of Rodinia. Lithos 102 (1), 341–357.
Li, Z.X., Bogdanova, S., Collins, A.S., Davidson, A., De Waele, B., Ernst, R.E., Fitzsimons, I.C.W., Fuck, R.A., Gladkochub, D.P., Jacobs, J., Karlstrom, K.E., Lu, S., Natapov, L.M., Pease, V., Pisarevsky, S.A., Thrane, K., Vernikovsky, V., 2008d. Assembly, configuration, and break-up history of Rodinia: a synthesis. Precambrian Res. 160 (1–2), 179–210.
Li, D.P., Chen, Y.L., Luo, Z.H., Zhao, J.X., 2009a. Zircon SHRIMP U-Pb dating and Neoproterozoic metamorphism of Kangding and Yuanmou intrusive complexes, Sichuan and Yunnan. J. Earth Sci. 20 (6), 897–908.
Li, X.H., Li, W.X., Li, Z.X., Lo, C.H., Wang, J., Ye, M.F., Yang, Y.H., 2009b. Amalgamation between the Yangtze and Cathaysia Blocks in South China: Constraints from SHRIMP U–Pb zircon ages, geochemistry and Nd–Hf isotopes of the Shuangxiwu volcanic rocks. Precambrian Res. 174 (1), 117–128.
Li, H., Lu, S., Su, W., Xiang, Z., Zhou, H., Zhang, Y., 2013a. Recent advances in the study of the Mesoproterozoic geochronology in the North China Craton. J. Asian Earth Sci. 72, 216–227.
Li, H.K., Zhang, C.L., Xiang, Z.Q., Lu, S.N., Zhang, J., Geng, J.Z., Qu, L.S., Wang, Z.X., 2013b. Zircon and baddeleyite U-Pb geochronology of the Shennongjia Group in the Yangtze Craton and its tectonic significance. Acta Petrol. Sin. 29 (2), 673–697 (in Chinese with English abstract).
Li, L.M., Lin, S.F., Xing, G.F., Davis, D.W., Davis, W.J., Xiao, W.J., Yin, C.Q., 2013c. Geochemistry and tectonic implications of Late Mesoproterozoic alkaline bimodal volcanic rocks from the Tieshajie Group in the southeastern Yangtze Block, South China. Precambrian Res. 230, 179–192.
Li, X.H., Li, Z.X., Li, W.X., 2014. Detrital zircon U–Pb age and Hf isotope constrains on the generation and reworking of Precambrian continental crust in the Cathaysia Block, South China: a synthesis. Gondwana Res. 25 (3), 1202–1215.
Li, Y., Xie, H.Q., Song, Z.R., 2017. SHRIMP U-Pb zircon ages of the northeastern Jiangxi ophiolites and the Zhangcun Group and a discussion on the tectonic evolution of the Jiangnan Orogen. Geol. Rev. 63 (4), 854–868 (in Chinese with English abstract).
Li, J.Y., Wang, X.L., Gu, Z.D., 2018a. Early Neoproterozoic arc magmatism of the Tongmuliang Group on the northwestern margin of the Yangtze Block: Implications for Rodinia assembly. Precambrian Res. 309, 181–197.
Li, M., Wang, C., Li, R.S., Peng, Y., Shao, D., Chen, F.M., Chen, S.J., Pan, X.P., 2018b. The Detrital Zircon Geochronology and Geological significance of the Zhoujieshan Formation, Quanji Group in the north margin of Qaidam Basin. Earth Sci. 43 (12), 4390–4398 (in Chinese with English abstract).
Li, M., Wang, C., Li, R.S., Meert, J.G., Peng, Y., Zhang, J.H., 2019. Identifying late Neoproterozoic-early Paleozoic sediments in the South Qilian Belt, China: A peri-Gondwana connection in the northern Tibetan Plateau. Gondwana Res. 76, 173–184.
Li, X.C., Fan, H.R., Zeng, X., Yang, K.F., Yang, Z.F., Wang, Q.W., Li, H.T., 2021. Identification of~ 1.3 Ga hydrothermal zircon from the giant Bayan Obo REE deposit (China): Implication for dating geologically-complicated REE ore system. Ore Geol. Rev. 138, 104405.
Li, C., Niu, M., Li, X., Yan, Z., Wu, Q., Sun, Y., Yuan, X., 2022. Origin and Precambrian paleogeography of the North Wulan terrane, northwestern China: a coherent model of the Tarim–Qilian–Quanji continent during the Columbia-Rodinia supercontinent cycle. Gondwana Res. 101, 132–155.
Li, C., Niu, M., Li, X., Yan, Z., Wang, L., 2024. Nature of early Mesoproterozoic magmatism in the Qilian-North Qaidam tectonic belt, NW China: Implications for prolonged extension processes and transition from Columbia to Rodinia. Gondwana Res. 126, 322–342.
Liao, F.X., Zhang, L., Chen, N.S., Sun, M., Santosh, M., Wang, Q.Y., Hassan, A.M., 2014. Geochronology and geochemistry of meta-mafic dykes in the Quanji Massif, NW China: Paleoproterozoic Evolution of the Tarim Craton and implications on the Assembly of the Columbia Supercontinent. Precambrian Res. 249, 33–56.
Lin, G.C., 2010. Zircon U-Pb age and petrochemical characteristics of Shimian granite in western Sichuan: Petrogenesis and tectonic significance. Earth Sci. 35 (4), 611–620 (in Chinese with English abstract).
Lin, G.C., Li, X.H., Li, W.X., 2007. SHRIMP U-Pb zircon age, geochemistry and Nd-Hf isotope of Neoproterozoic mafic dyke swarms in western Sichuan: Petrogenesis and tectonic significance. Sci. China (Ser. D) 50 (1), 1–16.
Lin, M.S., Peng, S.B., Jiang, X.F., Polat, A., Kysky, T., Wang, Q., Deng, H., 2016. Geochemistry, petrogenesis and tectonic setting of Neoproterozoic mafic-ultramafic rocks from the western Jiangnan Orogen, South China. Gondwana Res. 35, 338–356.
Lin, S., Xing, G., Davis, D.W., Yin, C., Wu, M., Li, L., et al., 2018. Appalachian-style multi-terrane Wilson cycle model for the assembly of South China. Geology 46 (4), 319–322.
Ling, W.L., Gao, S., Zhang, B.R., Li, H.M., Liu, Y., Cheng, J.P., 2003. Neoproterozoic tectonic evolution of the northwestern Yangtze Craton, South China: Implications for amalgamation and break-up of the Rodinia Supercontinent. Precambrian Res. 122 (1-4), 111–140.
Ling, W.L., Gao, S., Cheng, J.P., Jiang, L.S., Yuan, H.L., Hu, Z.C., 2006. Neoproterozoic magmatic events within the Yangtze continental interior and along its northern margin and their tectonic implication: Constraint from the ELA-ICPMS U-Pb geochronology of zircons from the Huangling and Hannan complexes. Acta Petrol. Sin. 22 (2), 387–396 (in Chinese with English abstract).
Ling, W.L., Ren, B.F., Duan, R.C., Liu, X.M., Mao, X.W., Peng, L.H., Liu, Z.X., Cheng, J.P., Yang, H.M., 2008. Timing of the Wudangshan, Yaolinghe volcanic sequences and mafic sills in South Qinling: U-Pb zircon geochronology and tectonic implication. Chin. Sci. Bull. 53 (14), 2192–2199.
Liu, S.W., Yan, Q.R., Li, Q.G., Wang, Z.Q., 2009. Petrogenesis of granitoid rocks in the Kangding Complex, western margin of the Yangtze Craton and its tectonic significance. Acta Petrol. Sin. 25 (8), 1883–1896 (in Chinese with English abstract).
Liu, Y.C., Liu, L.X., Gu, X.F., Li, S.G., Liu, J., Song, B., 2010. Occurrence of Neoproterozoic low-grade metagranite in the western Beihuaiyang zone, the Dabie Orogen. Chin. Sci. Bull. 55 (30), 3490–3498.
Liu, R.Y., Niu, B.G., He, Z.J., Ren, J.S., 2011. LA-ICP-MS zircon U-Pb geochronology of the eastern part of the Xiaomaoling composite intrusives in Zhashui area, Shaanxi, China. Geol. Bull. China 30 (2-3), 448–460 (in Chinese with English abstract).
Liu, Z., Jiang, Y.H., Wang, G.C., Ni, C.Y., Qing, L., Zhang, Q., 2015. Middle Neoproterozoic (~845Ma) continental arc magmatism along the northwest side of the Jiangshan-Shaoxing suture, South China: Geochronology, geochemistry, petrogenesis and tectonic implications. Precambrian Res. 268, 212–226.
Liu, Y.C., Liu, L.X., Li, Y., Gu, X.F., Song, B., 2017. Zircon U-Pb geochronology and petrogenesis of metabasites from the western Beihuaiyang zone in the Hong'an orogen, Central China: Implications for detachment within subducting continental crust at shallow depths. J. Asian Earth Sci. 145, 74–90.
Liu, H., Zhao, J.-H., Cawood, P.A., Wang, W., 2018a. South China in Rodinia: Constrains from the Neoproterozoic Suixian volcano-sedimentary group of the South Qinling Belt. Precambrian Res. 314, 170–193.
Liu, W., Yang, X., Shu, S., Liu, L., Yuan, S., 2018b. Precambrian Basement and Late Paleoproterozoic to Mesoproterozoic Tectonic Evolution of the SW Yangtze Block, South China: Constraints from Zircon U–Pb Dating and Hf Isotopes. Minerals 8, 333.
Liu, C.H., Zhao, G.C., Liu, F.L., Shi, J.R., Ji, L., 2020a. Detrital zircon records of late Paleoproterozoic to early Neoproterozoic northern North China Craton drainage reorganization: Implications for supercontinent cycles. Geol. Soc. Am. Bull. 132, 2135–2153.
Liu, J.N., Yin, C.Q., Zhang, J., Qian, J.H., Li, S., Xu, K.Y., et al., 2020b. Tectonic evolution of the Alxa Block and its affinity: Evidence from the U-Pb geochronology and Lu-Hf isotopes of detrital zircons from the Longshoushan Belt. Precambrian Res. 344, 105733.
Liu, H., Zi, J.-W., Cawood, P.A., Cui, X., Zhang, L., 2020c. Reconstructing South China in the Mesoproterozoic and its role in the Nuna and Rodinia supercontinents. Precambrian Res. 337, 105558.
Liu, C.H., Zhao, G., Liu, F.L., Xu, W., Sun, X., 2023. New geochronological results from late Mesoproterozoic to early Neoproterozoic successions in the eastern North China Craton and implications for the reconstruction of Rodinia. Bulletin 135 (9-10), 2575–2590.
Long, X., Yuan, C., Sun, M., Zhao, G., Xiao, W., Wang, Y., Yang, Y., Hu, A., 2010. Archean crustal evolution of the northern Tarim craton, NW China: Zircon U–Pb and Hf isotopic constraints. Precambrian Res. 180 (3-4), 272–284.
Long, X., Yuan, C., Sun, M., Kröner, A., Zhao, G., Wilde, S., Hu, A., 2011. Reworking of the Tarim Craton by underplating of mantle plume-derived magmas: evidence from Neoproterozoic granitoids in the Kuluketage area, NW China. Precambrian Res. 187 (1-2), 1–14.
Long, X., Yuan, C., Sun, M., Kröner, A., Zhao, G., 2014. New geochemical and combined zircon U–Pb and Lu–Hf isotopic data of orthogneisses in the northern Altyn Tagh, northern margin of the Tibetan plateau: Implication for Archean evolution of the Dunhuang Block and crust formation in NW China. Lithos 200–201, 418–431.
Long, X., Wilde, S.A., Yuan, C., Hu, A., Sun, M., 2015. Provenance and depositional age of Paleoproterozoic metasedimentary rocks in the Kuluketage Block, northern Tarim Craton: Implications for tectonic setting and crustal growth. Precambrian Res. 260, 76–90.
Long, X., Xu, B., Yuan, C., Zhang, C., Zhang, L., 2019. Precambrian crustal evolution of the southwestern Tarim Craton, NW China: Constraints from new detrital zircon ages and Hf isotopic data of the Neoproterozoic metasedimentary rocks. Precambrian Res. 334, 105473.
Lu, S.N., 2002. Preliminary Study of Precambrian Geology in the North Tibet–Qinghai Plateau. Geological Publishing House, Beijing, 125 p. [in Chinese].
Lu, S.N., Yuan, G.B., 2003. Geochronology of early Precambrian magmatic activities in Aketasdhtage, East Altyn Tagh. Acta Petrol. Sin. 77, 61–68 in Chinese with English abstract.
Lu, S.N., Yang, C.L., Li, H.K., Li, H.M., 2002. A group of rifting events in the terminal Paleoproterozoic in the North China Craton. Gondwana Res. 5 (1), 123–131.
Lu, S.N., Yu, H.F., Li, H.K., 2006. Research on Precambrian Major Problems in China. Geological Publishing House, Beijing, p. 206 [in Chinese].
Lu, S.N., Zhao, G.C., Wang, H.C., Hao, G.J., 2008a. Precambrian metamorphic basement and sedimentary cover of the North China Craton: a review. Precambrian Res. 160 (1–2), 77–93.
Lu, S.N., Li, H.K., Zhang, C.L., Niu, G.H., 2008b. Geological and geochronological evidence for the Precambrian evolution of the Tarim craton and surrounding continental fragments. Precambrian Res. 160, 94–107.
Lu, S.N., Li, H.K., Wang, H.C., Chen, Z.H., Zheng, J.K., Xiang, Z.Q., 2009. Detrital zircon population of Proterozoic metasedimentary strata in the Qinling-Qilian-Kunlun orogen. Acta Geol. Sin. 25, 2195–2208 [in Chinese with English abstract].
Lu, G.M., Wang, W., Ernst, R.E., Söderlund, U., Lan, Z.F., Huang, S.F., Xue, E.K., 2019. Petrogenesis of Paleo-Mesoproterozoic mafic rocks in the southwestern Yangtze Block of South China: Implications for tectonic evolution and paleogeographic reconstruction. Precambrian Res. 322, 66–84.
Ludwig, K.R., 2003. ISOPLOT 3.0: A geochronological toolkit for Microsoft Excel. Berkeley Geochronology Center Special Publication, pp. 1–70.
Lund, K., Aleinikoff, J.N., Evans, K.V., Fanning, C.M., 2003. SHRIMP U-Pb geochronology of Neoproterozoic Windermere Supergroup, central Idaho: Implications for rifting of western Laurentia and synchroneity of Sturtian glacial deposits. Geol. Soc. Am. Bull. 115, 349–372.

Lund, K., Aleinikoff, J.N., Evans, K.V., Dewitt, E.H., Unruh, D.M., 2010. SHRIMP U-Pb dating of recurrent Cryogenian and Late Cambrian–Early Ordovician alkalic magmatism in central Idaho: Implications for Rodinian rift tectonics. Geol. Soc. Am. Bull. 122, 430–453.
Luo, B.J., Liu, R., Zhang, H.F., Zhao, J.H., Yang, H., Xu, W.C., Guo, L., Zhang, L.Q., Tao, L., Pan, F.B., Wang, W., Gao, Z., Shao, H., 2018. Neoproterozoic continental back-arc rift development in the northwestern Yangtze Block. Evidence from the Hannan intrusive magmatism. Gondwana Res. 59, 27–42.
Ma, T.Q., Chen, L.X., Bai, D.Y., Zhou, K.J., Li, G., Wang, X.H., 2009. Zircon SHRIMP dating and geochemical characteristics of Neoproterozoic granites in southeastern Hunan. Geol. China 36 (1), 65–73 (in Chinese with English abstract).
Ma, X., Shu, L., Santosh, M., Li, J., 2013. Paleoproterozoic collisional orogeny in Central Tianshan: assembling the Tarim Block within the Columbia supercontinent. Precambrian Res. 228, 1–19.
Ma, X., Yang, K., Li, X., Dai, C., Zhang, H., Zhou, Q., 2016. Neoproterozoic Jiangnan Orogeny in southeast Guizhou, South China: evidence from U–Pb ages for detrital zircons from the Sibao Group and Xiajiang Group. Can. J. Earth Sci. 53, 219–230.
Ma, J.J., Wang, H., He, C., Wang, L., Wang, Q.Y., Chen, N.S., 2018. Neoproterozoic post-collision magmatism in South-Qilian block, western Qinghai, as evidenced by geochronology and geochemistry. J. Earth Sci. Environ. 40 (2), 133–154 [in Chinese with English abstract].
Maniar, P.D., Piccoli, P.M., 1989. Tectonic discrimination of granitoids. Geol. Soc. Am. Bull. 101, 635–643.
McDonough, W.F., Sun, S.S., 1995. The composition of the Earth. Chem. Geol. 120, 223–253.
McKenzie, N.R., Hughes, N.C., Myrow, P.M., Choi, D.K., Park, T.Y., 2011. Trilobites and zircons link north China with the eastern Himalaya during the Cambrian. Geology 39, 591–594.
Meert, J.G., 2012. What's in a name? The Columbia (Paleopangaea/Nuna) supercontinent. Gondwana Res. 21 (4), 987–993.
Meert, J.G., Gibsher, A.S., Levashova, N.M., Grice, W.C., Kamenov, G.D., Ryabinin, A.B., 2011. Glaciation and~ 770 Ma Ediacara (?) fossils from the lesser Karatau microcontinent, Kazakhstan. Gondwana Res. 19 (4), 867–880.
Meng, Q.R., Wei, H.H., Qu, Y.Q., Ma, S.X., 2011. Stratigraphic and sedimentary records of the rift to drift evolution of the northern North China craton at the Paleo- to Mesoproterozoic transition. Gondwana Res. 20, 205–218.
Meng, F.C., Cui, M.H., Wu, X.K., Wu, J.F., Wang, J.H., 2013. Magmatic and metamorphic events recorded in granitic gneisses from the Qimantag, East Kunlun Mountains, Northwest China. Acta Petrol. Sin. (Yanshi Xuebao) 29, 2107–2122 [in Chinese with English abstract].
Meng, E., Liu, F.L., Du, L.L., Liu, P.H., Liu, J.H., 2015. Petrogenesis and tectonic significance of the Baoxing granitic and mafic intrusions, southwestern China: Evidence from zircon U-Pb dating and Lu-Hf isotopes, and whole-rock geochemistry. Gondwana Res. 28 (2), 800–815.
Middlemost, E.A.K., 1994. Naming materials in the magma/igneous rock system. Earth Sci. Rev. 37, 215–224.
Mitchell, R.N., Zhang, N., Salminen, J., Liu, Y., Spencer, C.J., Steinberger, B., Murphy, J. B., Li, Z.X., 2021. The supercontinent cycle. Nat. Rev. Earth Environ. 2, 358–374.
Moores, E.M., 1991. Southwest US-East Antarctic (SWEAT) connection: A hypothesis. Geology 19, 425–428.
Mueller, P.A., Heatherington, A.L., Kelly, D.M., Wooden, J.L., Mogk, D.W., 2002. Paleoproterozoic crust within the Great Falls tectonic zone: Implications for the assembly of southern Laurentia. Geology 30, 127–130.
Müller, R.D., Gaina, C., Roest, W.R., Hansen, D.L., 2001. A recipe for microcontinent formation. Geology 29, 203–206.
Ning, W., Kusky, T., Wang, J., Wang, L., Deng, H., Polat, A., et al., 2020. From subduction initiation to arc–polarity reversal: Life cycle of an Archean subduction zone from the Zunhua ophiolitic mélange, North China Craton. Precambrian Res. 350, 105868.
Ning, W.B., Kusky, T.M., Wang, L., Huang, B., 2022. Archean eclogite-facies oceanic crust indicates modern-style plate tectonics. Proc. Natl. Acad. Sci. USA 119 (15), e2117529119.
Niu, B.G., He, Z.J., Ren, J.S., Wang, J., Deng, P., 2006. SHRIMP U-Pb ages of zircons from the intrusions in the western Douling-Xiaomaoling uplift and their geological significances. Geol. Rev. 52 (6), 826–835 (in Chinese with English abstract).
Pan, G.T., Ding, J., Yao, D., Wang, L., 2004. Geological Map of Qinghai- Xiang (Tibet) Plateau and Adjacent Areas. Chengdu Institute of Geology and Mineral Resources, China Geological Survey, Chengdu, China scale 1:1,500,000.
Pei, X.Z., Li, Z.C., Ding, S.P., Li, R.B., Feng, J.Y., Sun, Y., Zhang, Y.F., Liu, Z.Q., 2009. Neoproterozoic Jiaoziding peraluminous granite in the northwest margin of Yangtze Block: Zircon SHRIMP U-Pb age and geochemistry, and their tectonic significance. Earth Sci. Front. 16 (3), 231–249 (in Chinese with English abstract).
Peng, P., Zhai, M., Ernst, R.E., Guo, J., Liu, F., Hu, B., 2008. A 1.78 Ga large igneous province in the North China craton: The Xiong'er Volcanic Province and the North China dyke swarm. Lithos 101 (3–4), 260–280.
Peng, P., Guo, J., Zhai, M., Bleeker, W., 2010. Paleoproterozoic gabbronoritic and granitic magmatism in the northern margin of the North China Craton: Evidence of crust–mantle interaction. Precambrian Res. 183 (3), 635–659.
Peng, S.B., Kusky, T.M., Jiang, X.F., Wang, L., Wang, J.P., Deng, H., 2012. Geology, geochemistry and geochronology of the Miaowan ophiolite, Yangtze craton: Implications for South China's amalgamation history with the Rodinian supercontinent. Gondwana Res. 21 (2-3), 577–594.
Peng, P., Wang, X.P., Windley, B.F., Guo, J.H., Zhai, M.G., Li, Y., 2014. Spatial distribution of ~1950–1800 Ma metamorphic events in the North China craton: Implications for tectonic subdivision of the craton. Lithos 202–203, 250–266.
Peng, P., Xu, H., Mitchell, R.N., Teixeira, W., Kirscher, U., Qin, Z., 2022. Earth's oldest hotspot track at ca. 1.8 Ga advected by a global subduction system. Earth Planet. Sci. Lett. 585, 117530.
Peng, P., Liu, X., Feng, L., Zhou, X., Kuang, H., Liu, Y., Kang, J., Wang, X., Wang, C., Dai, K., Wang, H., Li, J., Miao, P., Guo, J., Zhai, M., 2023. Rhyacian intermittent large igneous provinces sustained Great Oxidation Event: evidence from North China craton. Earth Sci. Rev. 238, 104352.
Qin, X.F., Pan, Y.M., Li, J., Li, R.S., Zhou, F.S., Hu, G.A., Zhong, F.Y., 2006. Zircon SHRIMP U-Pb geochronology of the Yunkai metamorphic complex in southeastern Guangxi, China. Geol. Bull. China 25 (5), 553–559 (in Chinese with English abstract).
Rainbird, R.H., Stern, R.A., Khudoley, A.K., Kropachev, A.P., Heaman, L.M., Sukhorukov, V.I., 1998. U–Pb geochronology of Riphean sandstone and gabbro from southeast Siberia and its bearing on the Laurentia–Siberia connection. Earth Planet. Sci. Lett. 164 (3–4), 409–420.
Ren, J.H., Liu, Y.Q., Zhou, D.W., Feng, Q., Zhang, K., Dong, Z.L., Qin, P.L., 2010. Geochemical characteristics and LA-ICP-MS zircon U-Pb dating of basic dykes in the Xiaomian area: Eastern Kunlun: Journal of Jilin University. Earth Sci. Ed. 40, 856–868.
Rickwood, P.C., 1989. Boundary lines within petrologic diagrams which use oxides of major and minor elements. Lithos 22, 247–263. https://doi.org/10.1016/0024-4937(89)90028-5.
Rogers, J.J.W., Santosh, M., 2002. Configuration of Columbia, a Mesoproterozoic supercontinent. Gondwana Res. 5 (1), 5–22.
Rojas-Agramonte, Y., Kröner, A., Demoux, A., Xia, X., Wang, W., Donskaya, T., Liu, D., Sun, M., 2011. Detrital and xenocrystic zircon ages from Neoproterozoic to Palaeozoic arc terranes of Mongolia: Significance for the origin of crustal fragments in the Central Asian Orogenic Belt. Gondwana Res. 19, 751–763.
Rojas-Agramonte, Y., et al., 2014. Detrital and igneous zircon ages for supracrustal rocks of the Kyrgyz Tianshan and palaeogeographic implications. Gondwana Res. 26, 957–974.
Ross, G.M., Eaton, D.W., 2002. Proterozoic tectonic accretion and growth of western Laurentia: Results from Lithoprobe studies in northern Alberta. Can. J. Earth Sci. 39, 313–329.
Ross, G.M., Parrish, R.R., Winston, D., 1992. Provenance and U-Pb geochronology of the Mesoproterozoic Belt Supergroup (northwestern United States): Implications for age of deposition and pre-Panthalassa plate reconstructions. Earth Planet. Sci. Lett. 113, 57–76.
Ross, G.M., Eaton, D.W., Boerner, D.E., Miles, W., 2000. Tectonic entrapment and its role in the evolution of continental lithosphere: An example from the Precambrian of western Canada. Tectonics 19 (1), 116–134.
Şengör, A.M.C., Natal'in, B.A., Burtman, V.S., 1993. Evolution of the Altaid tectonic collage and Palaeozoic crustal growth in Eurasia. Nature 364, 299–307.
Şengör, A.M.C., Natal'in, B.A., 1996. Palaeotectonics of Asia: Fragments of A Synthesis. Tecton. Evol. Asia 486–640.
Şengör, A.C., Lom, N., Polat, A., 2022. The nature and origin of cratons constrained by their surface geology. Bulletin 134 (5–6), 1485–1505.
Shen, B., Xiao, S., Zhou, C., Kaufman, A.J., Yuan, X., 2010. Carbon and sulfur isotope chemostratigraphy of the Neoproterozoic Quanji Group of the Chaidam Basin, NW China: Basin stratification in the aftermath of an Ediacaran glaciation postdating the Shuram event? Precambrian Res. 177 (3–4), 241–252.
Shi, Y.R., Liu, D.Y., Zhang, Z.Q., Miao, L.C., Zhang, F.Q., Xue, H.M., 2007. SHRIMP zircon U-Pb dating of gabbro and granite from the Huashan ophiolite, Qinling orogenic belt, China: Neoproterozoic suture on the northern margin of the Yangtze Craton. Acta Geol. Sin. (Engl. Ed.) 81 (2), 239–243.
Shu, L., Deng, P., Yu, J., Wang, Y., Jiang, S., 2008. The age and tectonic environment of the rhyolitic rocks on the western side of Wuyi Mountain, South China. Sci. China Ser. D Earth Sci. 51 (8), 1053–1063.
Shu, L.S., Deng, X.L., Zhu, W.B., Ma, D.S., Xiao, W.J., 2011a. Precambrian tectonic evolution of the Tarim Block, NW China: New geochronological insights from the Quruqtagh domain. J. Asian Earth Sci. 42, 774–790.
Shu, L.S., Faure, M., Yu, J.H., Jahn, B.M., 2011b. Geochronological and geochemical features of the Cathaysia block (South China): New evidence for the Neoproterozoic breakup of Rodinia. Precambrian Res. 187 (3–4), 263–276.
Shu, L., Yao, J., Wang, B., Faure, M., Charvet, J., Chen, Y., 2021. Neoproterozoic plate tectonic process and Phanerozoic geodynamic evolution of the South China Block. Earth Sci. Rev. 216, 103596.
Sláma, J., Košler, J., Condon, D.J., Crowley, J.L., Gerdes, A., Hanchar, J.M., Whitehouse, M.J., 2008. Plešovice zircon—a new natural reference material for U–Pb and Hf isotopic microanalysis. Chem. Geol. 249 (1–2), 1–35.
Song, S.G., Su, L., Li, X.H., Niu, Y.L., Zhang, L.F., 2012. Grenville-age orogenesis in the Qaidam-Qilian block: The link between South China and Tarim. Precambrian Res. 220–221, 9–22.
Song, D.F., Xiao, W.J., Collins, A.S., Glorie, S., Han, C.M., Li, Y.C., 2017. New chronological constrains on the tectonic affinity of the Alxa Block, NW China. Precambrian Res. 299, 230–243.
Stacey, J.T., Kramers, J.D., 1975. Approximation of terrestrial lead isotope evolution by a two-stage model. Earth Planet. Sci. Lett. 26 (2), 207–221.
Strickland, A., Miller, E.L., Wooden, J.L., 2011. The Timing of Tertiary Metamorphism and Deformation in the Albion–Raft River–Grouse Creek Metamorphic Core Complex, Utah and Idaho. J. Geol. 119, 185–206.
Su, B., Cui, X., Tian, J., Lai, C.K., Ren, F., Ren, G., Liu, S., 2020. Detrital zircon provenance and palaeogeographic implications of the Ediacaran Shigu Group in the Zhongza Terrane, SW China. Int. Geol. Rev. 62, 2105–2124.

Su, W., Wang, Q., Kang, J., Song, X., 2023. Proterozoic evolution of the Alxa block in western China: A wandering terrane during supercontinent cycles. Precambrian Res. 389, 107002.

Sun, W.H., Zhou, M.F., Gao, J.F., Yang, Y.H., Zhao, X.F., Zhao, J.H., 2009. Detrital zircon U–Pb geochronological and Lu–Hf isotopic constraints on the Precambrian magmatic and crustal evolution of the western Yangtze Block, SW China. Precambrian Res. 172, 99–126.

Sun, H.Q., Huang, J.Z., Jiang, X.S., Luo, L., Ma, H.Y., Wu, H., 2013. The evolution of "Nanhuaian" rift basin on the southeastern margin of Yangtze platform: Age constraints from the Neoproterozoic granites. Geol. China 40 (6), 1725–1735 (in Chinese with English abstract).

Sun, J., Shu, L., Santosh, M., Wang, L., 2018. Precambrian crustal evolution of the central Jiangnan Orogen (South China): Evidence from detrital zircon U-Pb ages and Hf isotopic compositions of Neoproterozoic metasedimentary rocks. Precambrian Res. 318, 1–24.

Sun, J.P., Dong, Y.P., Ma, L.C., Peng, Y., Chen, S.Y., Du, J.J., Jiang, W., et al., 2019. Late Paleoproterozoic tectonic evolution of the Olongbuluke Terrane, northern Qaidam, China. Precambrian Res. 331, 105349.

Tan, S.X., Bai, Y.S., Chang, G.H., Tong, H.K., Bao, G.P., 2004. Discovery and geological significance of metamorphic and intrusive rock (system) of Qimantagh region in Jinning epoch. Nor. Geol. Unders. 37, 69–73 [in Chinese with English abstract].

Tang, Q.Y., Li, C.S., Zhang, M.J., Ripley, E.M., Wang, Q.L., 2014. Detrital zircon constraint on the timing of amalgamation between Alxa and Ordos, with exploration implications for Jinchuan-type Ni-Cu ore deposit in China. Precambrian Res. 255, 748–755.

Teng, X., Zhang, J., Mao, X., Lu, Z., Zhou, G., Wu, Y., Guo, Q., 2022. Qaidam block situated in the interior of Rodinia and Gondwana. New magmatic and metamorphic constraints. Precambrian Res. 381, 106866.

Trap, P., Faure, M., Lin, W., Le Breton, N., Monie, P., 2012. Paleoproterozoic tectonic evolution of the Trans-North China orogen: Toward a comprehensive model. Precambrian Res. 222–223, 191–211.

Tung, K.A., Yang, H.Y., Liu, D.Y., Zhang, J.X., Yang, H.J., Shau, Y.H., Tseng, C.Y., 2013. The Neoproterozoic granitoids from the Qilian block, NW China: Evidence for a link between the Qilian and South China blocks. Precambrian Res. 235, 163–189.

Turner, S.A., 2010. Sedimentary record of late Neoproterozoic rifting in the NW Tarim Basin, China. Precambrian Res. 181, 85–96.

Turner, S.P., Foden, J.D., Morrison, R.S., 1992. Derivation of some A-type magmas by fractionation of basaltic magma: An example from the Padthaway Ridge, South Australia. Lithos 28, 151–179.

Valentine, J.W., Moores, E.M., 1970. Plate-tectonic regulation of faunal diversity and sea level: a model. Nature 228 (5272), 657–659.

Vervoort, J.D., Plank, T., Prytulak, J., 2011. The Hf–Nd isotopic composition of marine sediments. Geochim. Cosmochim. Acta 75, 5903–5926.

Wan, Y., Song, B., Liu, D., Wilde, S.A., Wu, J., Shi, Y., Yin, X., Zhou, H., 2006. SHRIMP U–Pb zircon geochronology of Palaeoproterozoic metasedimentary rocks in the North China Craton: Evidence for a major Late Palaeoproterozoic tectonothermal event. Precambrian Res. 149, 249–271.

Wan, Y., Liu, D., Dong, C., Xu, Z., Wang, Z., Wilde, S.A., Yang, Y., Liu, Z., Zhou, H., 2009. The Precambrian Khondalite Belt in the Daqingshan Area, North China Craton: Evidence for Multiple Metamorphic Events in the Palaeoproterozoic Era. Geol. Soc. Lond. Spec. Publ. 323, 73–97.

Wan, Y., Xie, H., Yang, H., Wang, Z., Liu, D., Kröner, A., Wilde, S.A., Geng, Y.S., Sum, L., Ma, M.Z., Liu, S.J., Dong, C.Y., Du, L., 2013. Is the Ordos block Archean or Paleoproterozoic in age? Implications for the Precambrian evolution of the North China Craton. Am. J. Sci. 313, 683–711.

Wan, Y.S., Liu, D., Dong, C., Xie, H., Kröner, A., Ma, M., et al., 2015. Formation and evolution of Archean continental crust of the North China Craton. In: Precambrian Geology of China. Springer, pp. 59–136.

Wang, J., Li, Z.X., 2003. History of Neoproterozoic rift basins in South China: implications for Rodinia break-up. Precambrian Res. 122 (1–4), 141–158.

Wang, W., Zhou, M.F., 2012. Sedimentary records of the Yangtze Block (South China) and their correlation with equivalent Neoproterozoic sequences on adjacent continents. Sediment. Geol. 265–266, 126–142.

Wang, X., Zhou, J., Qiu, J., Gao, J., 2004. Geochemistry of the Meso- to Neoproterozoic basic–acid rocks from Hunan Province, South China: implications for the evolution of the western Jiangnan orogen. Precambrian Res. 135 (1–2), 79–103.

Wang, X.L., Zhou, J.C., Qiu, J.S., Zhang, W.L., Liu, X.M., Zhang, G.L., 2006. LA-ICP-MS U-Pb zircon geochronology of the Neoproterozoic igneous rocks from northern Guangxi, South China: Implications for tectonic evolution. Precambrian Res. 145 (1-2), 111–130.

Wang, X.C., Li, X.H., Li, W.X., Li, Z.X., Liu, Y., Yang, Y.H., et al., 2008a. The Bikou basalts in the northwestern Yangtze block, South China: Remnants of 820-810 Ma continental flood basalts? Geol. Soc. Am. Bull. 120 (11–12), 1478–1492.

Wang, X.L., Zhou, J.C., Qiu, J.S., Jiang, S.Y., Shi, Y.R., 2008b. Geochronology and geochemistry of Neoproterozoic mafic rocks from western Hunan, South China: implications for petrogenesis and post-orogenic extension. Geol. Mag. 145 (02).

Wang, Q.Y., Chen, N.S., Li, X.Y., Hao, S., Chen, H.H., 2008c. LA-ICPMS U-Pb dating for the basement Dakendaban group and thermal event in Quanji Block. Chin. Sci. Bull. 53 (14), 1693–1701.

Wang, Q.Y., Pan, Y.M., Chen, N.S., Li, X.Y., Chen, H.H., 2009. Proterozoic polymetamorphism in the Quanji Block, northwestern China: evidence from microtextures, garnet compositions and monazite CHIME ages. J. Asian Earth Sci. 34, 686–698.

Wang, M., Dai, C.G., Wang, X.H., Chen, J.S., Ma, H.Z., 2011. In-situ zircon geochronology and Hf isotope of muscovite-bearing leucogranites from Fanjingshan, Guizhou Province, and constraints on continental growth of the southern China block. Earth Sci. Front. 18 (5), 213–223 (in Chinese with English abstract).

Wang, D.B., Sun, Z.M., Yin, F.G., Wang, L.Q., Wang, B.D., Zhang, W.P., 2012a. Geochronology of the Hekou group on the western margin of the Yangtze Block: Evidence from zircon LA-ICP-MS U-Pb dating of volcanic rocks. J. Stratigr. 36 (3), 630–635 (in Chinese with English abstract).

Wang, W., Zhou, M.F., Yan, D.P., Li, J.W., 2012b. Depositional age, provenance, and tectonic setting of the Neoproterozoic Sibao Group, southeastern Yangtze Block, South China. Precambrian Res. 192, 107–124.

Wang, X.C., Li, X., Li, Z.X., Li, Q., Tang, G.Q., Gao, Y.Y., et al., 2012c. Episodic Precambrian crust growth: Evidence from U–Pb ages and Hf–O isotopes of zircon in the Nanhua Basin, central South China. Precambrian Res. 222–223, 386–403.

Wang, D.B., Yin, F.G., Sun, Z.M., Wang, L.Q., Wang, B.D., Liao, S.Y., Tang, Y., Ren, G.M., 2013a. Zircon U-Pb age and Hf isotope of Paleoproterozoic mafic intrusion on the western margin of the Yangtze Block and their implications. Geol. Bull. China 32 (4), 617–630 (in Chinese with English abstract).

Wang, Z.Z., Guo, Y., Yang, B., Wang, S.W., Sun, X.M., Hou, L., Zhou, B.G., Liao, Z.W., 2013b. Discovery of the 1.73Ga Haizi anorogenic type granite in the western margin of Yantze Craton, and its geological significance. Acta Geol. Sin. 87 (7), 931–942 (in Chinese with English abstract).

Wang, Y., Zhang, A., Cawood, P.A., Fan, W., Xu, J., Zhang, G., Zhang, Y., 2013c. Geochronological, geochemical and Nd–Hf–Os isotopic fingerprinting of an early Neoproterozoic arc–back-arc system in South China and its accretionary assembly along the margin of Rodinia. Precambrian Res. 231, 343–371.

Wang, C., Liu, L., Yang, W.Q., Zhu, X.H., Cao, Y.T., Kang, L., Chen, S.F., Li, R.S., He, S.P., 2013d. Provenance and ages of the Altyn Complex in Altyn Tagh: Implications for the early Neoproterozoic evolution of northwestern China. Precambrian Res. 230, 193–208.

Wang, L.Q., Pan, G.T., Ding, J., Yao, D.S., 2013e. Geological Map of the Tibetan Plateau at a Scale of 1:1.5 M with Explanations. Geological Publishing House, Beijing, p. 288.

Wang, X.L., Zhou, J.C., Griffin, W.L., Zhao, G.C., Yu, J.H., Qiu, J.S., Zhang, Y.J., Xing, G. F., 2014a. Geochemical zonation across a Neoproterozoic orogenic belt: Isotopic evidence from granitoids and metasedimentary rocks of the Jiangnan Orogen, China. Precambrian Res. 242, 154–171.

Wang, B., Liu, H.S., Shu, L.S., Jahn, B.M., Chung, S.L., Zhai, Y.Z., Liu, D.Y., 2014b. Early Neoproterozoic crustal evolution in the northern Yili block: Insights from migmatite, orthogneiss and leucogranite of the Wenquan metamorphic complex in the NW Chinese Tianshan. Precambrian Res. 242, 58–81.

Wang, Z.M., Han, C.M., Xiao, W.J., Su, B.X., Sakyi, P.A., Song, D.F., Lin, L.N., 2014c. The petrogenesis and tectonic implications of the granitoid gneisses from Xingxing Xia in the eastern segment of Central Tianshan. J. Asian Earth Sci. 88, 277–292.

Wang, C., Wang, Y.H., Liu, L., He, S.P., Li, R.S., Li, M., Yang, W.Q., Cao, Y.T., Meert, J.G., Shi, C., 2014d. The Paleoproterozoic magmatic-metamorphic events and cover sediments of the Tiekelik belt and their tectonic implications for the southern margin of the Tarim craton, northwestern China. Precambrian Res. 254, 210–225.

Wang, X.S., Gao, J., Klemd, R., Jiang, T., Zhai, Q.G., Xiao, X.C., Liang, X.Q., 2015a. Early Neoproterozoic multiple arc-back-arc system formation during subduction-accretion processes between the Yangtze and Cathaysia blocks: New constraints from the supra-subduction zone NE Jiangxi ophiolite (South China). Lithos 236-237, 90–105.

Wang, C., Li, R.S., Li, M., Meert, J.G., Peng, Y., 2015b. Paleoproterozoic magmatic-metamorphic history of the Quanji Massif, northwest China: Implications for a single North China–Quanji–Tarim craton within the Columbia supercontinent? Int. Geol. Rev. 57, 1772–1790.

Wang, L., Long, W.G., Xu, D.M., Xu, W.C., Zhou, D., Jin, X.B., Huang, H., Zhang, K., 2015c. Zircon U-Pb geochronology of metamorphic basement in Yunkai area and its implications on the Grenvillian event in the Cathaysia Block. Earth Sci. Front. 22 (2), 25–40 (in Chinese with English abstract).

Wang, M., Dai, C.G., Chen, J.S., Wang, X.H., Ma, H.Z., 2016a. Neoproterozoic geochronologic framework of magmatism in Fanjingshan area and its tectonic implications. Geol. China 43 (3), 843–856 (in Chinese with English abstract).

Wang, M.X., Nebel, O., Wang, C.Y., 2016b. The flaw in the crustal 'Zircon Archive': Mixed Hf isotope signatures record progressive contamination of late-stage liquid in mafic-ultramafic layered intrusions. J. Petrol. 57 (1), 27–52.

Wang, Y., Zhou, Y., Cai, Y., Liu, H., Zhang, Y., Fan, W., 2016c. Geochronological and geochemical constraints on the petrogenesis of the Ailaoshan granitic and migmatite rocks and its implications on Neoproterozoic subduction along the SW Yangtze Block. Precambrian Res. 283, 106–124.

Wang, L., Wang, H., He, C., Chen, N.S., Santosh, M., Sun, M., Wang, Q.Y., Jin, L., Liao, F. X., 2016d. Mesoproterozoic continental breakup in NW China: Evidence from gray gneisses from the North Wulan terrane. Precambrian Res. 281, 521–536.

Wang, J.P., Kusky, T., Wang, L., Polat, A., Deng, H., Wang, C., Wang, S., 2017a. Structural relationships along a Neoarchean arc-continent collision zone, North China craton. Geol. Soc. Am. Bull. 129 (1–2), 59–75.

Wang, R.R., Xu, Z.Q., Santosh, M., Xu, X.B., Deng, Q., Fu, X.H., 2017b. Middle Neoproterozoic (ca. 705~716Ma) arc to rift transitional magmatism in the northern margin of the Yangtze Block: Constraints from geochemistry, zircon U-Pb geochronology and Hf isotopes. J. Geodyn. 109, 59–74.

Wang, J., Shu, L., Santosh, M., 2017c. U-Pb and Lu-Hf isotopes of detrital zircon grains from Neoproterozoic sedimentary rocks in the central Jiangnan Orogen, South China: Implications for Precambrian crustal evolution. Precambrian Res. 294, 175–188.

Wang, G.G., Ni, P., Zhu, A.D., Wang, X.L., Li, L., Hu, J.S., Lin, W.H., Huang, B., 2018. 1.01~0.98 Ga mafic intra-plate magmatism and related Cu-Au mineralization in the eastern Jiangnan orogen: Evidence from Liujia and Tieshajie basalts. Precambrian Res. 309, 6–21.

Wang, J.P., Li, X.W., Ning, W.B., Kusky, T., Wang, L., Polat, A., Deng, H., 2019a. Geology of a Neoarchean suture: Evidence from the Zunhua ophiolitic mélange of the Eastern Hebei Province, North China Craton. Geol. Soc. Am. Bull. 131 (11–12), 1943–1964.

Wang, L., Johnston, S.T., Chen, N.S., 2019b. New insights into the Precambrian tectonic evolution and continental affinity of the Qilian block: Evidence from geochronology and geochemistry of metasupracrustal rocks in the North Wulan terrane. Geol. Soc. Am. Bull. 131 (9-10), 1723–1743.
Wang, P., Zhao, G., Liu, Q., Han, Y., Yao, J., Li, J., 2020. Zircons from the Tarim basement provide insights into its positions in Columbia and Rodinia supercontinents. Precambrian Res. 341, 105621.
Wang, C.Y., Yu, S.Y., Sun, D.Y., Lv, P., Feng, Z., Wang, G., Gou, J., 2021. Mesoproterozoic tectonic-thermal events in the Oulongbuluke Block, NW China: Constraints on the transition from supercontinent Columbia to Rodinia. Precambrian Res. 352, 106010.
Wang, D., Vervoort, J.D., Fisher, C.M., Lewis, R.S., Buddington, A., 2022. The Neoarchean and Paleoproterozoic crustal evolution of the Clearwater block, northwestern Laurentia: Implications for the assembly of supercontinents. Precambrian Res. 379, 106780.
Watts, K.E., Haxel, G.B., Miller, D.M., 2022. Temporal and petrogenetic links between Mesoproterozoic alkaline and carbonatite magmas at Mountain Pass, California. Econ. Geol. 117 (1), 1–23.
Wei, Y.X., Peng, S.B., Jiang, X.F., Peng, Z.Q., Peng, L.H., Li, Z.H., Zhou, P., Zeng, X.W., 2012. SHRIMP zircon U-Pb ages and geochemical characteristics of the Neoproterozoic granitoids in the Huangling anticline and its tectonic setting. J. Earth Sci. 23 (5), 659–675.
Wen, B., Evans, D.A., Li, Y.X., 2017. Neoproterozoic paleogeography of the Tarim Block: An extended or alternative "missing-link" model for Rodinia? Earth Planet. Sci. Lett. 458, 92–106.
Wen, B., Evans, D.A., Wang, C., Li, Y.X., Jing, X., 2018. A positive test for the Greater Tarim Block at the heart of Rodinia: Mega-dextral suturing of supercontinent assembly. Geology 46 (8), 687–690.
Whalen, J.B., Currie, K.L., Chappell, B.W., 1987. A-type granites: geochemical characteristics, discrimination and petrogenesis. Contrib. Mineral. Petrol. 95, 407–419.
Wiedenbeck, M., Allé, P., Corfu, F., Griffin, W.L., Meier, M., Oberli, F., Quadt, A.V., Roddick, J.C., Spiegel, W., 1995. Three natural zircon standards for U- Th- Pb, Lu-Hf, trace element and REE analyses. Geostand. Newslett. 19, 1–23.
Windley, B.F., Alexeiev, D., Xiao, W., Kröner, A., Badarch, G., 2007. Tectonic models for accretion of the Central Asian Orogenic Belt. J. Geol. Soc. 164 (1), 31–47.
Windley, B.F., Kusky, T.M., Polat, A., 2021. Onset of plate tectonics by the Eoarchean. Precambrian Res. 352, 105980.
Wingate, M.T., Pisarevsky, S.A., Evans, D.A., 2002. Rodinia connections between Australia and Laurentia: no SWEAT, no AUSWUS? Terra Nova 14 (2), 121–128.
Winston, D., 1986. Sedimentation and tectonics of the Middle Proterozoic Belt Basin and their influence on Phanerozoic compression and extension in western Montana and northern Idaho: Part II. Northern Rocky Mount. 87–118.
Wu, R.X., Zheng, Y.F., Wu, Y.B., 2005. Zircon U-Pb age, element and oxygen isotope geochemisty of Neoproterozoic granites at Shiershan in South Anhui Province. Geol. J. China Univ. 11 (3), 364–382 (in Chinese with English abstract).
Wu, R.X., Zheng, Y.F., Wu, Y.B., Zhao, Z.F., Zhang, S.B., Liu, X.M., Wu, F.Y., 2006. Reworking of juvenile crust: Element and isotope evidence from Neoproterozoic granodiorite in South China. Precambrian Res. 146 (3-4), 179–212.
Wu, C.Z., Santosh, M., Chen, Y.J., Samson, I.M., Lei, R.X., Dong, L.H., Qu, X., Gu, L.X., 2014. Geochronology and geochemistry of Early Mesoproterozoic meta-diabase sills from Quruqtagh in the northeastern Tarim Craton: implications for breakup of the Columbia supercontinent. Precambrian Res. 241, 29–43.
Wu, C., Yin, A., Zuza, A.V., Zhang, J., Liu, W., Ding, L., 2016. Pre-Cenozoic geologic history of the central and northern Tibetan Plateau and the role of Wilson cycles in constructing the Tethyan orogenic system. Lithosphere 8 (3), 254–292.
Wu, C., Zuza, A.V., Yin, A., Liu, C., Reith, R.C., Zhang, J., Liu, W., Zhou, Z., 2017. Geochronology and geochemistry of Neoproterozoic granitoids in the central Qilian Shan of northern Tibet: Reconstructing the amalgamation processes and tectonic history of Asia. Lithosphere 9, 609–636. https://doi.org/10.1130/L640.1.
Wu, C., Zhou, Z.G., Zuza, A.V., Wang, G.S., Liu, C.F., Jiang, T., 2018. A 1.9 Ga mélange along the northern margin of the North China craton: Implications for the assembly of Columbia supercontinent. Tectonics 37 (10), 3610–3646.
Wu, C., Zuza, A.V., Chen, X., Ding, L., Levy, D.A., Liu, C., Liu, W., Jiang, T., Stockli, D.F., 2019. Tectonics of the Eastern Kunlun Range: Cenozoic Reactivation of a Paleozoic-Early Mesozoic Orogen. Tectonics 38, 1609–1650. https://doi.org/10.1029/2018TC005370.
Wu, C., Zuza, A.V., Yin, A., Chen, X.H., Haproff, P.J., Li, J., et al., 2021. Punctuated Orogeny During the Assembly of Asia: Tectonostratigraphic Evolution of the North China Craton and the Qilian Shan from the Paleoproterozoic to Early Paleozoic. Tectonics 40 (4), e2020TC006503.
Wu, C., Wang, G.S., Zhou, Z.G., Haproff, P.J., Zuza, A.V., Liu, W.Y., 2022a. Paleoproterozoic Plate Tectonics Recorded in the Northern Margin Orogen, North China Craton. Geochem. Geophys. Geosyst. 23 (11), e2022GC010662.
Wu, C., Li, J., Zuza, A.V., Haproff, P.J., Yin, A., Ding, L., 2022b. Paleoproterozoic–Paleozoic tectonic evolution of the Longshou Shan, western North China craton. Geosphere 18 (3), 1177–1193.
Wu, Z.J., Lu, C., Qiu, L., Zhao, H., Wang, H., Tan, W., Zhong, M., 2022c. New detrital zircon geochronological results from the Meso-Neoproterozoic sandstones in the southern-eastern Liaoning region, North China craton, and their paleogeographic implications. Precambrian Res. 381, 106847.
Wu, C., Wang, G.S., Zhou, Z.G., Zhao, X.Q., Haproff, P.J., 2023. Late Archean–Paleoproterozoic plate tectonics along the northern margin of the North China craton. GSA Bull. 135 (3–4), 967–989.
Xia, L.Q., Xia, Z.C., Ma, Z.P., Xu, X.Y., Li, X.M., 2009. Petrogenesis of volcanic rocks from Xixiang Group in middle part of South Qinling Mountains. Northwest. Geol. 42 (2), 1–37 (in Chinese with English abstract).
Xia, Y., Xu, X.S., Zhao, G.C., Liu, L., 2015. Neoproterozoic active continental margin of the Cathaysia block: Evidence from geochronology, geochemistry, and Nd-Hf isotopes of igneous complexes. Precambrian Res. 269, 195–216.
Xiao, L., Zhang, H.F., Ni, P.Z., Xiang, H., Liu, X.M., 2007. LA-ICP-MS U-Pb zircon geochronology of early Neoproterozoic mafic-intermediat intrusions from NW margin of the Yangtze Block, South China: Implication for tectonic evolution. Precambrian Res. 154 (3-4), 221–235.
Xiao, D., Ning, W.B., Wang, J.P., Kusky, T., Wang, L., Deng, H., Zhong, Y.T., Jiang, K., 2021. Neoarchean to Paleoproterozoic tectonothermal evolution of the North China Craton: Constraints from geological mapping and Th-U-Pb geochronology of zircon, titanite, and monazite in Zanhuang massif. Precambrian Res. 359, 106214.
Xie, H., Zhu, X., Wang, X., He, Y., Shen, W., 2023. Petrological and geochemical characteristics of mafic rocks from the Neoproterozoic Sugetbrak Formation in the northwestern Tarim Block, China. China Geol. 6, 85–99.
Xin, Y.J., Li, J.H., Dong, S.W., Zhang, Y.Q., Wang, W.B., Sun, H.S., 2017. Neoproterozoic post-collisional extension of the central Jiangnan Orogen: Geochemical, geochronological, and Lu-Hf isotopic constraints from the ca. 820~800Ma magmatic rocks. Precambrian Res. 294, 91–110.
Xu, B., Jian, P., Zheng, H., Zou, H., Zhang, L., Liu, D., 2005. U-Pb zircon geochronology and geochemistry of Neoproterozoic volcanic rocks in the Tarim Block of northwest China: Implications for the breakup of Rodinia supercontinent and Neoproterozoic glaciations. Precambrian Res. 136, 107–123.
Xu, D.R., Xia, B., Li, P.C., Zhang, Y.Q., Chen, G.H., Ma, C., 2006. SHRIMP U-Pb Dating of zircon from the Precambrian granitoids in Northwest Hainan Island and its geological implications. Geotecton. Metallog. 30 (4), 510–518 (in Chinese with English abstract).
Xu, W.C., Zhang, H.F., Liu, X.M., 2007. U-Pb zircon dating constraints on formation time of Qilian high-grade metamorphic rock and its tectonic implications. Chin. Sci. Bull. 52, 531–538.
Xu, Z.Q., He, B.Z., Zhang, C.L., Zhang, J.X., Wang, Z.M., Cai, Z.H., 2013. Tectonic framework and crustal evolution of the Precambrian basement of the Tarim Block in NW China: new geochronological evidence from deep drilling samples. Precambrian Res. 235, 150–162.
Xu, Y., Yang, K.G., Polate, A., Yang, Z.N., 2016. The ~860Ma mafic dikes and granitoids from the northern margin of the Yangtze Block, China: A record of oceanic subduction in the early Neoproterozoic. Precambrian Res. 275, 310–331.
Xue, H.M., Ma, F., Song, Y.Q., Xie, Y.P., 2010. Geochronology and geochemistry of the Neoproterozoic granitoid association from eastern segment of the Jiangnan orogen, China: Constraints on the timing and process of amalgamation between the Yangtze and Cathaysia blocks. Acta Petrol. Sin. 26 (11), 3215–3244 (in Chinese with English abstract).
Xue, H.M., Ma, F., Song, Y.Q., 2012. Mafic ultramafic rocks from the Fanjingshan region, southwestern margin of the Jiangnan orogenic belt: Ages, geochemical characteristics and tectonic setting. Acta Petrol. Sin. 28 (9), 3015–3030 (in Chinese with English abstract).
Yan, Q.R., Hanson, A.D., Wang, Z.Q., Druschke, P.A., Yan, Z., Wang, T., Liu, D.Y., Song, B., Jian, P., Zhou, H., Jiang, C.F., 2004. Neoproterozoic subduction and rifting on the northern margin of the Yangtze Plate, China: Implications for Rodinia reconstruction. Int. Geol. Rev. 46 (9), 817–832.
Yan, C., Shu, L., Santosh, M., Yao, J., Li, J., Li, C., 2015. The Precambrian tectonic evolution of the western Jiangnan Orogen and western Cathaysia Block: Evidence from detrital zircon age spectra and geochemistry of clastic rocks. Precambrian Res. 268, 33–60.
Yang, C.H., Geng, Y.S., Du, L.L., Ren, L.D., Wang, X.S., Zhou, X.W., Yang, Z.S., 2009. The identification of the Grenvillian granite on the western margin of the Yangtze Block and its geological implications. Geol. China 36 (3), 647–657 (in Chinese with English abstract).
Yang, H., Liu, F.L., Du, L.L., Liu, P.H., Wang, F., 2012. Zircon U-Pb dating for metavolcanites in the Laochanghe Formation of the Dahongshan Group in southwestern Yangtze block, and its geological significance. Acta Petrol. Sin. 28 (9), 2994–3014 (in Chinese with English abstract).
Yang, B., Wang, W.Q., Dong, G.C., Guo, Y., Wang, Z.Z., Hou, L., 2015. Geochemistry, geochronology and their significances of Haizi bimodal intrusions in Kangdian fault-uplift zone, southwestern margin of Yangtze platform. Acta Petrol. Sin. 31 (5), 1361–1373 (in Chinese with English abstract).
Yang, H., Wu, G., Kusky, T.M., Chen, Y., Xiao, Y., 2018. Paleoproterozoic assembly of the North and South Tarim terranes: New insights from deep seismic profiles and Precambrian granite cores. Precambrian Res. 305, 151–165.
Yao, J., Shu, L., Santosh, M., Li, J., 2013. Geochronology and Hf isotope of detrital zircons from Precambrian sequences in the eastern Jiangnan Orogen: Constraining the assembly of Yangtze and Cathaysia Blocks in South China. J. Asian Earth Sci. 74, 225–243.
Yao, J., Shu, L., Santosh, M., 2014a. Neoproterozoic arc-trench system and breakup of the South China Craton: Constraints from N-MORB type and arc-related mafic rocks, and anorogenic granite in the Jiangnan orogenic belt. Precambrian Res. 247, 187–207.
Yao, J., Shu, L., Santosh, M., Zhao, G., 2014b. Neoproterozoic arc-related mafic–ultramafic rocks and syn-collision granite from the western segment of the Jiangnan Orogen, South China: Constraints on the Neoproterozoic assembly of the Yangtze and Cathaysia Blocks. Precambrian Res. 243, 39–62.
Yao, J., Shu, L., Santosh, M., Li, J., 2015. Neoproterozoic arc-related andesite and orogeny-related unconformity in the eastern Jiangnan orogenic belt: Constraints on the assembly of the Yangtze and Cathaysia blocks in South China. Precambrian Res. 262, 84–100.

Yao, J., Cawood, P.A., Shu, L., Santosh, M., Li, J., 2016a. An Early Neoproterozoic Accretionary Prism Ophiolitic Mélange from the Western Jiangnan Orogenic Belt, South China. J. Geol. 124 (5), 587–601.
Yao, J., Shu, L., Cawood, P.A., Li, J., 2016b. Delineating and characterizing the boundary of the Cathaysia Block and the Jiangnan orogenic belt in South China. Precambrian Res. 275, 265–277.
Yao, J., Shu, L., Cawood, P.A., Li, J., 2017. Constraining timing and tectonic implications of Neoproterozoic metamorphic event in the Cathaysia Block, South China. Precambrian Res. 293, 1–12.
Ye, M.-F., Li, X.-H., Li, W.-X., Liu, Y., Li, Z.-X., 2007. SHRIMP zircon U–Pb geochronological and whole-rock geochemical evidence for an early Neoproterozoic Sibaoan magmatic arc along the southeastern margin of the Yangtze Block. Gondwana Res. 12 (1–2), 144–156.
Ye, H.M., Li, X.H., Lan, Z.W., 2013. Geochemical and Sr–Nd–Hf–O–C isotopic constraints on the origin of the Neoproterozoic Qieganbulake ultramafic–carbonatite complex from the Tarim Block, Northwest China. Lithos 182–183, 150–164.
Ye, X.T., Zhang, C.L., Santosh, M., Zhang, J., Fan, X.K., Zhang, J.J., 2016. Growth and evolution of Precambrian continental crust in the southwestern Tarim terrane: New evidence from the ca. 1.4 Ga A-type granites and Paleoproterozoic intrusive complex. Precambrian Res. 275, 18–34.
Yin, A., 2010. Cenozoic tectonic evolution of Asia: A preliminary synthesis. Tectonophysics 488, 293–325.
Yin, A., Harrison, T.M., 2000. Geologic evolution of the Himalayan-Tibetan orogen. Annu. Rev. Earth Planet. Sci. 28, 211–280.
Yin, A., Nie, S., 1996. A Phanerozoic palinspastic reconstruction of China and its neighboring regions. In: Yin, A., Harrison, T.M. (Eds.), The Tectonics of Asia. Cambridge University Press, New York, pp. 442–485.
Yin, A., Dang, Y., Wang, L., Jiang, W., Zhou, S., Chen, X., Gehrels, G.E., Mcrivette, M.W., 2008a. Cenozoic tectonic evolution of Qaidam basin and its surrounding regions (Part 1): The southern Qilian Shan-Nan Shan thrust belt and northern Qaidam basin. GSA Bull. 120, 813–846.
Yin, A., Dang, Y., Zhang, M., Chen, X., Mcrivette, M.W., 2008b. Cenozoic tectonic evolution of the Qaidam basin and its surrounding regions (Part 3): Structural geology, sedimentation, and regional tectonic reconstruction. GSA Bull. 120, 847–876.
Yin, C.Q., Lin, S.F., Davis, D.W., Xing, G.F., Davis, W.J., Cheng, G.H., Xiao, W.J., Li, L.M., 2013. Tectonic evolution of the southeastern margin of the Yangtze Block: Constraints from SHRIMP U-Pb and LA-ICP-MS Hf isotopic studies of zircon from the eastern Jiangnan Orogenic Belt and implications for the tectonic interpretation of South China. Precambrian Res. 236, 145–156.
Yu, F.C., Wei, G.F., Sun, J.D., 1994. Metallogenic Modal for the Syntectonic Gold Deposits in Black Series-A Case Study of the Tanjianshan Deposit. Northwest University Press, Xi'an, pp. 1–130 in Chinese with English Abstract.
Yu, J.-H., O'Reilly, S.Y., Wang, L., Griffin, W.L., Zhang, M., Wang, R., et al., 2008. Where was South China in the Rodinia supercontinent? Precambrian Res. 164 (1–2), 1–15.
Yu, J.H., O'Reilly, S.Y., Wang, L., Griffin, W.L., Zhou, M.F., Zhang, M., Shu, L., 2010. Components and episodic growth of Precambrian crust in the Cathaysia Block, South China: Evidence from U–Pb ages and Hf isotopes of zircons in Neoproterozoic sediments. Precambrian Res. 181 (1–4), 97–114.
Yu, S.Y., Zhang, J.X., Zhao, X.L., Gong, J.H., Li, Y.S., 2014. Geochronology, geochemistry and petrogenesis of the late Palaeoproterozoic A-type granites from the Dunhuang block, SE Tarim Craton, China: implications for the break-up of the Columbia supercontinent. Geol. Mag. 151 (4), 629–648.
Yu, W.J., Luo, Z.H., Liu, Y.S., Sun, J.Y., Li, Z., Wang, Z., Tang, Z.X., 2017a. Petrogenesis of the Lala iron-copper deposit: Evidence by cryptoexplosive breccia CSD data and their zircon U-Pb data. Acta Petrol. Sin. 33 (3), 925–941 (in Chinese with English abstract).
Yu, X.J., Fu, S., Wang, Z., Li, Q., Guo, Z., 2017b. The discovery of early Paleoproterozoic high-Na trond-hjemite in the northeastern Qaidam Basin: Evidence from the drilling core samples. Precambrian Res. 298, 615–628.
Zhai, M.G., 2011. Cratonization and the ancient North China continent: A summary and review. Sci. China Earth Sci. 54 (8), 1110–1120.
Zhai, M.G., 2014. Multi-stage crustal growth and cratonization of the North China craton. Geosci. Front. 5 (4), 457–469.
Zhai, M.G., Santosh, M., 2011. The early Precambrian odyssey of the North China craton: A synoptic overview. Gondwana Res. 20 (1), 6–25.
Zhai, M.G., Guo, J.H., Yan, Y.H., Li, Y.G., Han, X.L., 1993. Discovery of high pressure basic granulite terrain in North China Archean craton and preliminary study. Sci. China (Ser. B) 36, 1402–1408.
Zhai, M.G., Li, T.S., Peng, P., Hu, B., Liu, F., Zhang, Y.B., Guo, J.H., 2010. Precambrian key tectonic events and evolution of the North China Craton. In: Kusky, T.M., Zhai, M.G., Xiao, W.J. (Eds.), The Evolving Continents, 338. Geological Society of London Special Publications, pp. 235–262.
Zhai, M.G., Zhao, L., Zhu, X.Y., Zhou, Y.Y., Peng, P., Guo, J.H., Li, X.H., 2021. Late Neoarchean magmatic–metamorphic event and crustal stabilization in the North China Craton. Am. J. Sci. 321 (1–2), 206–234.
Zhang, J.X., Gong, J.H., 2018. Revisiting the nature and affinity of the Alxa Block. Acta Petrol. Sin. 34, 940–962 (in Chinese with English abstract).
Zhang, W., Hu, Z.C., 2020. Estimation of isotopic reference values for pure materials and geological reference materials. At. Spectrosc. 41 (3), 93–102.
Zhang, Y., Wang, Y., 2016a. Early Neoproterozoic (~840 Ma) arc magmatism: Geochronological and geochemical constraints on the metabasites in the Central Jiangnan Orogen. Precambrian Res. 275, 1–17.
Zhang, Y.Z., Wang, Y.J., 2016b. Early Neoproterozoic (~840Ma) arc magmatism: Geochronological and geochemical constraints on the metab group and asites in the Central Jiangnan Orogen. Precambrian Res. 275, 1–17.
Zhang, S.B., Zheng, Y.F., 2013. Formation and evolution of Precambrian continental lithosphere in South China. Gondwana Res. 23 (4), 1241–1260.
Zhang, J.X., Wan, Y.S., Xu, Z.Q., Yang, J.S., Meng, F.C., 2001. Discovery of basic granulite and its formation age in Delingha area, North Qaidam Monutains. Acta Petrol. Sin. 17 (3), 453–458.
Zhang, J.X., Wan, Y.S., Meng, F.C., Yang, J.S., Xu, Z.Q., 2003. Geochemistry, Sm-Nd and U-Pb isotope study of gneisses (schists) enclosing eclogites in the North Qaidam Monutains—deeply subducted Precambrian metamorphic basement? Acta Petrol. Sin. 19 (3), 443–451.
Zhang, S.H., Li, Z.X., Wu, H., 2006. New Precambrian palaeomagnetic constraints on the position of the North China Block in Rodinia. Precambrian Res. 144, 213–238.
Zhang, S.H., Liu, S.W., Zhao, Y., Yang, J.H., Song, B., Liu, X.M., 2007a. The 1.75–1.68 Ga anorthosite-magnetite-alkali granitoid-rapakivi granite suite from the northern North China Craton: Magmatism related to a Paleoproterozoic orogen. Precambrian Res. 155 (3–4), 287–312.
Zhang, C.L., Li, X.H., Li, Z.X., Lu, S.N., Ye, H.M., Li, H.M., 2007b. Neoproterozoic ultramafic–mafic-carbonatite complex and granitoids in Quruqtagh of northeastern Tarim Block, western China: Geochronology, geochemistry and tectonic implications. Precambrian Res. 152 (3–4), 149–169.
Zhang, C.L., Li, Z.X., Li, X.H., Ye, H.M., 2009. Neoproterozoic mafic dyke swarms at the northern margin of the Tarim Block, NW China: Age, geochemistry, petrogenesis and tectonic implications. J. Asian Earth Sci. 35, 167–179.
Zhang, S.H., Zhao, Y., Yang, Z.Y., He, Z.F., Wu, H., 2009a. The 1.35 Ga diabase sills from the northern North China Craton: implications for breakup of the Columbia (Nuna) supercontinent. Earth Planet. Sci. Lett. 288 (3–4), 588–600.
Zhang, M., Kamo, S.L., Li, C., Hu, P., Ripley, E.M., 2010a. Precise U–Pb zircon–baddeleyite age of the Jinchuan sulfide ore-bearing ultramafic intrusion, western China. Mineral. Deposita 45 (1), 3–9.
Zhang, Y.J., Zhou, X.H., Liao, S.B., Zhang, X.D., Wu, B., Wang, C.Z., Yu, M.G., 2010b. Neoproterozoic crustal composition and orogenic process of the Zhanggongshan area, Anhui-Jiangxi. Acta Geol. Sin. 84 (10), 1401–1427 (in Chinese with English abstract).
Zhang, S.H., Li, Z.X., Evans, D.A., Wu, H., Li, H., Dong, J., 2012a. Pre-Rodinia supercontinent Nuna shaping up: A global synthesis with new paleomagnetic results from North China. Earth Planet. Sci. Lett. 353, 145–155.
Zhang, A.M., Wang, Y.J., Fan, W.M., Zhang, Y.Z., Yang, J., 2012b. Earliest Neoproterozoic (ca. 1.0Ga) arc-back-arc basin nature along the northern Yunkai Domain of the Cathaysia Block: Geochronological and geochemical evidence from the metabasite. Precambrian Res. 220-221, 217–233.
Zhang, C.L., Zou, H.B., Wang, H.Y., Li, H.K., Ye, H.M., 2012c. Multiple phases of the Neoproterozoic igneous activity in Quruqtagh of the northeastern Tarim Block, NW China: interaction between plate subduction and mantle plume? Precambrian Res. 222, 488–502.
Zhang, S.B., Wu, R.X., Zheng, Y.F., 2012d. Neoproterozoic continental accretion in South China: Geochemical evidence from the Fuchuan ophiolite in the Jiangnan orogen. Precambrian Res. 220–221, 45–64.
Zhang, Y., Wang, Y., Fan, W., Zhang, A., Ma, L., 2012e. Geochronological and geochemical constraints on the metasomatised source for the Neoproterozoic (~825Ma) high-mg volcanic rocks from the Cangshuipu area (Hunan Province) along the Jiangnan domain and their tectonic implications. Precambrian Res. 220–221, 139–157.
Zhang, C.L., Li, H.K., Santosh, M., Li, Z.X., Zou, H.B., Wang, H., Ye, H., 2012f. Precambrian evolution and cratonization of the Tarim Block, NW China: Petrology, geochemistry, Nd-isotopes and U–Pb zircon geochronology from Archaean gabbro-TTG–potassic granite suite and Paleoproterozoic metamorphic belt. J. Asian Earth Sci. Evol. Asian Continent Continent. Margins 47, 5–20.
Zhang, L., Ba, J., Chen, N.S., Wang, Q.Y., Liao, F.X., Li, X.Y., 2012g. U-Pb age spectra and trace elements of detrital zircon from Quanji Group: Implications for thermal events and early evolution in the basement. Earth Science—Journal of China University of. Geosciences 37 (Suppl), 28–37.
Zhang, C.L., Santosh, M., Zou, H.B., Li, H.K., Huang, W.C., 2013a. The Fuchuan ophiolite in Jiangnan Orogen: Geochemistry, zircon U-Pb geochronology, Hf isotope and implications for the Neoproterozoic assembly of South China. Lithos 179, 263–274.
Zhang, Y.Z., Wang, Y.J., Geng, H.Y., Zhang, Y.H., Fan, W.M., Zhong, H., 2013b. Early Neoproterozoic (~850Ma) back-arc basin in the Central Jiangnan Orogen (eastern South China): Geochronological and Petrogenetic constraints from meta-basalts. Precambrian Res. 231, 325–342.
Zhang, J., Yu, S., Gong, J., Li, H., Hou, K., 2013c. The latest Neoarchean–Paleoproterozoic evolution of the Dunhuang block, eastern Tarim craton, northwestern China: Evidence from zircon U–Pb dating and Hf isotopic analyses. Precambrian Res. 226, 21–42.
Zhang, H.F., Wang, J.L., Zhou, D.W., Yang, Y.H., Zhang, G.W., Santosh, M., Yu, H., Zhang, J., 2014a. Hadean to Neoarchean episodic crustal growth: Detrital zircon records in Paleoproterozoic quartzites from the southern North China Craton. Precambrian Res. 254, 245–257.
Zhang, C.H., Gao, L.Z., Shi, X.Y., Han, Y., Liu, Y.M., 2014b. SHRIMP age of the volcanic rock from the Fanjingshan Group and its chronostratigraphic significances. Earth Sci. Front. 21 (2), 139–143 (in Chinese with English abstract).
Zhang, C.L., Zou, H.B., Santosh, M., Ye, X.T., Li, H.K., 2014c. Is the Precambrian basement of the Tarim Craton in NW China composed of discrete terranes? Precambrian Res. 254, 226–244.
Zhang, C.L., Zou, H.B., Zhu, Q.B., Chen, X.Y., 2015a. Late Mesoproterozoic to early Neoproterozoic ridge subduction along southern margin of the Jiangnan Orogen: New evidence from the Northeastern Jiangxi Ophiolite (NJO), South China. Precambrian Res. 268, 1–15.

Zhang, H., Li, T.D., Gao, L.Z., Geng, S.F., Ding, X.Z., Liu, Y.X., Kou, C.H., 2015b. Zircon SHRIMP U-Pb dating, geochemical, zircon Hf isotopic features of the Mesoproterozoic Tieshajie Formation in northeastern Jiangxi. Geol. Rev. 61 (1), 65–78 (in Chinese with English abstract).
Zhang, Y.Z., Wang, Y.J., Zhang, Y.H., Zhang, A.M., 2015c. Neoproterozoic assembly of the Yangtze and Cathaysia blocks: Evidence from the Cangshuipu Group and associated rocks along the central Jiangnan Orogen, South China. Precambrian Res. 269, 18–30.
Zhang, H.J., Wang, X.L., Wang, X., Zhou, H.R., 2016. U-Pb zircon ages of tuff beds from the Hongzaoshan Formation of the Quanji Group in the north margin of the Qaidam Basin, NW China, and their geological significances. Earth Sci. Front. 23 (6), 202–218 (in Chinese with English abstract).
Zhang, S.H., Zhao, Y., Li, X.H., Ernst, R.E., Yang, Z.Y., 2017a. The 1.33–1.30 Ga Yanliao large igneous province in the North China Craton: Implications for reconstruction of the Nuna (Columbia) supercontinent, and specifically with the North Australian Craton. Earth Planet. Sci. Lett. 465, 112–125.
Zhang, F.F., Wang, X.L., Wang, D., Yu, J.H., Zhou, X.H., Sun, Z.M., 2017b. Neoproterozoic backarc basin on the southeastern margin of the Yangtze block during Rodinia assembly: New evidence from provenance of detrital zircons and geochemistry of mafic rocks. Geol. Soc. Am. Bull. 129, 904–919.
Zhang, J., Li, H.K., Zhang, C.L., Tian, H., Zhong, Y., Ye, X.T., 2018. New evidence for the breakup of the Columbia supercontinent from the northeastern margin of Tarim Craton: rock geochemistry, zircon U-Pb geochronology and Hf-O isotopic compositions of the ca. 1.55 Ga diabase sills in the Kuruktag area. Earth Sci. Front. 25 (6), 106–123.
Zhang, H.C., Zhao, G., Wang, C., Yao, J., Xu, N., 2022a. Phase equilibria modelling and zircon U-Pb geochronology of Paleoproterozoic mafic granulites from the Chengde Complex, North China Craton. Precambrian Res. 371, 106576.
Zhang, S.H., Ernst, R.E., Yang, Z., Zhou, Z., Pei, J., Zhao, Y., 2022b. Spatial distribution of 1.4-1.3 Ga LIPs and carbonatite-related REE deposits: Evidence for large-scale continental rifting in the Columbia (Nuna) supercontinent. Earth Planet. Sci. Lett. 597, 117815.
Zhao, G.C., 2015. Jiangnan Orogen in South China: Developing from divergent double subduction. Gondwana Res. 27 (3), 1173–1180.
Zhao, G.C., Cawood, P.A., 2012. Precambrian geology of China. Precambrian Res. 222–223, 13–54.
Zhao, G.C., Zhai, M.G., 2013. Lithotectonic elements of Precambrian basement in the North China Craton: Review and tectonic implications. Gondwana Res. 23, 1207–1240.
Zhao, J.H., Zhou, M.F., 2007. Geochemistry of Neoproterozoic mafic intrusions in the Panzhihua district (Sichuan Province, SW China): Implications for subduction-related metasomatism in the upper mantle. Precambrian Res. 152 (1-2), 27–47.
Zhao, J.H., Zhou, M.F., 2009. Secular evolution of the Neoproterozoic lithospheric mantle underneath the northern margin of the Yangtze Block, South China. Lithos 107 (3-4), 152–168.
Zhao, J.H., Zhou, M.F., 2013. Neoproterozoic high-Mg basalts formed by melting of ambient mantle in South China. Precambrian Res. 233, 193–205.
Zhao, G.C., Wilde, S.A., Cawood, P.A., Sun, M., 2001. Archean blocks and their boundaries in the North China craton: Lithological, geochemical, structural and P-T path constraints and tectonic evolution. Precambrian Res. 107 (1–2), 45–73.
Zhao, G.c., Cawood, P.A., Li, S.Z., Wilde, S.A., Sun, M., Zhang, J., He, Y.H., Yin, C.Q., 2012. Amalgamation of the North China Craton: key issues and discussion. Precambrian Res. 222, 55–76.
Zhao, G.C., Cawood, P.A., Wilde, S.A., Sun, M., 2002. Review of the global 2.1–1.8 Ga orogens: Implications for a pre-Rodinian supercontinent. Earth Sci. Rev. 59 (1–4), 125–162.
Zhao, G., Sun, M., Wilde, S.A., Li, S., 2004. A Paleo-Mesoproterozoic supercontinent: assembly, growth and breakup. Earth Sci. Rev. 67 (1–2), 91–123.
Zhao, G.C., Sun, M., Wilde, S.A., Li, S.Z., 2005. Late Archean to Paleoproterozoic evolution of the North China craton. Key issues revisited. Precambrian Res. 136 (2), 77–202.
Zhao, F.Q., Zhao, W.P., Zuo, Y.C., Li, Z.H., Xue, K.Q., 2006. U-Pb geochronology of Neoproterozoic magmatic rocks in Hanzhong, southern Shaanxi, China. Geol. Bull. China 25 (3), 383–388 (in Chinese with English abstract).
Zhao, G.C., Wilde, S.A., Sun, M., Guo, J.H., Kroner, A., Li, S.Z., Li, X.P., Zhang, J., 2008. SHRIMP U-Pb zircon geochronology of the Huai'an Complex: constraints on Late Archean to Paleoproterozoic magmatic and metamorphic events in the Trans-North China Orogen. Am. J. Sci. 308 (3), 270–303.
Zhao, J.H., Zhou, M.F., Zheng, J.P., Fang, S.M., 2010. Neoproterozoic crustal growth and reworking of the northwestern Yangtze Block: Constraints from the Xixiang dioritic intrusion, South China. Lithos 120 (3-4), 439–452.
Zhao, J.H., Zhou, M.F., Yan, D.P., Zheng, J.P., Li, J.W., 2011. Reappraisal of the ages of Neoproterozoic strata in South China: No connection with the Grenvillian orogeny. Geology 39 (4), 299–302.
Zhao, J.H., Zhou, M.F., Zheng, J.P., 2013a. Neoproterozoic high-K granites produced by melting of newly formed mafic crust in the Huangling region, South China. Precambrian Res. 233, 93–107.
Zhao, Y., Diwu, C.R., Sun, Y., Zhu, T., Wang, H.L., 2013b. Zircon geochronology and Lu-Hf isotope compositions for Precambrian rocks of the Dunhuang complex in Shuixiakou area, Gansu Province. Acta Petrol. Sin. 29.
Zhao, Y., Sun, Y., Yan, J., Diwu, C., 2015. The Archean-Paleoproterozoic crustal evolution in the Dunhuang region, NW China: Constraints from zircon U–Pb geochronology and in situ Hf isotopes. Precambrian Res. 271, 83–97.
Zhao, Y., Sun, Y., Ao, W., Zhang, H., Zhu, T., 2019. Depositional age, provenance and tectonic significance of Precambrian metasedimentary rocks from the Dunhuang Complex, NW China: Evidence from field investigation, zircon U–Pb geochronology and whole–rock geochemistry. Precambrian Res. 326, 272–294. https://doi.org/10.1016/j.precamres.2017.12.032.
Zheng, Y., Zhang, S., 2007. Formation and evolution of Precambrian continental crust in South China. Chin. Sci. Bull. 52 (1), 1–12.
Zhong, Y.T., Kusky, T., Wang, L., Polat, A., Liu, X.Y., Peng, Y.Y., Luan, Z.K., Wang, C.H., Wang, J.P., Deng, H., 2021. Alpine-style nappes thrust over ancient North China continental margin demonstrate large Archean horizontal plate motions. Nat. Commun. 12, 6172.
Zhong, Y., Kusky, T.M., Wang, L., 2022. Giant sheath-folded nappe stack demonstrates extreme subhorizontal shear strain in an Archean orogen. Geology 50 (5), 577–582.
Zhou, Y.Y., Zhai, M.G., 2022. Mantle plume-triggered rifting closely following Neoarchean cratonization revealed by 2.50–2.20 Ga magmatism across North China Craton. Earth Sci. Rev. 230, 104060.
Zhou, M.F., Kennedy, A.K., Sun, M., Malpas, J., Lesher, C.M., 2002a. Neo-proterozoic arc-related mafic intrusions along the northern margin of South China: Implications for the accretion of Rodinia. J. Geol. 110 (5), 611–618.
Zhou, M.F., Yan, D.P., Kennedy, A.K., Li, Y.Q., Ding, J., 2002b. SHRIMP U-Pb zircon geochronological and geochemical evidence for Neoproterozoic arc-magmatism along the western margin of the Yangtze Block, South China. Earth Planet. Sci. Lett. 196 (1-2), 51–67.
Zhou, M., Ma, Y., Yan, D., Xia, X., Zhao, J., Sun, M., 2006. The Yanbian Terrane (Southern Sichuan Province, SW China): A Neoproterozoic arc assemblage in the western margin of the Yangtze Block. Precambrian Res. 144 (1–2), 19–38.
Zhou, J., Li, X.H., Ge, W., Li, Z.X., 2007a. Age and origin of middle Neoproterozoic mafic magmatism in southern Yangtze Block and relevance to the break-up of Rodinia. Gondwana Res. 12 (1–2), 184–197.
Zhou, J.B., Li, X.H., Ge, W.C., Li, Z.X., 2007b. Age and origin of Middle Neoproterozoic mafic magmatism in southern Yangtze Block and relevance to the break-up of Rodinia. Gondwana Res. 12 (1-2), 184–197.
Zhou, J.C., Wang, X.L., Qiu, J.S., 2009. Geochronology of Neoproterozoic mafic rocks and sandstones from northeastern Guizhou, South China: Coeval arc magmatism and sedimentation. Precambrian Res. 170 (1-2), 27–42.
Zhou, J.Y., Mao, J.W., Liu, F.Y., Tan, H.Q., Shen, B., Zhu, Z.M., Chen, J.B., Luo, L.P., Zhou, X., Wang, Y., 2011. SHRIMP U-Pb zircon chronology and geochemistry of albitite from the Hekou Group in the western Yangtze Block. J. Mineral. Petrol. 31 (3), 66–73 (in Chinese with English abstract).
Zhou, Z.G., Hu, M.M., Wu, C., Wang, G.S., Liu, C.F., Cai, A.R., 2018. Coupled U-Pb dating and Hf isotopic analysis of detrital zircons from Bayan Obo Group in Inner Mongolia: Constraints on the evolution of the Bayan Obo rift belt. Geol. J. 53 (6), 2649–2664.
Zhou, X., Hu, X., Jiang, R., Gao, T., Ma, X., Xing, G., Sun, G., Shu, X., Zhao, X., 2020. Sedimentary Facies, Provenance and Geochronology of the Heshangzhen Group: Implications for the Tectonic Evolution of the Eastern Jiangnan Orogen, South China. Acta Geol. Sin. Engl. Ed. 94, 1138–1158.
Zhou, Y., Zhai, M., Mitchell, R.N., Cawood, P.A., Huang, G., Spencer, C.J., et al., 2024. Low δ18O and δ30Si TTG at ca. 2.3 Ga hints at an intraplate rifting onset of the Paleoproterozoic supercontinent cycle. J. Geophys. Res. Solid Earth 129, e2023JB027306.
Zhu, X.Y., Chen, F.K., Wang, W., Pham, T.H., Wang, F., Zhang, F.Q., 2008a. Zircon U-Pb ages of volcanic and sedimentary rocks of the Wudang Group in the Qinling Orogenic Belt within western Henan Province. Acta Geosci. Sin. 29 (6), 817–829 (in Chinese with English abstract).
Zhu, W., Zhang, Z., Shu, L., Lu, H., Su, J., Yang, W., 2008b. SHRIMP U-Pb zircon geochronology of Neoproterozoic Korla mafic dykes in the northern Tarim Block, NW China: Implications for the long-lasting breakup process of Rodinia. J. Geol. Soc. Lond. 165, 887–890.
Zhu, W., Zheng, B., Shu, L., Ma, D., Wan, J., Zheng, D., Zhang, Z., Zhu, X., 2011. Geochemistry and SHRIMP U-Pb zircon geochronology of the Korla mafic dykes: Constrains on the Neoproterozoic continental breakup in the Tarim Block, northwest China. J. Asian Earth Sci. 42, 791–804.
Zhu, Q., Zhao, X., Hong, W., Jin, G., Huang, W., Wang, C., Liu, K., Gao, T., Wen, H., 2023. Geochronology, Hf isotope and trace element of zircon and apatite for neoproterozoic granodiorites in the eastern Jiangnan Orogen: Implications for the neoproterozoic tectonic evolution. Lithos 446–447, 107134.
Zhuo, J.W., Jiang, X.S., Wang, J., Cui, X.Z., Wu, H., Xiong, G.Q., Lu, J.Z., Jiang, Z.F., 2015. LA-ICP-MS zircon U-Pb ages for pisolitic welded tuff from the bottom of the Neoproterozoic Suxiong Formation in western Sichuan and their geological significance. Sediment. Geol. Tethyan Geol. 35 (4), 85–91 (in Chinese with English abstract).
Zonenshain, L.P., Kuzmin, M.I., Natapov, L.M., Page, B.M. (Eds.), 1990. Geology of the USSR: A Plate-Tectonic Synthesis. Am. Geophys. Union Geodyn. Ser. Vol. 21, 242.
Zong, K., Liu, Y., Zhang, Z., He, Z., Hu, Z., Guo, J., Chen, K., 2013. The generation and evolution of Archean continental crust in the Dunhuang block, northeastern Tarim craton, northwestern China. Precambrian Res. 235, 251–263.
Zuza, A.V., Yin, A., 2017. Balkatach hypothesis: A new model for the evolution of the Pacific, Tethyan, and Paleo-Asian oceanic domains. Geosphere 13 (5), 1664–1712.
Zuza, A.V., Wu, C., Reith, R.C., Yin, A., Li, J.H., Zhang, J.Y., Zhang, Y.X., Wu, L., Liu, W. C., 2018. Tectonic evolution of the Qilian Shan: An early Paleozoic orogen reactivated in the Cenozoic. Geol. Soc. Am. Bull. 130, 881–925.